

Radiation, Clouds, Water Vapor, Precipitation, and Atmospheric Circulation

LEAD AUTHOR D. L. Hartmann

CONTRIBUTING AUTHORS C. S. Bretherton
 T. P. Charlock
 M. D. Chou
 A. Del Genio
 R. E. Dickinson
 R. Fu
 R. A. Houze
 M. D. King
 K. M. Lau
 C. B. Leovy
 S. Sorooshian
 J. Washburne
 B. Wielicki
 R. C. Willson

CHAPTER 2 CONTENTS

2.1 Introduction	43
2.1.1 Role of radiation, clouds, atmospheric water, and precipitation in climate and global change	43
2.2 Major scientific issues	43
2.2.1 Total solar irradiance and the Earth's climate	43
2.2.1.1 Role of TSI in climate change	43
2.2.1.2 Space-based observations of TSI variability	43
2.2.1.3 Remaining uncertainties	45
2.2.1.3.1 Uncertainties resulting from measurement technology	45
2.2.1.3.2 Present and planned TSI monitoring	46
2.2.1.4 Needed observations and observational strategy	46
2.2.1.4.1 The "overlap" strategy with ambient temperature radiometers	46
2.2.2 Role of radiation fluxes in the climate system	47
2.2.2.1 Atmospheric and surface radiative fluxes and heating	48
2.2.2.2 Absorption, scattering, and emission by gases	49
2.2.2.3 Absorption, scattering, and emission from aerosols	50
2.2.2.4 Absorption, scattering, and emission from clouds	51
2.2.2.5 Absorption, scattering, and emission by the Earth's surface	52
2.2.2.6 Radiation in global climate models	55
2.2.3 Role of convection and clouds in climate	56
2.2.3.1 Cloud effects on the Earth's energy balance	56
2.2.3.2 Cloud effects on the surface energy balance	58
2.2.3.3 Observations of cloud properties	58
2.2.3.3.1 Surface observations	58
2.2.3.3.2 Satellite observations	59
2.2.3.4 Modeling of clouds in the climate system	59
2.2.3.4.1 Global climate models–cloud parameterization and role in sensitivity	60
2.2.3.4.2 Regional mesoscale modeling of clouds	62
2.2.3.4.3 Cloud-scale models	64
2.2.3.5 Observational strategy for radiative fluxes and cloud properties	65
2.2.3.5.1 TOA radiative fluxes	70
2.2.3.5.2 Surface radiative fluxes	70
2.2.3.5.3 Radiative fluxes within the atmosphere	71
2.2.3.5.4 Cloud properties	72
2.2.3.5.4.1 Cloud fraction	72
2.2.3.5.4.2 Cloud height	73
2.2.3.5.4.3 Cloud visible optical depth and thermal infrared emittance	74
2.2.3.5.4.4 Cloud particle size	75
2.2.3.5.4.5 Cloud liquid/ice water path	75
2.2.3.5.4.6 Cloud mesoscale organization and structure	76
2.2.4 Water vapor and climate	76
2.2.4.1 Water vapor feedback and climate sensitivity	77
2.2.4.2 Water vapor distribution and variability	78
2.2.4.3 Maintenance of the global water vapor distribution	78
2.2.4.3.1 Role of convection and clouds	78
2.2.4.3.2 Role of large-scale atmospheric motions	79
2.2.4.3.3 Role of surface temperature	80
2.2.4.4 Water vapor in global climate models	80
2.2.4.5 Needed observations of water vapor	81
2.2.4.5.1 Available climatologies	81
2.2.4.5.2 Needed improvements	82
2.2.5 Precipitation	82
2.2.5.1 Role and importance of precipitation	82
2.2.5.1.1 Role in climate system operation	83
2.2.5.1.2 Importance in global change scenarios	84

CHAPTER 2 CONTENTS (CONT.)

2.2.5.2	Spatial and temporal distribution of precipitation	85
2.2.5.3	Integration of ground data	86
2.2.5.4	Precipitation in climate models	86
2.2.5.5	Needed satellite measurements and algorithms	87
2.2.6	Atmospheric circulation, hydrologic processes, and climate	88
2.2.6.1	Hydrologic processes and the tropospheric circulation	88
2.2.6.2	Large-scale circulation and climate feedback processes	88
2.2.6.3	Need for satellite measurements of wind	89
2.2.7	Strategy for combining observations and modeling	89
2.3	Required satellite measurements and data sets	91
2.3.1	Summary of required satellite observations	91
2.3.1.1	Total solar irradiance	91
2.3.1.2	Radiative fluxes	91
2.3.1.2.1	TOA fluxes	92
2.3.1.2.2	Surface and internal atmospheric fluxes	93
2.3.1.3	Cloud properties	93
2.3.1.3.1	Cloud fractional area coverage	94
2.3.1.3.2	Cloud height	96
2.3.1.3.3	Cloud visible optical depth and infrared emissivity	97
2.3.1.3.4	Cloud particle size and phase	97
2.3.1.3.5	Cloud liquid/ice water path	97
2.3.1.3.6	Lightning	97
2.3.1.4	Atmospheric temperature profiles	97
2.3.1.5	Water vapor	99
2.3.1.6	Precipitation	99
2.3.1.7	Winds and circulation	99
2.3.2	Critical surface observations and field experiments	99
2.3.2.1	FIRE	100
2.3.2.2	GEWEX	101
2.3.2.3	Climate Variability (CLIVAR) Project	101
2.3.2.4	ARM	102
2.3.2.5	BSRN	102
2.3.2.6	ECLIPS	102
2.3.2.7	Ties to other research areas	102
2.3.2.7.1	Oceanic processes	102
2.3.2.7.2	Land processes	103
2.4	Summary of EOS contributions	103
2.4.1	Observation and monitoring of key climate variables	103
2.4.1.1	Total solar irradiance	103
2.4.1.2	Radiative energy fluxes—TOA, surface, atmospheric	104
2.4.1.3	Cloud properties	104
2.4.1.4	Precipitation	104
2.4.2	Understanding of the processes that relate clouds and water vapor to global climate and their effect on climate sensitivity	104
2.4.3	More-accurate treatment of cloud and water vapor and their radiative effects in global climate models	104
2.4.4	Better measurement of precipitation and understanding of the role of precipitation in connecting atmospheric and surface processes, and more-accurate modeling of precipitation in global climate models	105
2.4.5	Synergism with oceanic and land-surface processes	105
2.4.6	Enhanced assessment of global change: monitoring and trend detection	105
2.4.7	Improved predictions of future climates and the influence of climate change on humanity	106
	References	106
	Chapter 2 Index	113

2.1 Introduction

2.1.1 *Role of radiation, clouds, atmospheric water, and precipitation in climate and global change*

The temperature near the surface of the Earth is in thermodynamic equilibrium when the absorption of radiant energy from the sun is in approximate balance with the emission of radiant energy to space by the planet. Sources of heat that are internal to the Earth system are negligible in a global sense. The energy output of the sun is a critical control on the Earth's climate. The amount of available solar energy absorbed by the Earth depends on its reflectivity, which is strongly dependent on the fractional coverage and optical properties of clouds in the atmosphere, aerosol amount and properties, atmospheric humidity, and the condition of the surface. These properties in turn interact with the temperature distribution and circulation of the atmosphere. Surface ice cover is sensitive to the global mean temperature of the Earth, and cloud amount and properties may also change with the mean climate.

The surface temperature of the Earth depends not only on the absorbed solar radiation, but also on the relationship between the surface temperature and the rate at which energy is returned to space by the radiative emission of the Earth. This relationship is controlled by the amount and vertical distribution of greenhouse gases, clouds and aerosols, and their relationship with the temperature profile. The most important greenhouse gas is

water vapor, whose distribution is determined by a complex web of interactions within the climate system itself. The dependence of saturation vapor pressure of water on temperature provides one of the potentially most powerful positive feedback processes in the climate system. The water vapor distribution interacts strongly with convection and the associated clouds, precipitation, large-scale circulations, and the thermal structure of the atmosphere.

Understanding the interactions among radiative transfer, clouds, water vapor, and precipitation, and incorporating this understanding into appropriate models, constitutes a critical step in predicting future climate changes and their regional and global impacts. In addition, these processes are also important for seasonal and interannual variability. In particular, mechanical and thermodynamic interactions between the atmosphere and the ocean on these time scales are strongly modulated by clouds, water vapor, and large-scale circulations.

EOS will collect a set of global observations that bear directly on the radiative, cloud, and hydrologic processes in the Earth's atmosphere. Through instrument team investigations, interdisciplinary science investigations, and use by the wider scientific community, these observations will be translated into an improved understanding of these processes and into improvements in our models of climate (Hartmann 1994).

2.2 Major scientific issues

2.2.1 *Total solar irradiance (TSI) and the Earth's climate*

2.2.1.1 *Role of TSI in climate change*

Monitoring TSI, the energy from the sun that is available to be received at the average distance of the Earth from the sun, has been a goal of science for more than a century. At any time in the Earth's history the climate regime of the biosphere has been determined by the TSI, the atmospheric chemical composition, the distribution of oceans and land masses, and the circulations of the oceans and atmosphere that act in combination to determine the net retention of solar energy, its distribution within the climate system, and its ultimate return to space by radiative emission.

2.2.1.2 *Space-based observations of TSI variability*

The first long-term solar monitoring utilizing an Electrically Self-Calibrating Cavity (ESCC) sensor in space was the Earth Radiation Budget (ERB) experiment on the National Aeronautics and Space Administration (NASA) Nimbus 7 spacecraft. The ERB database, beginning in late 1978 and continuing to early 1993, is the longest currently available (Hickey et al. 1980; Hoyt et al. 1992). Unambiguous evidence of TSI variability was first detected in the highly precise results of the Active Cavity Radiometer Irradiance Monitor (ACRIM I) experiment on the NASA Solar Maximum Mission (SMM) in 1980 (Willson et al. 1981). The principal features of TSI variability have been identified in the ERB results as well. The mutually corroborative function of the ACRIM I and

ERB results has played an important role in verifying TSI variability on the solar activity cycle time scale.

A series of short-term TSI experiments have been flown on or deployed from the space shuttle to provide comparison experiments for satellite solar monitors. The Spacelab 1 and Atmospheric Laboratory for Applications and Science (ATLAS) flights between 1983 and 1993 employed two different TSI experiments, as has the shuttle-deployed and -retrieved European Retrieval Carrier (EURECA) platform that operated during 1992-1993 (Frohlich 1994; Crommelynck et al. 1994; Willson 1994). The shuttle ACRIM experiment has demonstrated a capability of sustaining flight-to-flight precision of the order of 100 parts-per-million (ppm). This precision is comparable to the accuracy achievable by radiometers operating at cryogenic temperatures, but significantly inferior to the precision accessible using an overlap strategy with "ambient temperature" satellite experiments (Willson 1995).

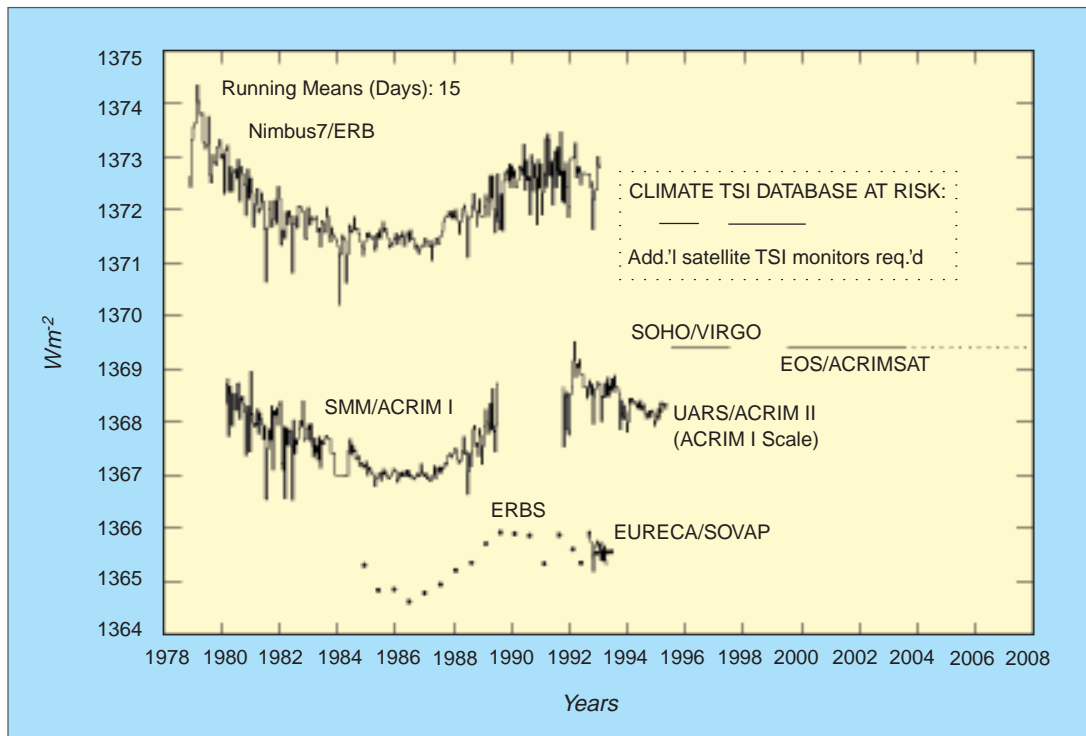
The results of modern TSI monitoring are shown in Figure 2.1. The Nimbus7/ERB, SMM/ACRIM I and Upper Atmosphere Research Satellite (UARS)/ACRIM

II experiments have documented the direct dependence of TSI on solar activity during solar cycles 21 and 22. Qualitatively similar results have been obtained with the Earth Radiation Budget Satellite (ERBS) solar monitor (Lee et al. 1995).

One of the most significant findings from the precision TSI database thus far is on solar cycle time scales: a direct correlation of luminosity and solar activity (Willson and Hudson 1986, 1988, 1991; Foukal and Lean 1988; Hoyt et al. 1992; Frohlich 1994). TSI showed a 0.1% peak-to-peak amplitude during solar cycle 21. The observed maximum of TSI at the maximum in solar activity agrees in sense with that predicted from the coincidence of the "Little Ice Age" climate anomaly and the "Maunder Minimum" of solar activity during the seventeenth and eighteenth centuries (Eddy 1977).

Solar cycle TSI variation is predicted with varying degrees of success by linear regression models using the precision TSI database and "proxies" of solar activity, such as the Zürich sunspot number, the 10.7-cm microwave flux, the He I 1083-nm full-disk equivalent width, and the "core-to-wing ratio" of the Mg II line at 280 nm. The

FIGURE 2.1



Record of total solar irradiance (TSI) monitoring from space. Includes data from Nimbus 7/ERB, Solar Maximum Mission, UARS/ACRIM, and ERBE solar monitor, plus some shuttle observations.

use of the He I model led to the initial realization of the primary role of faculae and the bright network in the solar cycle TSI variation (Foukal and Lean 1988, 1990; Livingston et al. 1988; Willson and Hudson 1988). The “proxy models” of TSI have been useful in providing qualitative explanations of solar phenomena, but in view of the fact that they are simple statistical constructs and not physical models, it is not surprising that significant differences are found between predictions of TSI and satellite observations.

An inverse relationship between sunspot area and total irradiance has been found on the solar rotational time scale (27 days) with deficits in total irradiance of up-to-0.3% (Willson et al. 1981, Willson 1982; Hudson and Willson 1982; Foukal and Lean 1988). There is growing evidence that most of the missing flux is balanced by excess facular radiation on the active region time scale (months) (Willson 1984; Foukal and Lean 1986).

On the shortest time scales, solar global oscillations of low degree have been detected in the ACRIM I total irradiance data, including pressure modes (time scales of minutes—the so-called 5-minute oscillations or “P-modes”) and possible gravity modes (time scales of hours to days). Interpretation of the 5-minute-oscillation results from the ACRIM I experiment has placed an upper limit on differential rotation of the outer solar atmosphere as a function of solar radius, and therefore on solar oblateness, providing support for the relativistic interpretation of the perihelion of Mercury observations (Woodard and Hudson 1983; Woodard 1984; Frohlich 1987; Woodard and Noyes 1985).

P-mode oscillations are constrained to the convection zone or just below, limiting the depth within the sun for which their analysis can provide new physical insight. Should gravity mode oscillations be verified in TSI data, their analysis would yield information on physical processes extending to the solar core.

TSI variations on time scales shorter than a year do not appear to be of direct climatological interest but contain information on solar variability that has provided new insight into the physics of the sun. Continuous TSI monitoring, particularly by satellites with a high solar-pointing duty cycle during each orbit can provide the observations that will facilitate future solar models that may predict TSI variability with sufficient precision to anticipate possible corresponding climate variations.

2.2.1.3 Remaining uncertainties

2.2.1.3.1 Uncertainties resulting from measurement technology
The “absolute” uncertainty of the *current generation* of TSI flight instruments, which operate at ambient temperatures, is about 1000 ppm in the laboratory and about two-to-three times larger in flight experiments (Willson 1973, 1979, 1982; Frohlich 1994). Ambient temperature TSI radiometry is a mature technology that has been thoroughly flight tested in various configurations on balloon, rocket, space shuttle, and satellite flight platforms (Willson 1973, 1979, 1982; Duncan et al. 1977; Hickey et al. 1988). The principal remaining sources of uncertainty for well-designed ambient temperature sensors are the determination of their aperture areas and the myriad of small, parasitic thermal interactions between the cavity detector and its surroundings.

The absolute uncertainty of a *new generation* of TSI sensors operating near the temperature of liquid Helium approaches 100 ppm in the laboratory environment—a 10-fold improvement relative to “ambient temperature” sensors. Cryogenic sensors face some daunting challenges in their transformation into space flight experiments, however. They must use small apertures (~0.3-cm diameter compared to 0.8 cm for “ambient temperature” radiometers) to minimize solar heating that would otherwise prevent their cryogenic coolers from reaching the required temperatures (< 20 K). The singular advantage of cryogenic sensors is that the parasitic thermal uncertainties are reduced to negligible levels. Aperture-area determination remains the most limiting source of uncertainty since their small apertures cannot be determined with the same accuracy as the larger ones employed in ambient temperature sensors.

Contamination is a major source of uncertainty in any TSI flight experiment, and it is of particular concern for cryogenic sensors. At low temperatures they would function as attractors for condensables and particulates. Accumulation of contaminants on the rims of their small apertures would cause larger errors than for ambient temperature instrumentation. A realistic expectation for their eventual in-flight performance would likely be in the several hundred ppm uncertainty range. Moreover, functional lifetime in orbit is a greater concern with cryogenic instruments.

2.2.1.3.2 Present and planned TSI monitoring

The impact of ambient temperature sensor “absolute” uncertainties on TSI monitoring can be seen in Figure 2.1. The highest (Nimbus7/ERB) and lowest (ERBS) lie at $\pm 0.25\%$ about the mean (1369 Wm^{-2}). This is within the expected uncertainty of these sensors’ “native” scales. Should the series of long-term TSI experiments be interrupted, the continuity of the long-term TSI database could not be re-established by deployment of another experiment with an uncertainty less than $\pm 0.25\%$. Since climate changes comparable to the “Little Ice Age” may involve TSI changes as small as 0.5% over 200+ years, the loss of contiguity in the satellite solar-monitoring experiments would render the database useless for climatology.

The ACRIM I experiment terminated with the re-entry of the SMM spacecraft in late 1989. The Nimbus7/ERB experiment ceased operations in early 1993. The precision TSI climate database is currently being sustained by two experiments: the UARS/ACRIM II launched in 1991 and the European Space Agency’s (ESA) Solar Heliospheric Observatory (SOHO)/Variability of solar Irradiance and Gravity Oscillations (VIRGO) launched in late 1995. The connection to the database compiled by the ERB and ACRIM I is conserved by the ACRIM II experiment. The ERBS TSI instrument is also contributing data, but it was launched in 1984 and is limited by aging spacecraft batteries.

The UARS has on-board resources and an orbit that could last to the year 2000. Problems with the batteries and solar panel drive systems raised some doubts about its life expectancy early in the mission but work-arounds appear to have stabilized the satellite. The SOHO/VIRGO experiment became fully operational in March 1996 and has a two-year minimum mission lifetime that could extend significantly by virtue of its Lagrangian point orbit. VIRGO has experienced some initial problems with its two TSI instruments, but appears to be capable of providing high-quality results using work-arounds.

The next planned TSI experiments are a series of ACRIMs designed to provide the database during the 15 years of the Earth Observation System (EOS) program. The first EOS/ACRIM will launch in 1999. The major concern in the effort to sustain the TSI database during the late 1990s is the possible cessation of UARS/ACRIM II and SOHO/VIRGO observations prior to the inception of EOS/ACRIM. Failure to overlap these experiments could result in a catastrophic loss of relative precision between the first 20 years of the long-term, precision TSI database and that to follow.

2.2.1.4 Needed observations and observational strategy

Sustained changes in TSI of as little as a few tenths of one percent per century could be causal factors for significant climate change on time scales ranging from decades to centuries (Lean et al. 1995). A precise, long-term record of solar luminosity variation is required to provide empirical evidence of the sun’s role in climate change and to separate its effect from other climate drivers. The same record, together with climate and other solar observations, will yield a valuable empirical record of TSI variability against which climate observations can be tested, and will also yield an improved understanding of the physics of the sun and the causes of luminosity variations. The record could also eventually lead to a predictive capability for solar-driven climate change.

The National Research Council (NRC) recently published its findings regarding research priorities for Solar Influences on Global Change, one of the seven science elements of the U.S. Global Change Research Program (USGCRP) (NRC 1994). Their recommendations include “monitoring total and spectral solar irradiance from an uninterrupted, overlapping series of spacecraft radiometers employing in-flight sensitivity tracking” as this element’s highest priority and most urgent activity.

Monitoring solar luminosity variability with maximum precision demands not only state-of-the-art technology but the use of an optimum research strategy. Following is an evaluation of approaches to sustain the precision TSI database with the requisite 10-ppm or smaller discontinuities between experiments.

2.2.1.4.1 The “overlap” strategy with ambient temperature radiometers

A relative precision smaller than 10 ppm should be readily achievable for the data of overlapped satellite solar monitors, assuming a sufficiency of overlapping comparisons and adequate degradation calibrations. The principal source of uncertainty for satellite experiments is degradation of their sensors by extended solar exposure during multi-year missions. The series of ACRIM experiments has employed a three-fold sensor redundancy and a phased operational modality that can calibrate such degradation with a residual uncertainty of less than 50 ppm per decade. Fully-implemented three-fold sensor redundancy is essential for adequate calibration of degradation in long-term satellite experiments.

The optimum overlap strategy is the intercomparison of successive, high-precision satellite solar-monitoring experiments at a precision level defined by their operation in the space-flight environment. A backup overlap

strategy would involve intercomparisons by a “third party” flight experiment, such as another satellite experiment or the shuttle-based TSI experiments that have made intercomparisons with two successive but non-overlapping satellite solar monitors.

The “overlap strategy” was to have begun with the in-flight comparison of the SMM/ACRIM I and UARS/ACRIM II experiments. Unfortunately, the SMM mission ended in late 1989, two years before the UARS could be launched. The relationship between the ACRIM I and ACRIM II experiments has instead been established using a “third party” overlap strategy based on the results of mutual comparisons of ACRIM I and ACRIM II with the less precise, but long-lived, Nimbus 7/ERB and ERBS experiments. The results are shown in Table 2.1. The ratio of ACRIM I to ACRIM II is 1.002069 with linear detrending of the slowly-degrading Nimbus7/ERB results. The Nimbus7/ERB experiment does not have a degradation calibration capability, and linear detrending can only approximate the effects of degradation on the comparison results. The uncertainties of the results in Table 2.1 therefore include some systematic errors and, as such, represent an upper limit for the backup overlap strategy. The statistical uncertainty of 10 ppm demonstrates the ability of the “overlap strategy” to produce high precision even when the comparison experiments are not optimized for the purpose.

The overlap strategy employing flight-tested ambient temperature TSI radiometers is the only approach currently available capable of sustaining the long-term climate TSI database with the precision required. A sensibly conservative overlap requires launch of an EOS/ACRIM experiment at the earliest possible time, now 1999, which will be in the eighth year of the UARS/ACRIM II experiment and near the end of SOHO/VIRGO’s third year.

The EOS/ACRIM experiment uses the ACRIM technology flown successfully on NASA’s SMM, UARS, Spacelab 1, and ATLAS missions. Two approaches to the EOS implementation of ACRIM observations appropri-

ate to the “mission-of-opportunity” status are under consideration. The basic philosophy of both is the use of inexpensive instrumentation made from commercial parts. The required five-year EOS data-segment lifetime reliability is achieved through the deployment of redundant instruments. The new, compact form of the ACRIM sensor assembly can be mated with small-satellite technology to construct a dedicated ACRIM satellite, or flown as secondary payloads on other satellites of opportunity using derated versions of compact, flight-proven gimbals for solar pointing.

The ACRIM implementation plan involves the initial launch of two ACRIM instruments as secondary payloads. Following intercomparisons on orbit, one will be used as the primary TSI monitor and the second held in reserve. Upon failure of the primary instrument, the reserve will assume that role, and another ACRIM will be deployed at the earliest opportunity to replace the reserve function. The first two ACRIMs can be on orbit within 24 months of project startup, enhancing the possibility of implementing the overlap strategy with the UARS/ACRIM II experiment during its extended mission and the SOHO/VIRGO experiment prior to the end of its two-year minimum mission. The series of ACRIMs proposed would provide overlapping satellite TSI observations throughout the EOS mission.

2.2.2 Role of radiation fluxes in the climate system

The climate system is a heat engine that is driven by the spatial and temporal displacement of the entry and exit of broadband radiant energy. A net flow of radiant energy at the top of the atmosphere enters the tropics and leaves at high latitudes. The resulting equator-to-pole heating gradient drives the circulations of the atmosphere and ocean. The largest fraction of radiant energy entering the climate system is absorbed at the surface in the form of solar radiation, but leaves from the atmosphere in the form of thermal infrared emission. This radiative heating below and cooling above drives the convective activity of the troposphere, resulting in abundant rainfall and cleansing

TABLE 2.1

<i>DATA</i>	<i>POLYNOMIAL FIT (DEGREE)</i>	<i>RATIO ACRIM I/ACRIM II</i>	<i>STANDARD ERROR (PPM)*</i>
Original Data	0	1.001890	13
Detrended Data	1	1.002069	10

* 1 sigma error

Ratio of SMM/ACRIM I and UARS/ACRIM II results constructed using mutual intercomparisons with the Nimbus7/ERB experiment. Demonstration of the backup capability of the overlap strategy for preserving the precision of the total solar irradiance database.

of the atmosphere. The general circulation and the hydrological cycle are maintained in their current states partly by the requirements of thermodynamic balance, whereby they transport and store heat, transporting energy from the point of absorption to the point of emission to space. The main processes for cycling energy by radiation, wind, and latent heating interact on a wide range of scales, from boundary-layer turbulence with scales of less than a meter to the large-scale components of atmospheric circulation with dimensions of 10^7 meters.

Radiation is the primary forcing of climate change; anthropogenic radiative forcing by changes in trace gases, aerosols, and surface optical properties is on the scale of decades; astronomical radiative forcing (Milankovitch orbital variations) is on the slower scale of the ice ages. Radiation is important for climate feedback. It is widely acknowledged that uncertainties in the radiative feedback to climate by clouds pose the most formidable obstacle to climate prediction by general circulation models (GCMs). The strong coupling of radiative and hydrological processes and the general importance of this coupling in environmental prediction has led to development of the complex Global Energy and Water Cycle Experiment (GEWEX) by the World Climate Research Program. The GEWEX Radiation Panel oversees a wide range of international activities involving satellite and surface measurements and modeling.

Pre-EOS satellite sensors have observed radiation in various narrow bands for remote-sensing applications and in the broadband shortwave (SW, solar wavelengths) and longwave (LW, thermal infrared) to monitor the ERB at the top of the atmosphere (TOA). The newer EOS sensors have more spectral coverage, a larger number of independent channels, and greater calibration accuracy. Further advances in our understanding of the role of radiative fluxes in climate can be expected from EOS implementation through:

- 1) simultaneous measurement of different quantities by multiple instruments to provide a more-complete picture of the Earth system and facilitate a more-comprehensive understanding;
- 2) synergistic integration of pairs of instruments to improve the accuracy of the retrieval for individual parameters;
- 3) commitment to a 15-year time series of observations, which is long enough to resolve some modes of natural interannual variability;

- 4) modeling and analysis within Interdisciplinary Science (IDS) investigations to provide scientific guidance for the prioritization of remote sensing, apply EOS satellite products to critical science questions, and apply ancillary data to improve the accuracy of EOS remote sensing and supply additional observables; and
- 5) a readily-accessible EOS Data and Information System (EOSDIS) for producing and distributing EOS data, precursor satellite data sets, and critical aircraft and in situ data.

2.2.2.1 Atmospheric and surface radiative fluxes and heating

Advances in thermodynamics, electromagnetic theory, and physical chemistry permitted Arrhenius (1896) to predict a global warming associated with increasing concentrations of CO_2 , because increased carbon dioxide would inhibit the upward radiative transfer of energy from the surface to space. Modern climate models have consistently indicated that CO_2 and other anthropogenic trace gases will change the vertical distribution of radiative fluxes in the atmospheric column so as to warm the troposphere and cool the stratosphere. These global model results are consistent with those of one-dimensional radiative-convective (RC) models, which demonstrate the large radiative forcing of the climate system by clouds and trace gases (Manabe and Wetherald 1967). Sellers (1969) and Budyko (1969) devised other simple climate models that focused on surface radiation and quantified a highly significant ice-albedo feedback mechanism. The potential significance of cloud-climate feedback was found to be very large in other low-order model studies (Paltridge 1980; Charlock 1981, 1982; Wang et al. 1981), and it remains such in state-of-the-art global climate models (GCMs) (e.g., Mitchell 1993a, b). The climate response to a given radiative forcing is still not reliably predictable because GCMs, which do not convincingly simulate clouds (Rossow et al. 1991) and their relation to TOA radiation (Barkstrom et al. 1989), are sensitive to uncertain radiative feedbacks, especially due to clouds (Cess et al. 1991). There have been fairly good simulations of transient temperature variations due to the radiative forcing of the 1991 Pinatubo volcanic eruption (Hansen et al. 1994) and even to the 1963 Agung eruption. However, see Hansen et al. (1978), and see also Chapter 8.

The simulation of the atmospheric circulation and climate requires an adequate vertical profile of diabatic heating (e.g., Hartmann et al. 1984), including radiation and latent heating. Surface fluxes are important for studies of ocean circulation and heat transport (e.g., Liu et al.

1994). Table 2.2 shows annually-averaged Earth Radiation Budget Experiment (ERBE) results (Harrison et al. 1990) for TOA SW and LW radiation and present estimates for surface radiation (Gupta et al. 1995) based on International Satellite Cloud Climatology Project (ISCCP) data. Confidence in the TOA results is tempered by the ~5 Wm⁻² discrepancy between the SW and LW results in Table 2.2; this may be due to ERBE angular modeling (Green and Hinton 1996). The surface radiative fluxes in Table 2.2 have errors that are probably larger than the errors at the TOA (see also Kiehl and Trenberth 1997).

2.2.2.2 Absorption, scattering, and emission by gases
 Atmospheric gases have a greater effect on the climate than any other component of the Earth’s climate system. It is estimated that absorption of infrared radiation by atmospheric gases reduces the escaping longwave radiation by about 120 Wm⁻², whereas the reflection of solar radiation by clouds and the surface each return only about 50 Wm⁻² to space, when globally averaged. Emission and absorption of terrestrial thermal infrared energy by vibrational and rotational transitions in gases generate the so-called clear-sky greenhouse effect; H₂O, CO₂, and O₃ are the primary agents, with significant impact by CH₄, N₂O, and CFCs. In Figure 2.2, the calculated spectral distributions of downwelling longwave radiation for tropical and subarctic atmospheres under clear skies indicate two distinct wavelength regimes. At wavelengths less than 8 mm and greater than 12 mm, the atmosphere is opaque, mostly because of absorption by H₂O and CO₂; so that the downward longwave radiation follows the blackbody emission curve for a temperature close to that of the surface. Strongly-absorbed thermal wavelengths are useful for satellite sounding at altitudes well above the surface. Electronic transitions of gaseous molecules induce considerable absorption of the incoming solar energy, most of the atmospheric absorption in Table 2.2, for example. In Figure 2.3, the calculated spectral distribution of

downwelling solar radiation at the tropical surface under clear skies is shown for a solar zenith angle of 60°. Solar energy at wavelengths below 0.5 mm is strongly absorbed by O₃ and scattered by all molecules. The attenuation in Figure 2.3 between 0.5 and 0.8 mm is mostly due to scattering, though there is some absorption by O₂ and H₂O. Absorption by H₂O dominates the attenuation above 0.8 mm, and CO₂ also absorbs above 2.5 mm.

The two principal contributions that EOS can make in the area of absorption and emission by atmospheric gases are:

- 1) production of more-accurate vertical profiles and time histories of water vapor and other radiatively active gases; and
- 2) validation of the radiative transfer physics for natural and anthropogenic gases.

Because of the enormous importance of H₂O to both radiative and hydrological processes, it is retrieved by several EOS sensors, as described in Section 2.2.4.

The Measurements of Pollution in the Troposphere (MOPITT) instrument will provide CH₄ retrievals on EOS AM-1. This will be useful for careful budget studies of the radiative effect of anthropogenic trace gases. After 2000, retrievals of the radiatively significant species O₃, H₂O, CH₄, N₂O, and CFCs will be made by the High-Resolution Dynamics Limb Sounder (HIRDLS) in the upper troposphere and above; these are needed for studies of the secular trend in radiation near the tropopause and for the stratospheric radiation budget. The Microwave Limb Sounder (MLS) will also measure H₂O, O₃, and N₂O in the upper troposphere and is unique in providing data which are not degraded by cirrus. The Tropospheric Emission Spectrometer (TES) will cover most infrared active species from the surface to the lower stratosphere.

TABLE 2.2

SHORTWAVE		LONGWAVE		NET	
Incoming TOA Flux	341				
Absorbed TOA Flux	239	TOA OLR	235	Net TOA	+4*
Surface Insolation	184	Surface Downward	348		
Surface Absorbed	160	Surface Cooling	47	Net Surface	+113
Absorbed in Atmosphere	79	Atmosphere Cooling	188	Net Atmosphere	-109

* Net TOA radiation is a measure of ERBE estimate error, and is probably close to zero in reality.

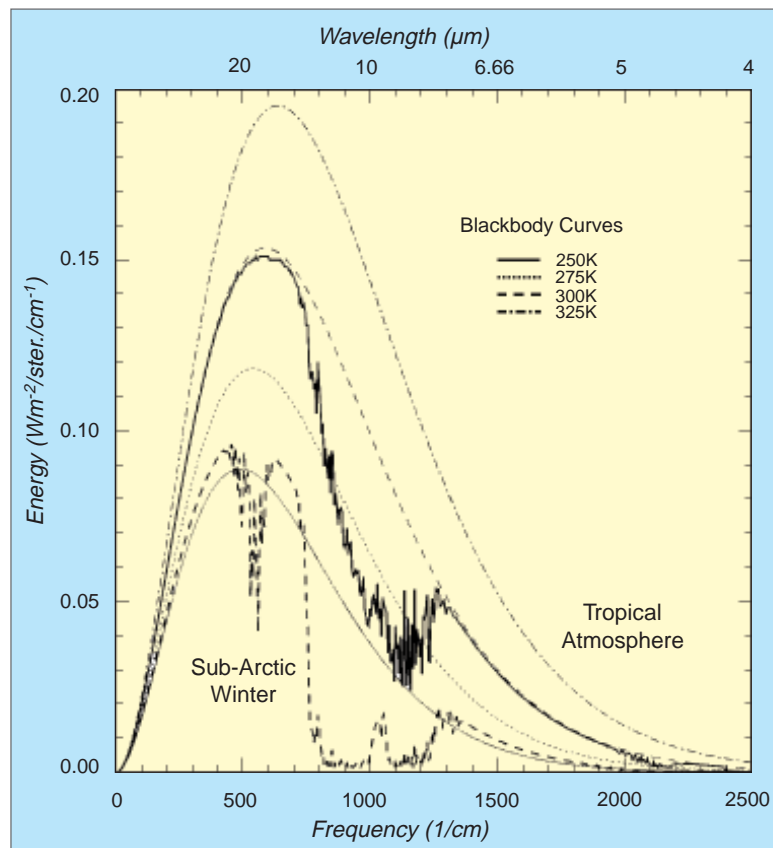
Radiation budget at surface and top of atmosphere (TOA) for February 1985 to January 1989. Units are Wm⁻². TOA values are ERBE estimates, and surface estimates are from surface radiation budget (SRB) calculations (Gupta et al. 1996). Atmospheric heating rates are calculated as residuals from the TOA and surface estimates.

The large spread of broadband radiative fluxes in the Intercomparison of Radiative Codes for Climate Models (ICRCCM) studies (e.g., Ellingson et al. 1991) clearly shows that the problem of calculating such fluxes for a given distribution of gases still exists. There are particular uncertainties in regard to the H₂O continuum. The Atmospheric Radiation Measurement (ARM) program is providing data for a continuation of ICRCCM at high spectral resolution. The Atmospheric Infrared Sounder (AIRS) and especially TES can make significant contributions to the extension of ICRCCM by issuing radiance data sets that can be used as a testbed for radiative transfer codes. The Clouds and the Earth's Radiant Energy System (CERES) will observe the net effect of all radiatively active constituents including gases at the TOA. CERES will also attempt retrievals of the radiation budget throughout the atmospheric column; this will constitute a time series of the greenhouse effect.

2.2.2.3 Absorption, scattering, and emission from aerosols

Aerosols have both direct and indirect radiative effects on the climate system; both effects constitute the largest uncertainties in the anthropogenic radiative forcing of climate. The direct effect is the scattering and absorption of solar energy by aerosols, which are composed mainly of insoluble dust, hydrocarbons, and hydrophilic particles. The direct optical effects are mainly due to aerosols with radii of a few tenths of a micrometer. The global aerosol optical thickness in the LW radiation is quite small, and aerosols usually make only a small contribution to the greenhouse effect. The direct radiative forcing of tropospheric aerosol is highly regional. Anthropogenic sulfate aerosols mostly scatter SW radiation and cool the climate; the global optical depth of sulfate aerosol is only roughly inferred from budgets of sulfur gases (e.g., Charlson et al. 1991). Soot from industrial areas can absorb strongly and induce heating; however, we lack both accurate budgets for the soot and reliable calculations for its small

FIGURE 2.2



Calculated spectral distributions of downwelling longwave radiation for tropical and subarctic atmospheres under clear skies. Blackbody curves for various temperatures are shown for reference.

optical impact (Penner et al. 1994). Natural and anthropogenic biomass burning produces huge quantities of smoke and may have a global cooling effect of 0.2 to 2 Wm⁻². The 1994 Intergovernmental Panel on Climate Change (IPCC) estimate of the direct radiative forcing of anthropogenic aerosols is small but uncertain. This uncertainty will remain large until: 1) a more-sophisticated surface-based network is in place to monitor the aerosol and radiative fluxes; and 2) EOS sensors like the Moderate Resolution Imaging Spectroradiometer (MODIS), the Multi-angle Imaging Spectroradiometer (MISR), the Earth Observing Scanning Polarimeter (EOSP), and CERES can be combined with outputs from such a network to produce more reliable estimates of the global amount and radiative forcing of aerosols.

Measurements of aerosols and their effects on the climate system are discussed more fully in Chapter 8 of this Plan, "Volcanoes and the Climate Effects of Aerosols."

2.2.2.4 Absorption, scattering, and emission from clouds

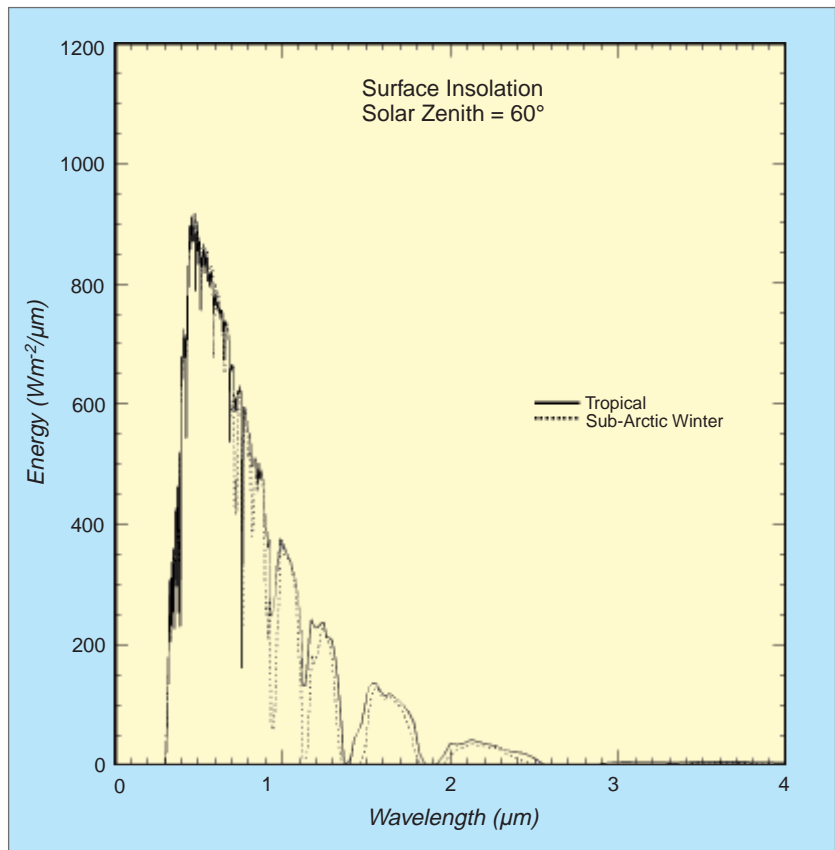
In terms of the radiative forcing of natural constituents, the effect of clouds on climate is second only to greenhouse gases, although it has been argued that the uncertainty in cloud radiative forcing and feedback is larger than that for greenhouse gases (Cess et al. 1991). The uncertainty posed by cloud-radiative feedback to climate has been widely recognized as a key problem in climate prediction. The cloud forcing has been observed by ERBE (Ramanathan et al. 1989; Harrison et al. 1990) at the TOA. The ISCCP of the World Climate Research Program (WCRP) (Rossow and Schiffer 1991) has striven to provide estimates of cloud areas, cloud top heights, and cloud visible optical thickness based on an analysis of operational narrowband meteorological imagers. Estimating the radiative effects of clouds and retrieving cloud properties from space both require a detailed understanding of the scattering and absorption properties of clouds. Important problems remain in the directional scattering of solar radiation by realistic clouds, the radiative effects of the overlap of cloud fragments, and perhaps even in the basic absorption properties of cloudy atmospheres.

A debate on the net SW radiation absorbed by the atmosphere, perhaps founded on different interpretations of the few available in situ atmospheric radiation measurements, is in progress. Cess et al. (1996), Ramanathan et al. (1995), and Pilewskie and Valero (1995) contend that clouds increase the absorption of SW of the atmospheric column by 25-40 Wm^{-2} , resulting in a corresponding error in the present global SW budget of the atmosphere and surface. However, global surveys by Li et al. (1995) and Whitlock et al. (1995) imply that the SW budget of the atmosphere is correct to within 10-15 Wm^{-2} ; measurements by Hayasaka et al. (1995) and theoretical calculations by Chou et al. (1995) do not support the “anomalous” SW

absorption by clouds, either. EOS will have improved retrievals of radiatively active constituents (gases, aerosols, clouds, surfaces) and TOA fluxes, and it has excellent prospects for generating accurate fluxes of surface radiation and usable estimates for vertical profiles of radiation, particularly through combined use of satellite and in situ data.

The CERES record of radiation fluxes and cloud forcing will surpass ERBE in accuracy and in its ability to accurately estimate the radiative forcing by clouds. CERES will use multi-angle sampling for its broadband scanner and incorporate MODIS-based cloud and surface scene identifications for the development of angular distribution models. The development of such angular distribution models is needed to accurately measure the albedo of the planet. The solar radiance reflected from a particular region depends on the angle from which the region is viewed and the position of the sun. To estimate albedo, an angular distribution model is needed to relate measurements at particular angles to a total reflected short-

FIGURE 2.3



Calculated surface insolation as a function of wavelength under clear conditions for tropical and subarctic conditions.

wave flux integrated over all angles. The present ERBE record reveals a shortcoming in our understanding of directional reflection of solar radiation in that the estimated albedo shows a spurious dependence on satellite viewing angle. The directional aspects of cloud radiation will be investigated with MISR, which has a higher resolution than CERES. EOSP will also provide cloud optical thickness and phase. Cloud particle phase is important radiatively, for both remote sensing and for the energy budget, because liquid water and ice scatter radiation quite differently. MISR retrievals of the absorbing properties of aerosol will be needed as inputs to radiative transfer simulations of cloud SW absorption. An important aspect of EOS observations of clouds and radiation fluxes is the relatively long, homogenous, 15-18 year record that is its goal. Such a long homogenous record would allow seasonal and interannual variability to be adequately sampled and used to understand connections within the climate system that only appear on longer time scales, such as the El Niño-Southern Oscillation (ENSO) and decadal variabilities that are known to exist (e.g., Rasmusson and Wallace 1983; Deser and Blackmon 1993).

Landsat-based studies have shown that small-scale cloud structure causes systematic errors in the retrieval of cloud area with moderate-resolution instruments like Advanced Very High Resolution Radiometer (AVHRR), Visible and Infrared Scanner (VIRS), and even MODIS (Wielicki and Parker 1992). The same small-scale structure influences the broadband TOA albedo of cloudy regions (Cahalan et al. 1995). Plane parallel radiative transfer calculations with the “independent pixel” approximation show that when a homogeneous cloud field and an inhomogeneous cloud field present the same TOA albedo to space, the total atmospheric absorption for the inhomogeneous field is usually slightly larger. These problems will be addressed in detail with EOS AM-1 data, which will have the high-resolution Advanced Spaceborne Thermal Emission and Reflection Radiometer (ASTER), as well as MODIS, MISR, and CERES. The first-generation CERES IDS products will test the ability of plane parallel radiative transfer physics and MODIS cloud property retrievals to match the observed CERES instrument broadband TOA flux. The resolution of some discrepancies at TOA is expected to require advances in 3-D radiative transfer modeling and in the retrieval of cloud microphysical parameters as well as cloud geometry.

Cloud vertical structure poses another barrier to the attempt in EOS to retrieve the full vertical profile of radiation within the atmosphere. This is illustrated in Figure 2.4 where the cloud forcing to the global atmospheric LW cooling rate has been calculated with ISCCP cloud, temperature, and humidity data, and the Wang et al. (1991)

radiative transfer code. The mean LW cooling rate of the troposphere is roughly 2 K day^{-1} , and clouds obviously have an enormous impact in the LW, inducing more cooling in some regions and significant relative heating in others. In the left panel of Figure 2.4, it is assumed that the ISCCP clouds do not overlap. In the right panel of Figure 2.4, the cloud forcing difference for the randomly overlapped minus nonoverlapping clouds is shown; it is dramatic and spans roughly a full quarter of the cloud forcing range. Both random overlapping clouds and nonoverlapping clouds show the same picture to the operational LW radiometers used by ISCCP. EOS will begin to resolve the cloud overlap and cloud geometrical thickness dilemma by using combinations of passive sensors such as:

- MODIS and Advanced Microwave Scanning Radiometer (AMSR-E) sensors over ocean (e.g., MODIS will sense optically-thick ice clouds, while AMSR-E will detect underlying water clouds),
- MODIS and AIRS longwave sensors (e.g., for optically-thin cirrus over extensive low water clouds), and
- MISR multi-angle stereo views of broken and isolated cloud fields.

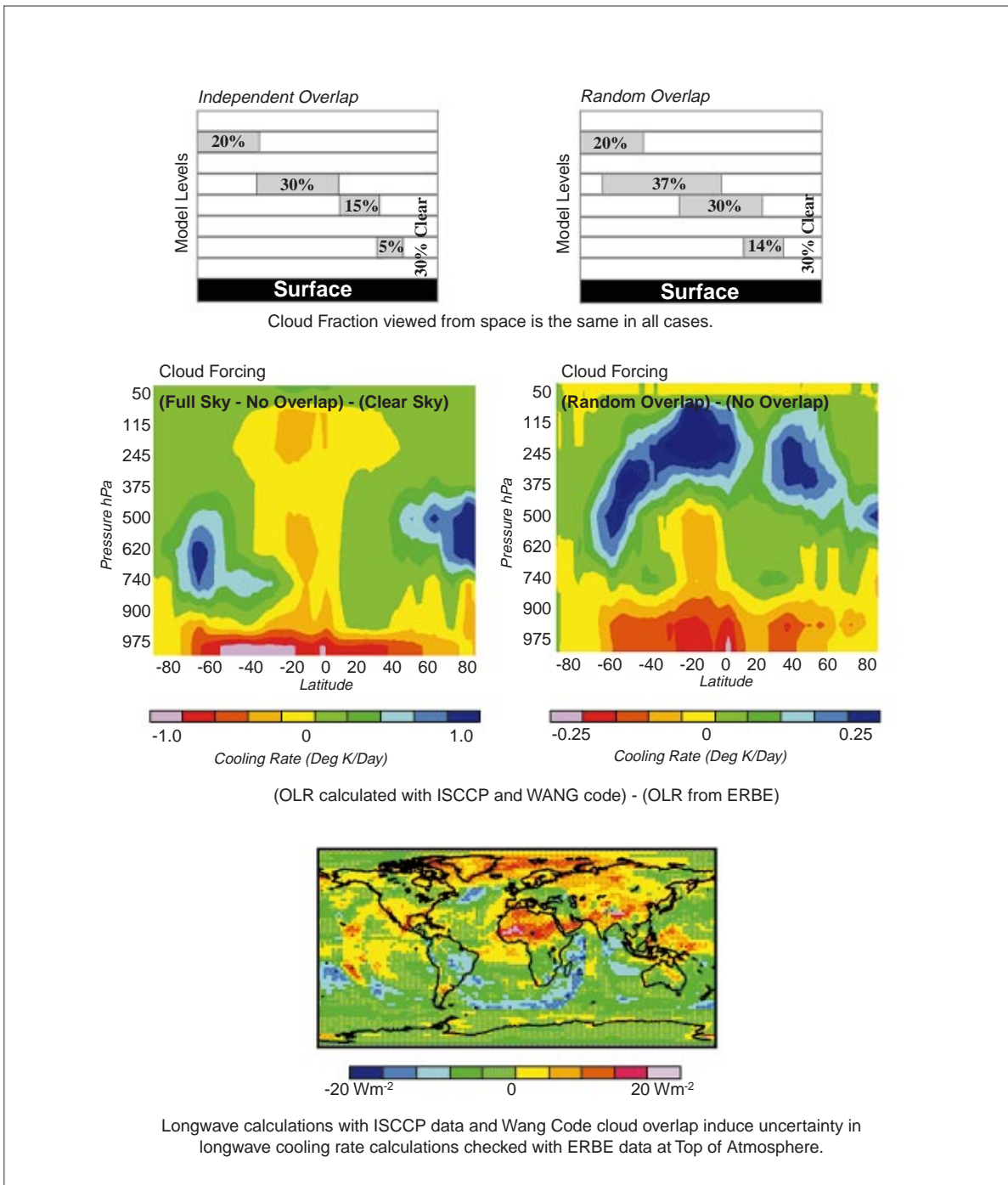
Active sensors have the best prospects for determining cloud geometry. Unfortunately, the sampling of the EOS Geoscience Laser Altimeter System (GLAS) lidar will be limited to nadir. GLAS can determine the geometrical thickness of optically thin clouds. The GLAS record of cloud top height will be a vital tool for evaluating the accuracy of cloud retrievals from passive sensors. A complete resolution of the problem posed by Figure 2.4 may require that a new type of instrument be flown on satellites, the Cloud Profiling Radar (CPR), which can detect the vertical distribution of cloud-size particles.

More-detailed plans for observing cloud properties are presented in Section 2.2.3.5.

2.2.2.5 *Absorption, scattering, and emission by the Earth's surface*

Table 2.2 shows that the surface absorbs about twice as much solar radiation as does the atmospheric column. Surface solar absorption is modulated by a surface solar albedo that ranges from 0.06 for diffuse radiation striking the ocean to approximately 0.90 for some of the freshest snow. Upward and downward LW fluxes at the surface are larger than any other radiative fluxes in the atmosphere, but their sum, the net LW flux, is generally not as large as surface SW net flux. Retrievals of surface fluxes by the

FIGURE 2.4



Effect of cloud overlap assumptions on longwave cooling in the atmosphere (Charlock and Rose 1994).

ongoing GEWEX Surface Radiation Budget (SRB) Project (Whitlock et al. 1995) are probably accurate to within 10-20 Wm^{-2} for a monthly average in the $280 \times 280\text{-km}^2$ equivalent-area grid boxes of ISCCP.

The SRB Project errors for SW and LW over snow and ice surfaces and for LW in persistently cloudy regions are larger than those in other regions. Both ERBE and ISCCP have difficulty distinguishing between low clouds and a snow-covered surface. Higher accuracy is needed from EOS to monitor secular trends in snow and ice albedo associated with global warming and to test this important feedback mechanism in GCMs; Groisman et al. (1994) describe a 10% decrease in the coverage of Northern Hemisphere seasonal snow during the past two decades. A similar problem is faced over sea ice; more-accurate surface radiation measurements are needed to develop models and monitor trends.

The surface albedo and radiative fluxes over snow-free land are not known to sufficient accuracy, either. Surface optical properties have been adequately determined with localized, in situ measurements in the First ISLSCP Field Experiment (FIFE) (e.g., Sellers and Hall 1992). The formation of the GEWEX Continental-Scale International Project (GCIP) is partly due to the fact that numerical weather prediction (NWP) is hampered by the limitations of parameterizations for surface hydrology, and one key to the improvement of the Soil-Vegetation-Atmosphere Transfer (SVAT) model or the Simple Biosphere (SiB) model systems is a more-accurate SRB. Over a typical land surface, the surface albedos retrieved by two satellite systems (using either different instruments or different algorithms) differ by a few percent. A change in land use or crop pattern would also induce a difference of a few percent; a change in regional climate can be forced by perturbing the surface albedo by the same magnitude. Until EOS determines the surface albedo of all land surfaces to greater accuracy, we cannot adequately quantify the radiative forcing to climate that is associated with changes in land use. The uncertainty to climate prediction posed by anthropogenic surface albedo forcing is anticipated to be regional. This problem will be best treated in tandem with the related issue of anthropogenic surface hydrological forcing (i.e., changes in evapotranspiration associated with land use; Shuttleworth and Dickinson 1989).

A more-accurate SRB is also needed for the development and validation of ocean modeling, wherein the surface energy budget is a key forcing to circulation (see also discussion in Chapter 3). The limiting factor on the SRB over the oceans provided by EOS will be due to downwelling LW over the extratropics, where downwelling LW from cloud bases is only slightly masked

by sub-cloud water vapor. The retrieval in EOS of downwelling LW over the oceans could be improved with a few ocean-based monitoring stations for SRB and cloud base height. If aerosol sun photometers were deployed at the same monitoring stations, EOS could validate retrievals of maritime aerosols. A satellite-based cloud radar would enable cloud base heights to be determined, which would greatly improve estimates of net longwave radiation at the surface.

The EOS AM-1 platform is well suited to provide a more-accurate SRB. The keys to implementation involve the deployment of field measurements before and after launch and integration of multiple EOS sensors. Present satellite-based retrievals of the SW SRB are limited by inadequacies in cloud screening (which will be handled by MODIS), quantification of aerosol optical properties (MODIS for scattering properties and MISR for absorbing and scattering properties), and specification of the directional characteristics of radiation throughout the spectrum (CERES and MISR). For monitoring secular trends, stable and broadband spectral coverage of an ERB sensor like CERES is essential. Climate is forced by broadband energy. Imager channels can be expected to change frequencies with time, so the monitoring of spectrally-dependent features like aerosol and surface scattering will not be fully consistent without an integration over the broadband. The retrieval of global land-surface radiation with MODIS, MISR, and CERES will be buttressed by ASTER, the space-borne "microscope," and by in situ monitoring of surface and atmospheric properties. ASTER will permit the reliable identification of a small subset of the global surface that is observed twice daily by MODIS and CERES at coarser resolution.

The surface information from the Pathfinder land program will prepare the research community to apply EOS data. (The EOS Program Office at NASA Headquarters has initiated the Pathfinder data set concept. Pathfinders provide access to large remote-sensing data sets applicable to global change research prior to the availability of data from the EOS satellites. Landsat data, held primarily by USGS/EDC, have been analyzed with support from NASA, EPA, and USGS.) The successful development of models for biospheric processes is dependent on an accurate specification of surface radiation parameters. Individually, the MODIS, MISR, CERES, and ASTER algorithms for surface remote sensing are on generally sound footing. The limited prelaunch exercises by each of the instrument teams have not, however, focused on the potential synergism of the instruments. A common focus of field programs on a very limited set of sites, preferably with continuous monitoring, would foster synergism. The same sites could serve for the validation

of EOS. The most obvious candidate is presently the ARM Southern Great Plains (SGP) site. Atmospheric measurement is thorough at the SGP site, especially during the ARM Intensive Observing Periods (IOPs), affording an excellent opportunity for space-based surface remote sensing. When the atmosphere is well characterized, it can be more reliably “subtracted.” The preparation and validation of EOS surface products would be advanced with in situ determinations of surface optical properties at the same sites. The in situ measurement of surface optical properties is the cornerstone of effective cooperation of EOS radiation programs with ARM and GCIP. Well-determined surface optics would provide a validation for the EOS remote sensing of the surface; the same surface optics provide ARM and GCIP with the means to “subtract” the surface and reliably specify the properties of the large fraction of the clouds that are optically thin. For the ASTER archive, a record at the ARM and the Baseline Surface Radiation Network (BSRN) sites is a must. A desert monitoring site is also suggested because of the unique optical properties of arid regions (i.e., nonblack surface LW emissivity); note the large discrepancy in Figure 2.4 between observed and calculated Outgoing Longwave Radiation (OLR) over the Sahara Desert, which is mostly cloudless.

2.2.2.6 Radiation in global climate models

The most general goal of the USGCRP is the development of global models for climate prediction. EOS will supply the global validation for the models, and theory indicates that radiation is the most critical component of the models and observations. The main radiative uncertainties are cloud feedback, water vapor feedback, direct and indirect forcing by anthropogenic aerosols, surface albedo feedback over land (snow and vegetation) and sea (sea ice), and anthropogenic surface albedo forcing (land use). Radiation and hydrology are closely linked through their shared dependence on water and energy cycles. Some of the main issues in the application of EOS to the task of improving the radiation in climate models can be highlighted by comparing a present model to satellite data. Focus will be placed on LW because it is less directional than SW and easier to both observe and calculate. In Figure 2.5, the OLR from the GEOS Data Assimilation System (Schubert et al. 1995; essentially a GCM run with analyzed meteorological data) is compared with ERBE data. The differences are huge, of opposite sign in the tropics and midlatitudes, and due mostly to cloud deficiencies. The right panel of Figure 2.5 compares a recalculation of OLR with the Wang et al. (1991) code using GEOS soundings but with observed ISCCP clouds.

While the OLR calculated with ISCCP is not perfect (note “rings” at the edge of coverage for the geostationary satellites used by ISCCP), the satellite clouds produce a more-accurate regional OLR than does the GCM. Many other models in the Atmospheric Model Intercomparison Project (AMIP) (Gates 1993) perform similarly to GEOS, when compared with satellite data. It should be noted that the GEOS fields of geopotential height, temperature, and wind compare very well with available observations. Therefore, a major challenge for EOS is to make models assimilate and predict cloud, water vapor, and radiation data as well as they currently do temperature, pressure, and wind data.

What about the modeled greenhouse effect inside the atmosphere? Figure 2.6 shows the difference between the LW heating rates in GEOS and those recalculated using the ISCCP clouds. To span the differences in the LW heating rate, scientists have been forced to use a span of 3.0 K day⁻¹ (−1.5 to 1.5). In contrast, the mean LW heating rate (not shown) is approximately 2.0 K day⁻¹ with a span of 4.0 K day⁻¹ (−4 to 0). The probable error in the profile of the atmospheric greenhouse heating rates in the GCM has a span of 75% compared with the full range in the natural profile of the atmospheric greenhouse heating rates. GEOS does not use the Wang et al. (1991) code, but the differences due to the radiative transfer codes are fairly small. Most of the differences are due to clouds, and they greatly exceed estimates for error in the satellite clouds (i.e., nonoverlapping and randomly overlapping clouds in Figure 2.4).

There is clearly an important task in the application of EOS data to building better radiation simulations in climate models. In the comparison with the GEOS model and ERBE, better clouds are needed than in present models (Figure 2.5 and 2.6). Thought experiments (Figure 2.4) and comparisons with ERBE (the rings in the right panel of Figure 2.5) show that the clouds in present ISCCP observations need improvement, too. EOS PM-1 has a number of instruments to observe the state variables that generate clouds (AIRS, the Advanced Microwave Sounding Unit [AMSU], and the Humidity Sounder, Brazil [HSB]), cloud properties (MODIS and AMSR), and cloud-induced radiation (CERES). Implementing GCM radiation validation with EOS is straightforward: produce quality products from EOS AM-1 and EOS PM-1, get the data to the Distributed Active Archive Centers (DAACs), and have the IDS teams lead the way in utilizing the data in climate models. Fostering the development of better GCM parameterizations for radiation and cloudiness is an important mission of several EOS IDS investigations.

2.2.3 Role of convection and clouds in climate

Clouds have a strong effect on the radiative energy fluxes in the atmosphere. They scatter and absorb solar radiation, and absorb and emit terrestrial radiation, and these effects have a strong influence on the energy balances at the TOA, within the atmosphere, and at the surface. In addition, the vertical motions that are associated with clouds produce important convective transports of energy and moisture. The large-scale, mesoscale, and microscale interactions of clouds with the clear environment around them play a critical role in determining both the amount of water vapor that is retained in the clear atmosphere, and the amount of precipitation reaching the surface.

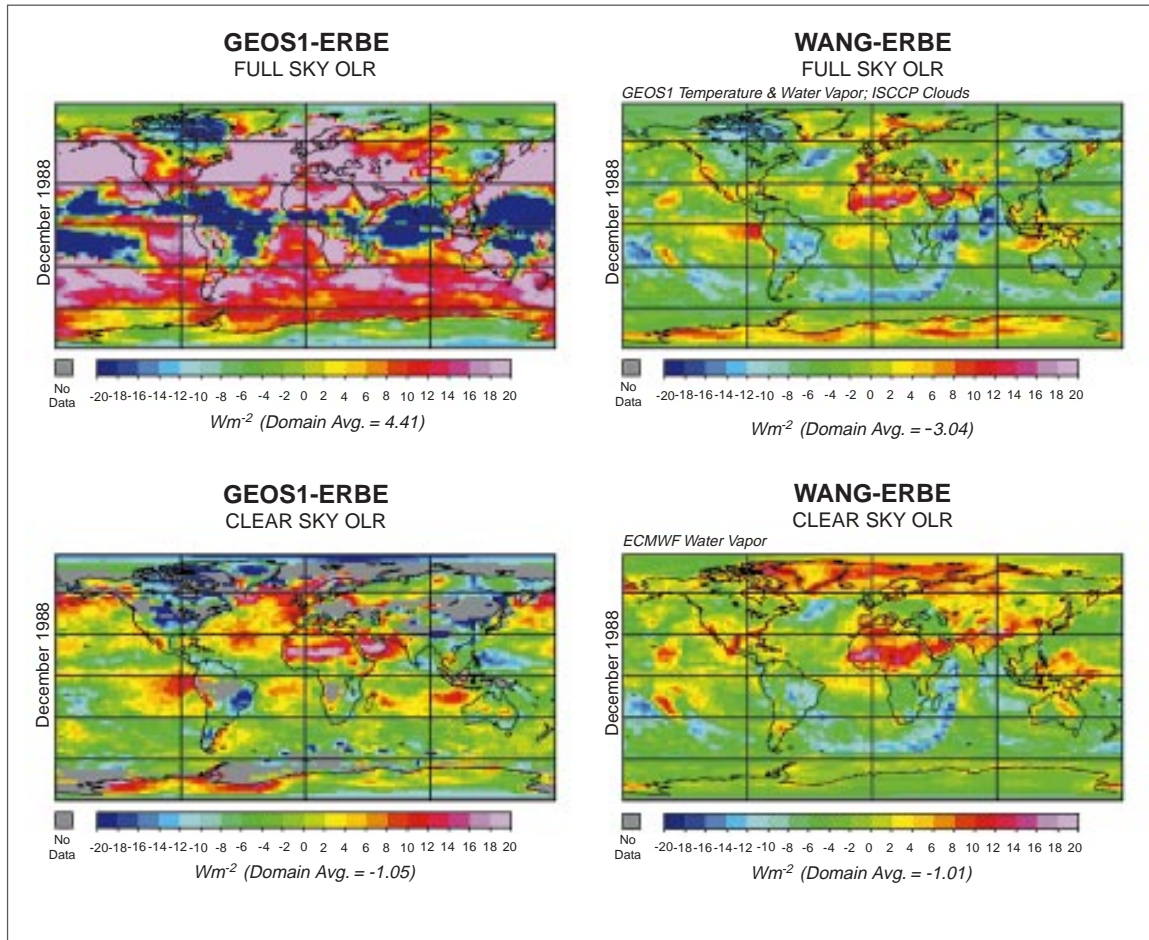
2.2.3.1 Cloud effects on the Earth's energy balance

The Earth's global radiation budget is illustrated in Figure 2.7 (pg. 59). Averaged over the globe and over a year,

about 340 Wm^{-2} of incident SW radiation is available from the sun. Of this, 30%, or about 100 Wm^{-2} , is reflected back to space, so that the climate system accepts 240 Wm^{-2} from the sun which, under equilibrium conditions, is equal to the LW emission to space by the climate system. The influence of clouds on the radiation balance of the Earth was estimated by ERBE (ERBE; Ramanathan et al. 1989; Harrison et al. 1990). These estimates revealed that if clouds were suddenly removed, and nothing else changed, the absorbed solar radiation would increase by about 50 Wm^{-2} and the emitted longwave radiation would increase by about 30 Wm^{-2} , yielding a net positive change in the energy balance of the Earth of about 20 Wm^{-2} (Table 2.3, pg. 59).

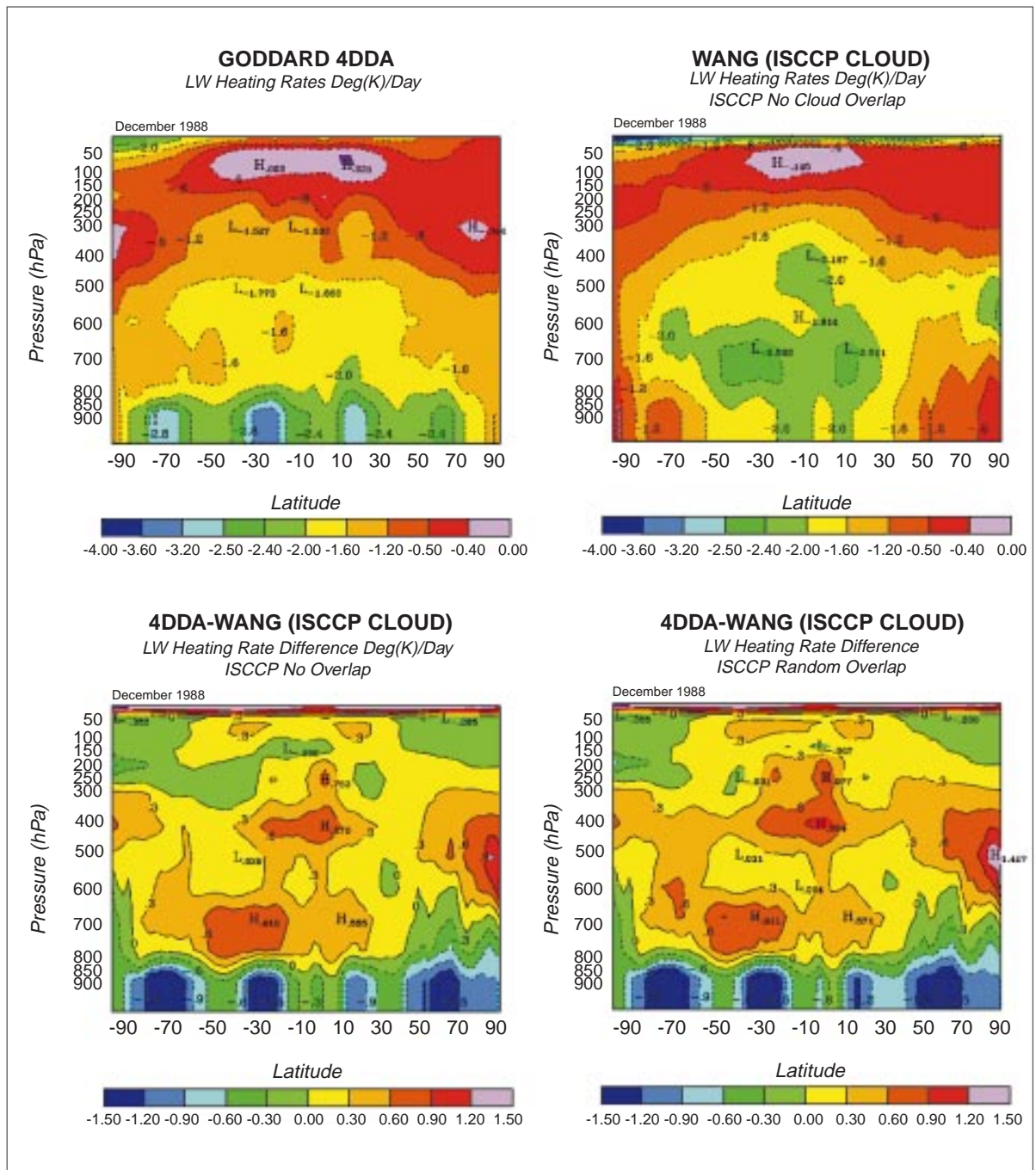
A convenient means of gauging the magnitude of a climate forcing such as that associated with the radiative effect of clouds is to compare it with the calculated

FIGURE 2.5



Comparison of outgoing longwave radiation in the GEOS data assimilation and in ERBE observations (Schubert et al. 1995; essentially a GCM run with analyzed meteorological data).

FIGURE 2.6



Comparison of longwave heating rates in the GEOS data assimilation product and estimates derived from ISCCP data (Charlock et al. 1994).

effect of a doubling of atmospheric CO₂. If the CO₂ concentration is instantaneously doubled, emission by the climate system is reduced by roughly 4 Wm⁻², or about 1.7% (Houghton et al. 1990), because of the increased greenhouse effect. This 4 Wm⁻² radiative imbalance would induce a time-dependent climate change, ultimately resulting in a new equilibrium climate. If it is simplistically assumed that climate change involves solely temperature changes, then the Earth would warm until radiative balance is achieved. That is, the LW emission must increase from 236 to 240 Wm⁻², which requires an increase in emission temperature of 1.2 K, or about 0.4% of its globally-averaged value of 288 K. Current GCMs produce a greater warming at the surface than this, but estimated warmings vary greatly from model to model, ranging from 1.7 to 5.4 K (Houghton et al. 1990). This disagreement stems from the different depictions of climate feedback mechanisms in GCMs that can either amplify or moderate the warming. For example, a warmer climate means a warmer troposphere that will contain more water vapor, which itself is a greenhouse gas. Thus water vapor provides a positive (amplifying) feedback mechanism. An intercomparison of 19 GCMs (Cess et al. 1990) showed the models to be in remarkable agreement regarding water-vapor feedback, though this does not guarantee that this assessment of the water-vapor feedback is correct (e.g., Lindzen 1990).

A common misconception is that because clouds cool the present climate, they will likewise act to moderate global warming. It is, however, the change in net cloud radiative forcing associated with a change in climate that governs cloud feedback. Cess et al. (1990) have shown that calculations of this cloud feedback vary widely from one global climate model to another, and that this feedback explains a substantial fraction of the variance in climate sensitivity in a sample of 19 global climate models.

2.2.3.2 *Cloud effects on the surface energy balance*

Since the clear atmosphere absorbs much of the same frequencies of solar radiation that are absorbed by clouds, the effect of clouds is a redistribution of solar heating in the atmosphere and, through the scattering of radiation by clouds, a reduction in absorbed solar radiation at the surface. Because the atmosphere is fairly opaque to terrestrial radiation, the reduction of emitted longwave radiation caused by clouds is felt mostly as reduced cooling of the atmosphere, except at high latitudes or altitudes where the water vapor content of the atmosphere is small. Therefore clouds represent a redistribution of energy between the surface and the atmosphere that may be larger

than the net effect of clouds on the energy balance measured at the top of the atmosphere. The convection with which clouds are associated is also of first-order importance in the exchange of heat between the surface and the atmosphere, so that more than radiation is involved in understanding the role of convection and clouds in the energy balance at the surface. The detailed physical and radiative properties of clouds are important, which in turn are related to the mechanisms that generate them and the environment in which they are found.

2.2.3.3 *Observations of cloud properties*

2.2.3.3.1 *Surface observations*

A nearly-global record of cloud observations by surface observers is available from surface weather observations (Warren et al. 1986, 1988). These data provide a longer record than that available from satellite observations, and also provide a wealth of information about the morphology of cloud systems observed over the Earth. The bottom-up view of surface observers is complementary to the top-down view from satellites. The cloud typing based on human visual observations of clouds provides valuable information on cloud genesis mechanisms and associated atmospheric structure. On the other hand, surface observations of clouds do not provide the quantitative information on radiative effects, drop size and phase, and cloud top structure that are recoverable from satellite-based observations.

Long records of surface observations of clouds show trends that may be related to corresponding decadal changes in sea surface temperature (SST). Long records of cloud observations can also be used in conjunction with upper-air observations from balloons to investigate the relationship of particular cloud types to atmospheric structure (e.g., Klein and Hartmann 1993b, Klein et al. 1995). Figure 2.8 (pg. 60) shows the trend in SST and low marine cloud amount for the period between 1952 and 1981 as determined from surface observations (Norris and Leovy 1994). Significant decadal trends over the oceans are observed in both SST and marine cloudiness. To evaluate the importance of such trends for climate requires detailed observations of cloud optical properties such as will be made available by EOS. To observe decadal changes such as these, an initial observing period of 15-18 years has been planned for EOS.

Observations of clouds by surface remote sensing and aircraft instrumentation are necessary to investigate mesoscale and microscale aspects of cloud development and interaction with the large-scale environment.

2.2.3.3.2 Satellite observations

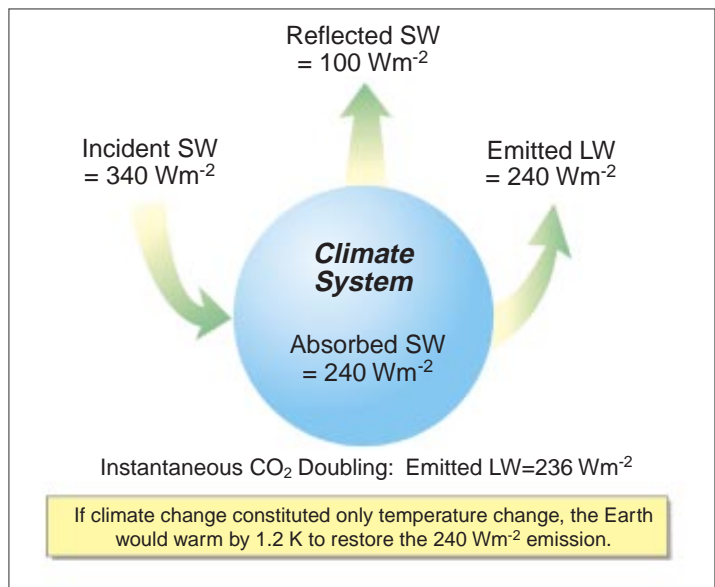
Satellites provide a means of developing global observations of cloud amounts and properties. The ISCCP attempts to take advantage of the visible and infrared information available from operational meteorological satellites to construct a climatology and time series of the abundance of clouds with optical depth and cloud top pressures paired into 35 categories, in three-hour intervals of time. These data are extremely valuable in characterizing global cloud coverage and type in a variety of other studies.

The greater spatial and spectral resolution from visible and infrared imagers that are part of the EOS program will allow clouds to be characterized from space more accurately and in greater detail. A key instrument in this regard is MODIS. MODIS offers spatial resolution as fine as 250 meters from some channels, which will reduce errors associated with partially-filled fields of view. MODIS will provide more-accurate, better-calibrated retrievals for cloud area, height, and optical thickness, and will further retrieve cloud particle size and phase, and estimate the cloud geometrical thickness (especially when combined with AMSR-E). MISR and EOSP will also contribute new information on cloud phase and particle size spectra. Distinguishing between cloud particle size and water amount contributions to cloud albedo is critical to monitoring and understanding key cloud forcing and feedback processes. The improvement in cloud sensing by EOS will be aided by the more-accurate EOS soundings of temperature and humidity from AIRS/AMSU/HSB.

2.2.3.4 Modeling of clouds in the climate system

The representation of clouds in climate models in a manner that accurately expresses their effect on climate and climate sensitivity is a critical goal of EOS. To this end

FIGURE 2.7



Schematic illustration of the Earth's radiative energy balance and how a doubling of atmospheric carbon dioxide would perturb that balance (Wielicki et al. 1995. Reproduced with permission from the American Meteorological Society).

EOS observations will be incorporated in the validation and testing of numerical models that simulate clouds. A substantial amount of work will be done within EOS IDS investigations, but the EOS data will be useful to the entire climate and cloud modeling community. Because of the large difference between the scales of individual cloud systems and the size of the Earth, cloud modeling is currently conducted on three scales. The first scale is that of the global climate model. While the whole planet is included, as it must be in a climate simulation and prediction, and the model may be integrated for 100 years or more, the grid points used to represent the climate are separated by a horizontal distance of about 100 km, and cloud processes must be represented implicitly through a so-called "parameterization." Cloud parameterizations in global models can be validated in two ways. In climate models the seasonal means and other statistics of cloud proper-

TABLE 2.3

	AVERAGE CONDITIONS	CLOUD-FREE CONDITIONS	CLOUD RADIATIVE FORCING
OLR	235	266	31
Absorbed Solar	239	288	-49
Net Radiation	4	22	-18

Global-annual-average conditions of top-of-atmosphere fluxes for average conditions, for clear-sky conditions, and cloud radiative forcing estimated from ERBE (Harrison et al. 1992). Units are Wm^{-2} .

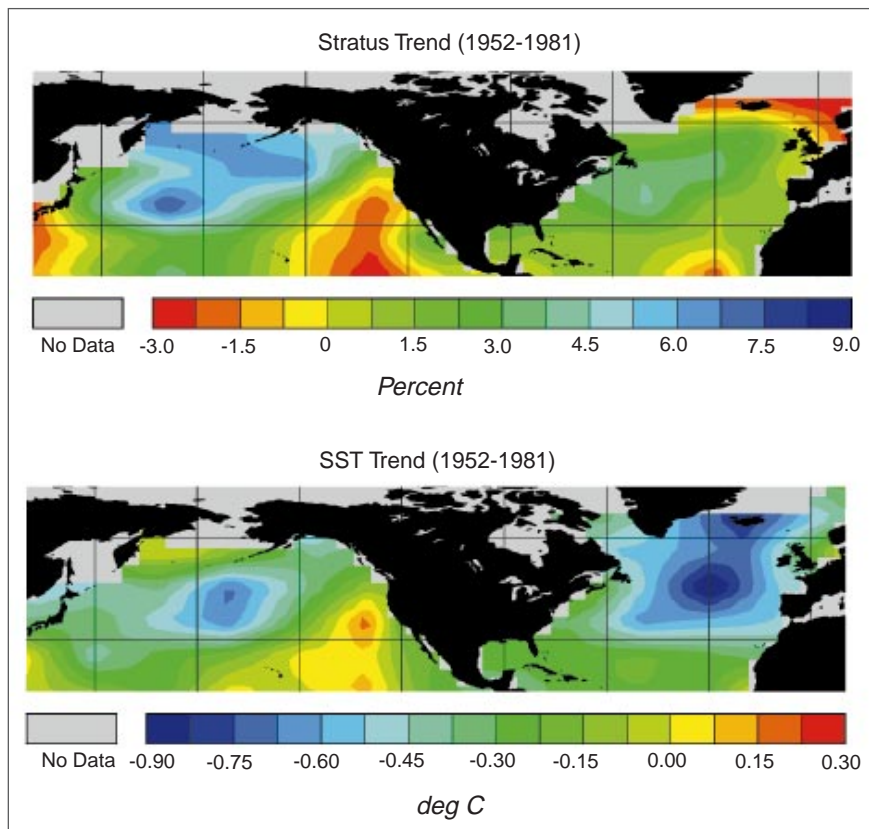
ties can be verified against similar statistics derived from observations. In weather forecast models, the day-to-day evolution of cloud properties can be verified against instantaneous observations. Both methods are useful and give different insights into the quality of the model simulation of clouds and water vapor. If a regional mesoscale model that represents only a part of the Earth is used, current computer technology will allow increasing the spatial resolution by a factor of 10 to about 10 km, but such models are normally run for no longer than a few weeks. A regional model can represent the mesoscale circulations that often develop in association with cloud systems, but the cloud-scale processes must still be parameterized. A cloud-resolving model requires a horizontal grid spacing of about 1 km or less, and only a small geographical region, perhaps incorporating only a single cloud, can be simulated with current computers. To make progress on the cloud problem, EOS investigations will pursue cloud modeling in each of these three categories: global, regional, and cloud-resolving models (Figure 2.9). EOS observations will provide data for validation on all of these horizontal scales, and for both instantaneous and

climatological comparisons. When EOS observations are coupled with in situ and ground-based observations and a rigorous program of numerical experimentation, the observations will offer the promise of a qualitative enhancement of our confidence in our ability to predict the role of clouds in global climate change, and thereby a refinement in our ability to predict future climate changes in response to natural and human influences. Numerical weather forecasting and seasonal and interannual forecasting will also benefit from this program of observation and research.

2.2.3.4.1 Global climate models—cloud parameterization and role in sensitivity

The history of prevailing opinion about the sensitivity of the Earth's climate to external perturbations roughly parallels that of developments in the parameterization of clouds in global climate models. The earliest GCMs assumed a fixed distribution of clouds and predicted modest equilibrium climate sensitivity. The advent of GCM cloud parameterizations resulted in generally higher estimates of sensitivity (Hansen et al. 1984; Washington and Meehl

FIGURE 2.8



Trends in SST and marine cloudiness (Adapted from Norris and Leovy 1994).

1984; Wetherald and Manabe 1986; Wilson and Mitchell 1987) for several reasons.

The most surprising result from these and later GCMs is the tendency of cloud cover to decrease with warming, especially low and middle clouds. To date, no theoretical basis for predicting the sign of cloud-cover feedback has emerged. This cloud-cover decrease, combined with the better-understood tendency of cloud height (and thus greenhouse effect) to increase with warming, caused the majority of GCMs from this period to predict net positive cloud feedback. Early parameterizations prescribed cloud optical properties, typically assuming decreasing albedo or optical thickness with increasing altitude. Increased cloud height then implies that column optical thickness decreases with warming, thus producing large positive cloud feedback.

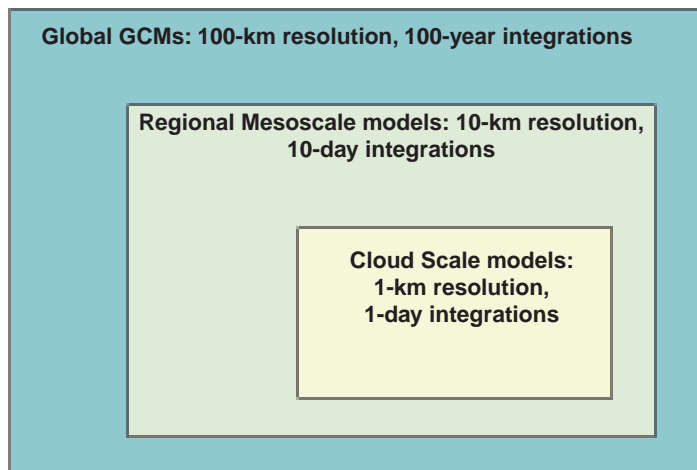
Radiative-convective models (Somerville and Remer 1984), based on observations of increasing cloud liquid water with temperature (Feigelson 1978), suggested that climate sensitivity might be halved if cloud optical thickness variations were taken into account. This has been incorporated diagnostically in some GCMs via a calculation of the adiabatic water content of a lifted cloud (Betts and Harshvardhan 1987) or the condensation required to remove supersaturation. An assumption about cloud particle effective radius is also needed. Since the albedo effect dominates the greenhouse effect of clouds globally, such models tend to produce negative cloud optics feedback and thus reduced sensitivity (cf., GCMs described in Appendices A and B of Cess et al. 1990).

The recent trend in GCMs has been to include cloud water as a prognostic variable, permitting fully interactive optical thickness calculations (Sundqvist 1978; Roeckner et al. 1987; Smith 1990; LeTreut and Li 1991; Tiedtke 1993; Fowler et al. 1996; Del Genio et al. 1996). This requires parameterization of a variety of poorly understood microphysical and small-scale dynamical processes (e.g., autoconversion, accretion, evaporation, Bergeron-Findeisen growth, cumulus detrainment, cloud top entrainment instability). Depending on how these details are represented, GCMs with prognostic parameterizations can produce either positive or negative cloud optics feedback. Uncertainties in the details of prognostic schemes, combined with the fact that some GCMs still prescribe optical properties or diagnose their temperature dependence, largely explain the persistent wide

range of GCM estimates of equilibrium climate sensitivity to a doubling of carbon dioxide (1.7-5.4 K). A critical goal of EOS is to incorporate more-detailed global observations of cloud liquid water and ice contents, cloud particle size, and the spatial and temporal distribution of cloud into a better understanding of how these properties depend on the climate, and to translate this into better models for climate predictions on a variety of time scales from weather forecasting to decadal climate change.

Climate sensitivity and cloud feedback depend on the nature of the climate change experiment that is performed. Prescribed uniform SST changes are a simple, inexpensive test of sensitivity (Cess et al. 1990). Recent intercomparisons of such experiments involving many GCMs indicate a significant convergence of results im-

FIGURE 2.9



Schematic diagram of the three types of models, including clouds.

plying small cloud feedback (Cess et al. 1996). But these simulations are not representative of an actual climate change, in which SST gradients can change because of regionally-varying climate forcing, changes in ocean circulation, etc. The same model can produce either small negative or large positive cloud feedbacks depending on the presence or absence of changes in SST gradients, because feedbacks are inherently regional and interactions with the dynamics affect climatic changes in cloud properties (Senior and Mitchell 1993; Del Genio et al. 1996).

Prognostic cloud parameterizations are of most interest to EOS, since they are laboratories for assessing which uncertain aspects of clouds should be focused on by future observational programs. Among the first-order questions faced by climate modelers are: What controls the detrainment of ice from cumulus updrafts into

mesoscale cirrus anvil clouds, and thus determines their shortwave reflectance? What causes the transition from nearly overcast marine stratus to scattered trade cumulus off the west coasts of continents in the subtropics, and is this indicative of a climate feedback mechanism? Why do satellite data suggest that low clouds generally get optically thinner with increasing temperature (Tselioudis et al. 1992)? Why do GCMs characteristically underpredict cloud forcing in the midlatitude storm tracks, thus compromising simulations of ocean heat transport (Gleckler et al. 1995)? What role do cloud interactions with sea ice play in determining the degree of polar amplification of climate warming? How large are the indirect effects of changes in tropospheric aerosols on cloud properties? How can small-scale cloud inhomogeneities be accounted for in relating grid-scale cloud water path to cloud albedo and emissivity? How can cloud cover be parameterized as a function of grid-scale climate parameters?

The cloud type that appears to exert the greatest effect on climate sensitivity in state-of-the-art GCMs is the tropical mesoscale anvil cloud that accompanies cumulus convection (Heymsfield and Donner 1990; Del Genio et al. 1996). The central question is how to represent the detrainment of ice from cumulus updrafts into anvil clouds. EOS observations can contribute to the answer in two ways:

- 1) By characterizing the microphysical and radiative properties of anvil clouds. CERES will provide the net radiative effect of anvils at the TOA. The liquid water path (LWP) of these clouds can be estimated by AMSR. Anvils are thought to be largely ice though, so microwave techniques for estimating ice water path from scattering at high frequencies must be pursued as a high priority by EOS. The scattering properties of ice clouds are not yet well defined; MISR will help constrain the phase function for anvil clouds while MODIS will estimate particle sizes and optical thicknesses. The same instruments will characterize these properties for the more ubiquitous and poorly understood thin cirrus that exist at all latitudes. Stratiform precipitation, the major water sink for anvils, will be measured by AMSR-E as well.
- 2) By relating anvil properties to convection strength. Direct measurements of vertical velocities are not possible, but the Lightning Imaging Sensor (LIS) lightning occurrence measurements will serve as an index of convection intensity, while AIRS temperature and moisture profiles will yield estimates of convective available potential energy.

Subtropical marine stratus and trade cumulus clouds are important to climate models not only as a source of cloud feedback but also as a key deficiency that causes climate drift in coupled ocean-atmosphere GCMs. A central question about these clouds is the reality of the ISCCP finding that the optical thickness of low clouds over ocean tends to decrease with temperature (Tselioudis et al. 1992). MODIS, with better than an order-of-magnitude higher resolution than ISCCP, should determine whether subpixel cloudiness variations contribute at all to this result. AMSR-E LWP data will provide corroborating information on larger spatial scales.

A related question for GCMs is how to translate grid-scale predicted cloud water content into cloud albedo, given small-scale inhomogeneities. The 250-m resolution of MODIS is sufficient to capture the most important scales of inhomogeneity (cf., Wielicki and Parker 1992), permitting optical thickness probability density functions to be characterized for different cloud types. This combined with MODIS particle-size estimates will help define parameterizations for albedo as a function of LWP.

Another particle-size issue is the poorly-defined indirect effects of aerosols on clouds, both the radiative effect of smaller droplets and the suppression of drizzle (Charlson et al. 1992). EOSP and MISR will define the tropospheric aerosol distribution, which can be combined with MODIS optical thickness and particle size to isolate the indirect radiative effect. In principle, AMSR can complement this by measuring drizzle rates for stratus, but current microwave algorithms are insensitive to light precipitation.

A key decision in GCMs is when to form liquid water vs. ice. Phase information is currently lacking on a global scale; field studies suggest that it is not simply temperature-dependent, but may be sensitive to cloud dynamics, age, etc. The altitude of transition from liquid to ice affects cloud feedback because of the different microphysical characteristics of liquid and ice (cf., Mitchell et al. 1989; Li and LeTreut 1992) and the unique physics of the mixed-phase region (Del Genio et al. 1996). EOSP is sensitive to cloud-top phase because of the different angular distributions of polarization of liquid and ice particles. MODIS can also discriminate phase via the different spectral dependences of liquid and ice absorption.

2.2.3.4.2 Regional mesoscale modeling of clouds

Many atmospheric circulations are organized on the mesoscale, which is defined as encompassing horizontal length scales of 20-200 km (Fujita 1984). An example of paramount importance for climate is mesoscale convective systems, which dominate weather over most of the

tropics and the summertime midwestern United States, throwing out cirrus anvils whose feedback on climate has been a subject of intense controversy (e.g., Ramanathan and Collins 1991; Wallace 1992; Fu et al. 1992; Hartmann and Michelsen 1993; Lau et al. 1994). Severe midlatitude cyclones, hurricanes, orographically-forced flow, fronts, and thermally-forced flows such as land/sea breezes are other examples of mesoscale organization. These circulations produce distinctive cloud features on the mesoscale. Ubiquitous cloud types such as boundary-layer stratocumulus and midlatitude cirrus clouds also show strong mesoscale patterning that affects the mean radiative impact of the cloud. Understanding the feedbacks between clouds, the associated mesoscale circulation patterns, and climate is a particularly challenging, important, and poorly-understood problem because of the range of length scales involved. Typically, processes inside the cloud involve circulations 1 km or less in size, and the mesoscale circulations evolve as part of atmospheric flow patterns thousands of kilometers across. Thus, our understanding of those aspects of the feedback between clouds and climate that are modulated by mesoscale processes is particularly rudimentary.

In the past decade, mesoscale models (MMs) have become a powerful tool for understanding and forecasting mesoscale atmospheric circulations. Examples of MMs widely used in this country include the National Center for Atmospheric Research (NCAR)/Pennsylvania State University (PSU) mesoscale model or MM5 (Grell et al. 1993) and the Colorado State University Regional Atmospheric Modeling System (RAMS). An MM is typically used to simulate a region 1000 km or more on a side with a horizontal resolution of 5-40 km and a vertical resolution of 1 km or less, and is typically used for time intervals of 24-72 hours. Usually, the boundary conditions for a simulation are taken from analyses generated by a larger-scale numerical model. Often, grid nesting is used to increase resolution in regions of particular interest or flow complexity. A mesoscale model typically includes a parameterization for cumulus convection. Other model physics may vary greatly in complexity depending on the model and the problem being investigated. For simulations of organized cumulus convection, models such as the MM5 and RAMS include cloud water and ice physics parameterizations similar to cumulus ensemble models (see below). A typical MM includes terrain-following coordinates and sophisticated land and ocean surface parameterizations. Recent MMs are nonhydrostatic and allow the user to embed a small region of particularly-fine mesh refinement as a cloud ensemble model.

Mesoscale models have very successfully simulated a variety of complex weather phenomena, including rapidly-deepening midlatitude cyclones, squall lines and their interaction with fronts, hurricanes, topographic damping, and trapped waves on inversions. Many of these phenomena depend on cloud processes, especially deep convection. The feedbacks can be quite subtle. Braun and Houze (1994) showed that improvements in the ice-physics parameterization of the MM5 made a substantial improvement to the longevity of a simulated squall line and completely changed its feedback on the large scale. Changes in the choice of cumulus parameterization can suppress the development of a hurricane. However, few studies have focused on applying MMs to the radiative impact of clouds or to the forecasting of cloud properties. In the coming decade, we foresee an exciting opportunity for using MMs to apply knowledge gained from small-scale models and observations of clouds to understand the climatically-important feedbacks between clouds and the larger-scale circulation systems in which they are embedded.

The increased use of MMs has particular promise in the following four areas:

1) *Tropical convection*

MMs have been successfully used to study severe midlatitude organized convection, which generally takes place in a highly conditionally-unstable environment in which a synoptic-scale weather system acts as a trigger to locally initiate convection. However, MMs have only just begun to be applied to the enormous regions of convection over the tropical west Pacific, over the ITCZs, and the monsoonal convection over the tropical land masses, even though this convection is predominantly organized on the mesoscale. Recent work done within an EOS IDS investigation has shown that the MM5 can simulate many important mesoscale features of tropical convection observed in the Tropical Ocean Global Atmosphere (TOGA)/Coupled Ocean-Atmosphere Response Experiment (COARE) experiment, such as the development of boundary-layer cold pools driven by convective downdrafts, the triggering of new convection at cold pool edges, and the degree of the localization of convection over the warmest water (Chen 1996). In the future, the optical properties of the modeled cirrus anvils will be compared with observations. MMs could be used in the future for climate-sensitivity studies, similar to cumulus ensemble models (CEMs) but using a larger domain, and for simulations of other parts of the tropics, such as the East Pacific and Central America, in which mesoscale

variability of convection can interact with mesoscale variability of surface characteristics and topography.

2) *Cirrus cloud evolution*

Cirrus cloud has a crucial radiative impact on the atmosphere, but it is perhaps the most difficult to model of all cloud types because it is very thin, its modeling is dependent on microphysical assumptions such as ice crystal size distribution, and because it is patchy, both due to the internal convective circulations that cause the cirrus fallstreaks often seen on a summer day (Houze 1993) and due to the large-scale circulations that maintain cirrus cloud. As part of NASA's First ISCCP Regional Experiment (FIRE) program, Cotton and coworkers (DeMott et al 1994; Harrington et al. 1995) have begun to forecast midlatitude cirrus cloud using the RAMS mesoscale model coupled to a sophisticated parameterization of cirrus microphysics, with moderate success. The evolution of tropical cirrus clouds, which start as anvils from Mesoscale Convective Systems (MCS), is of paramount importance to tropical-cloud climate interactions, but so far has not been investigated with an MM (DeMott et al. 1994; Harrington et al 1995).

3) *Midlatitude cyclonic cloud systems*

Persistent boundary-layer cloud over the summertime midlatitude oceans produces by far the strongest net cloud radiative forcing of any cloud type (e.g., Hartmann et al. 1992; Klein and Hartmann 1993b). However, both our observational and theoretical understanding of this cloud is rudimentary compared to subtropical stratocumulus cloud, which forms over cold upwelled water off the west coast of the major continents. The subtropical cloud forms in a relatively synoptically-steady regime of equatorward winds blowing from cold to warm water, in a region of strong mean subsidence. The midlatitude cloud forms in a much more synoptically-variable regime, making it much harder to interpret the observations. Mesoscale modeling of the boundary-layer evolution induced by passing synoptic-scale systems could help gain more insight into how this cloud is maintained.

4) *Boundary-layer fog and cloud prediction*

In coastal locations such as San Francisco or Los Angeles, the summertime weather is highly dependent on the inland penetration of air and cloud from the marine boundary layer. There is a strong diurnal cycle of cloud caused mainly by the strong daytime heating; the albedo of the cloud affects this heating cycle so that the clouds and circulations are strongly coupled. Ballard et al. (1991) used an MM for forecasting cloud and visibility on and near the coast of Scotland. A difficulty with such simula-

tions (and with mesoscale simulations of boundary-layer cloud in general) is the need to start with cloud in the initial conditions to achieve a realistic forecast, because cloud-topped boundary layers are typically strongly forced by cloud-top longwave radiative cooling (Lilly 1968). However, as representations of the interactions between boundary cloud, turbulence, and radiation in MMs improve, they should provide increased insight into both the weather and climate of coastal zones.

While mesoscale models have achieved popularity as a tool for understanding severe weather events, which often involve clouds and convection, their potential for understanding cloud-climate feedbacks still remains largely untapped. Aggressive pursuit of the above four areas should go a long way toward both using this potential and improving forecasts by better representation of cloud processes in mesoscale models. Such studies are being conducted with several EOS IDS investigations. The higher spatial resolution, new cloud variables, and greater accuracy of EOS cloud observations will enable better validation of regional cloud simulations.

2.2.3.4.3 Cloud-scale models

An important class of models that may emerge as a powerful tool for studies of the role of clouds on climate are the cloud-resolving models (also known as cumulus ensemble models [CEMs]). In CEMs cloud-scale dynamics are resolved based on nonhydrostatic governing equations. Subgrid-scale turbulence is included using higher-order closure schemes and latent heating is explicitly computed; therefore, no cumulus parameterization is required. In addition, the budgets of all three phases of water are explicitly computed by parameterized cloud microphysics. For example, the Goddard cumulus ensemble model (CEM) includes a parameterized Kessler-type-two-category scheme for cloud water and rain, and a three-category ice scheme for cloud ice, snow, and hail/graupel (cf., Tao and Soong 1986; Tao and Simpson 1993). The Goddard CEM also includes detailed shortwave and infrared radiation (cf., Chou 1991). CEMs have been used to study the mechanisms of cloud generation, microphysical processes in clouds, interactions and merging of cloud clusters, cloud-environment interactions and trace gas transport (Krueger 1988; Xu and Krueger 1991; Lipps and Hemler 1986). They have been used widely in simulations of convective processes in conjunction with major field experiments, i.e., PRE-STORM, EMEX, MONEX, TAMEX, and TOGA/COARE. Another very important application of CEMs is in the development of hybrid satellite retrieval algorithms for clouds, water vapor, precipitation, and related dynamical quantities such as the vertical profile of latent heating. For example, the Goddard

CEM is the centerpiece of the rainfall and latent heating profile retrieval algorithm for the Tropical Rainfall Measuring Mission (TRMM).

A typical CEM has a spatial resolution of 1-3 km and variable vertical resolution of 0.2-1 km, with finer resolution in the atmospheric boundary layer and coarser resolution in the upper troposphere or lower stratosphere above cloud top. Because of the large computational resources required, three-dimensional versions of CEMs are typically integrated for 24-36 hours over a domain of 500-km squares. For many applications, such as simulating line-type convection or organized mesoscale cloud clusters, two-dimensional versions of the CEMs with a larger domain are often used for economy of computation.

More recently, CEMs have been applied to the study of water and energy cycles within tropical clusters and climate cloud-radiative feedback processes (Lau et al. 1993; Held et al. 1993). Sui et al. (1993) used the Goddard cumulus ensemble model to study the water and energy cycles in tropical convection and their role in the climate system. They documented the importance of stratiform clouds in maintaining the moisture content of the tropical atmosphere. They found that the rate of conversion of ice-phase water into the vapor phase associated with the dissipation of upper-level cirrus clouds contributes to upper-tropospheric moisture about as much as moisture transport from deep convection. In the lower troposphere, the re-evaporation of rainwater and cloud water are the dominant sources of atmospheric moisture. These results will have important consequences regarding the role of stratiform clouds and water vapor in climate feedback processes. More recently, using cumulus ensemble models, Lau et al. (1994) have demonstrated that changes in cloudiness and related cloud radiative forcing are more sensitive to remote forcing due to the large-scale circulation than to the variation of local SST. CEMs have also been coupled to oceanic mixed-layer models to elucidate the mechanisms of diurnal variability of clouds and precipitation over the ocean.

Another potential application of CEMs in climate studies is the nesting of CEMs in MMs and in GCMs. One approach is to use the large-scale conditions generated by coarse resolution GCMs (typically $4^\circ \times 5^\circ$ or $2^\circ \times 2.5^\circ$ latitude-longitude) as a boundary condition to the CEMs. Alternatively, this may be achieved by double nesting between CEMs, MMs, and GCMs. Experimentation with one-way interaction, i.e., using larger models to force CEMs and MMs, has demonstrated some success in documenting the modification of regional convective processes due to climate changes such as deforestation. The nesting of models has the advantage of focusing computational resources only in the region of interest, thus saving un-

necessary calculation. However, the numerical treatment of interactions across the nesting boundaries can be a major problem. The challenge is to include the feedback from the cloud scale and mesoscale to the global-scale climate. Telescoping grids or polar rotations are viable alternatives, but these methods are only in early stages of development. Undoubtedly, the use of nested models will be important for understanding scale interaction between hydrologic systems and climate.

2.2.3.5 *Observational strategy for radiative fluxes and cloud properties*

Observations of net radiative energy fluxes at the top of the atmosphere have proven valuable in understanding the global energy balance, in determining horizontal energy transport by the ocean, and in defining the role of clouds in the energy balance of the Earth. Despite the scientific consensus that cloud-radiation effects strongly regulate ocean temperatures and climate, and despite the acknowledged inadequacy of current simulations of surface radiation by climate models, there currently is very little data on the global climatology of surface radiation fluxes. A global surface radiation climatology data set is a requirement for further advances in understanding the ocean-atmosphere interactions in the climate system, and for development and testing of more-realistic climate models. Efforts to produce such a climatology from satellite measurements are now underway (Li and Leighton 1993; Darnell et al. 1992; Gupta et al. 1992).

If the net radiative energy flux at the TOA is combined with the net radiative energy flux at the Earth's surface, the net atmospheric radiative cooling is obtained. The atmospheric radiative cooling is the net effect of infrared emission by the atmosphere, the absorption by the atmosphere of infrared radiation emitted by the Earth's surface, and the absorption by the atmosphere of solar radiation.

The vertical distribution of radiative cooling/heating inside the atmosphere is also very important. For example, simulations of the climatic effects of increasing carbon dioxide concentrations predict warming of the troposphere and cooling of the stratosphere (e.g., Cess et al. 1993), and there is some empirical evidence for such changes (Houghton et al. 1990). For this reason, measurements of the radiative energy flux at the tropopause are particularly important. Unfortunately, they are almost completely nonexistent. Additional resolution of the vertical structure of the radiative cooling would also be useful, particularly for the troposphere where cloud layers can produce very sharp local features.

In summary, following the TOA radiative flux, the next most valuable measurement would be of the surface

radiative flux, because of its importance for atmosphere-ocean and atmosphere-land interactions. After that, it would be best to obtain the radiative flux at the tropopause. Additional details of the radiative cooling profile within the troposphere would also be useful, but information at more than about 4-to-10 levels might be of marginal utility.

Radiative fluxes are the highest priority measurements necessary to understand the role of cloud feedback mechanisms in the climate system. Current global climate models cannot accurately model even the gross zonal mean seasonal changes in cloud radiative forcing, much less the desired regional effects. In order to improve simulations of cloud forcing and its effect on climate sensitivity, more-detailed measurements of cloud properties are needed to provide understanding and model validation. Wielicki et al. (1995) have suggested that measurements of the following cloud properties be developed to better understand cloud feedbacks and to validate their simulation in global climate models:

- *cloud LWP (or ice water path)*
- *cloud visible optical depth*
- *cloud particle size*
- *cloud particle phase/shape*
- *cloud fractional coverage*
- *cloud temperature/height*
- *cloud infrared emittance*

At least five of these cloud properties can vary independently (optical depth, size, phase, coverage, height). Since TOA SW and LW fluxes represent only two constraints, it must be concluded that GCM agreement with TOA SW and LW fluxes is a necessary, but not sufficient, condition to guarantee correct cloud physics and thereby correct cloud/climate feedback mechanisms.

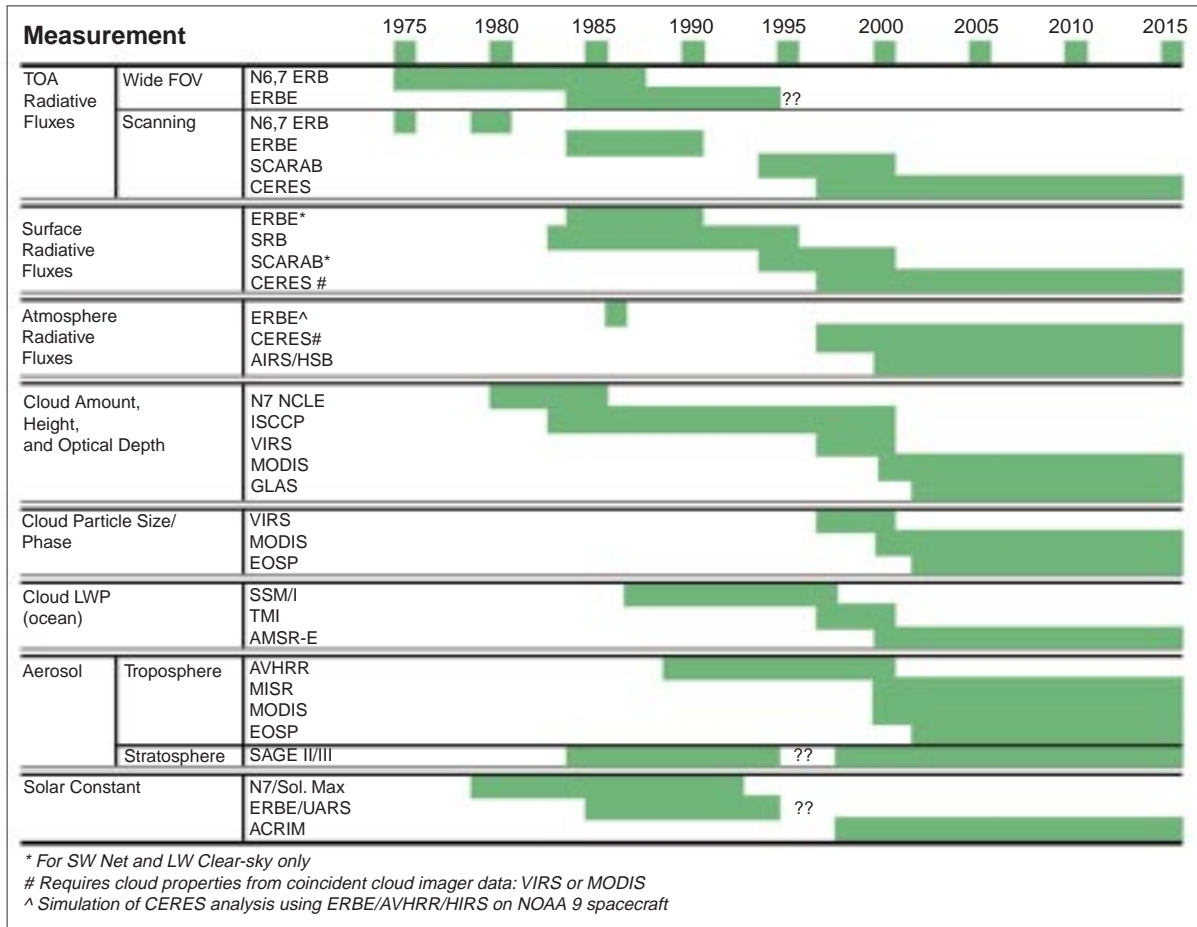
Figure 2.10 shows a timeline of satellite-based global radiation budget and cloud observations from 1975 to 2015. A major improvement in remote sensing capabilities began with the U.S./Japanese TRMM satellite in 1997 and continues with the NASA EOS AM-1 satellite as well as the ESA Environmental Satellite (ENVISAT) starting in 1998. An observational gap is already apparent for scanner-based radiation budget data from ERBE. Fortunately, the French/German/Russian Scanner for Radiation Budget (SCARAB) instrument was launched in December 1993 and should provide overlapping intercalibration with the ERBE nonscanners, which continue to operate. The first SCARAB instrument provided data for 1 year, and a second instrument will launch in 1997. EOS CERES (Wielicki et al. 1996) radiation budget measurements began with TRMM and continue with the EOS AM-1 and

PM-1 sun-synchronous orbits. The CERES measurements will improve the calibration, time sampling, and angular sampling over the earlier ERBE and SCARAB data sets. Cloud observations will be successively improved by VIRS in 1997, and later by MODIS, to be launched on the EOS AM-1 (1999) and PM-1 (2000) satellites. VIRS on TRMM adds improved calibration, spatial resolution (2 km IR), and cloud particle size information (1.6 μm channel) over the current AVHRR and geostationary cloud data sets, and will also provide diurnal sampling from its low-inclination orbit. MODIS adds improved detection of cirrus clouds (CO_2 slicing channels and 1.38- μm channel), improved resolution of boundary-layer cellular cloud fields (250-m-1-km spatial resolution), and improved cloud microphysics for both day and nighttime observations (1.6 and 2.1 μm , day, and 8.5 μm , night).

Table 2.4a summarizes the time and space sampling of the primary global and regional satellite observations for clouds and radiation in three time intervals: past/current, TRMM, and EOS. For the EOS-era observations, instruments are listed by spacecraft orbit. The first EOS AM-1 platform will be launched in 1999 in a sun-synchronous descending orbit at 10:30 a.m. The first EOS PM-1 platform will be launched in 2000 in a sun-synchronous ascending orbit at 1:30 p.m. These measurements are planned to provide a 15-year time series to allow studies of climate processes. The EOS orbits were chosen to optimize measurements of the diurnal cycle, surface land processes, and ocean biological processes. For the critical diurnal cycle of clouds and radiative fluxes, a third precessing orbit is provided by TRMM in 1997-2000, and potentially a TRMM follow-on mission beyond 2000. The ACRIM platform is planned for launch in 1999, the ICESat-1-GLAS platform in 2001, and the European Meteorological Operational Satellite (METOP) platform in 2002.

While Table 2.4a summarizes the major cloud and radiation satellite instruments, there are several instruments shown in Table 2.4b that provide critical supporting data. In general, these supporting instruments sacrifice time or space sampling capabilities in order to achieve additional special measurement capabilities. These capabilities can be used to test assumptions utilized in the global data sets. For example, pixel-beam filling issues and cloud inhomogeneity can be examined using the very-high-spatial-resolution Landsat-7 and ASTER data. Multiple-view-angle solar-reflectance data from Polarization and Directionality of the Earth's Reflectance (POLDER) and MISR can be used to test the assumptions of shortwave anisotropy and to examine non-plane-parallel radiative transfer effects of broken cloud fields. Medium Resolution Imaging Spectrometer

FIGURE 2.1 □



Timeline of the primary global and regional satellite observations for clouds and radiative properties (Wielicki et al. 1995, reproduced with permission from the American Meteorological Society).

(MERIS) and Global Imager (GLI) can provide an early independent method for the determination of daytime cloud height using oxygen A-band absorption of solar reflected radiation. Later observations by the GLAS lidar will provide a more-definitive test of cloud top height using active lidar for both day and night, and allowing better discrimination of multilayer cloud cases such as thin cirrus over low- or middle-level cloud. The Advanced Along Track Scanning Radiometer (AATSR) can test whether the determination of remotely-sensed cloud data is independent of viewing zenith angle. The EOSP measurements can provide an independent estimate of aerosols and cloud microphysics. While these tests do not replace the need for ground- and aircraft-based verification, they have the advantage of allowing tests over a complete range of global climate conditions. Field experiments give the most accurate and complete cloud and radiation data sets,

but for extremely limited time periods and climatic regions. Ultimately, the highest confidence is achieved only through a combination of field experiment data, special local high-resolution data, and global satellite data.

Improvements in global satellite observations of key climate parameters depend critically on two efforts. First, the derivation of advanced remote-sensing algorithms (often called inversion methods) is required to utilize the new measurements provided by EOS. Second, the new data must be rigorously validated against independent surface and aircraft in situ or remote-sensing observations. This section will summarize the state of the art in remote sensing of the key cloud and climate parameters discussed previously. This section will also identify problem areas critical to future advances in remote sensing, data analysis, and validation.

TABLE 2.4A

	<i>PAST AND CURRENT</i>	<i>TIME SPAN</i>	<i>CLOUD AND RADIATION</i>	<i>TIME SAMPLING (EQ. CROSSING, LT) OBSERVATIONS</i>	<i>MONTHLY AVERAGE GRID</i>	<i>NADIR FIELD OF VIEW (KM)</i>	<i>DATA SOURCE</i>
Pre-EOS	N7 ERB	1979-1990	SW, LW fluxes: top of atmosphere	1200	500 km	90; 1000	NSSDC
	N7 NCLE	1979-1990	Cloud amount, height	1200	500 km	8; 60	NSSDC
	HIRS	1989-1993	Cirrus height, emittance	0700, 1400	2.5°	20	NOAA
	ERBE	1984-1995+	SW, LW fluxes: top of atmosphere, cloud forcing	0700, 1400, Preprocessing	2.5°	40; 1000	LaRC V0 DAAC
	ISCCP	1983-1995+	Cloud amount, height, optical depth	Every 3 h	280 km	4-8	LaRC V0 DAAC
	SRB	1983-1995+	SW, LW fluxes: surface	Every 3 h	280 km	4-8	LaRC V0 DAAC
	SSM/I	1987-1995+	Cloud liquid water path (ocean only)	0630, 1630	1.0°	32-55	Wetnet
	SCARAB	1994-1997+	SW, LW fluxes: top of atmosphere	Preprocessing	2.5°	80	CNES/France
TRMM (45°N-45°S)	CERES	1997-2000	SW, LW fluxes: top of atmosphere, surface,* in atmosphere*	Preprocessing	1.0°	10	LaRC V1 DAAC
	VIRS	1997-2000	Cloud amount, height, optical depth, particle size/phase	Preprocessing	1.0°	2	LaRC V1 DAAC
	TMI	1997-2000	Cloud liquid water path (ocean only)	Preprocessing	TBD	4.5-37	TBD

	<i>EOS (PLATFORM INSTRUMENT)</i>	<i>TIME SPAN</i>	<i>CLOUD AND RADIATION</i>	<i>TIME SAMPLING (EQ. CROSSING, LT) OBSERVATIONS</i>	<i>MONTHLY AVERAGE GRID</i>	<i>NADIR FIELD OF VIEW</i>	<i>DATA SOURCE</i>
EOS	AM-CERES	1999-2013	SW, LW fluxes: top of atmosphere, surface,* in atmosphere*	1030	1.0°	20	LaRC V1 DAAC
	AM-MODIS	1999-2013	Cloud amount, height, optical depth, particle size/phase	1030	5 km, 1.0°	0.25-1	GSFC, LaRC
	PM-CERES	2000-2015	SW,LW fluxes: top of atmosphere, surface,* in atmosphere*	1330	1.0°	20	LaRC V1 DAAC

TABLE 2.4A (CONT.)

EOS	EOS (PLATFORM INSTRUMENT)	TIME SPAN	CLOUD AND RADIATION	TIME SAMPLING (EQ. CROSSING, LT) OBSERVATIONS	MONTHLY AVERAGE GRID	NADIR FIELD OF VIEW	DATA SOURCE
	PM-MODIS	2000-2015	Cloud amount, height, optical depth, particle size/phase	1330	5 km, 1.0°	0.25-1	GSFC, LaRC
	PM-AMSR#	2000-2015	Cloud liquid water path (ocean only)	1330-1030	TBD	10-20	TBD
	PM-AIRS/HSB	2000-2015	Temp/water vapor, cloud and surface emissivity	1330	TBD	15	JPL V1 DAAC
	ACRIM	1999-2015	Solar constant	TBD	N/A	N/A	LaRC V1 DAAC
	*Requires both CERES broadband scanner data and cloud imager data for within-atmosphere fluxes, and surface LW fluxes (cloudy). #Also planned for EUMETSAT METOP beginning in 2000 in a 1030 LT sun-synchronous orbit.						

Primary global and regional satellite observations of clouds and radiation in the pre-EOS and EOS era. Satellite data with 1/8 to 2-day coverage, and both day and night observations (*Wielicki et al. 1995, used with permission from the American Meteorological Society*).

TABLE 2.4B

PLATFORM INSTRUMENT	TIME SPAN	CLOUD AND RADIATION OBSERVATIONS	SPECIAL CAPABILITIES	NADIR FIELD OF VIEW	SAMPLING LIMITATIONS	DATA SOURCE
ADEOS 1: POLDER	1996-1999	Narrowband SW cloud anisotropy,	multiangle, polarization	day only, 50% duty	6 km	ESA
Landsat-7	1999-2002	Cloud properties at scales << 1 km	spatial resolution, calibration	1 per 16 days	15-120 m	EDC V1 DAAC
EOS AM: ASTER	1999-2003	Cloud properties at scales << 1 km	spatial, spectral resolution	1 per 48 days	15-90 m	EDC V1 DAAC
EOS AM: MISR	1999-2003	Aerosols, narrowband anisotropy, stereo cloud height	multiangle, calibration	1 per 9 days	200 m, 2 km	LaRC V1 DAAC
ENVISAT: AATSR	1998-2003	Dual-pathlength cloud properties	2-angle views	1 per 5 days	1 km	ESA
ENVISAT: MERIS	1998-2003	Oxygen A-band cloud height	oxygen A-band	day only	1 km	ESA
ADEOS II: AMSR	2000-2002	Cloud liquid water path	spatial resolution	oceans only	5-50 km	NASDA
ADEOS II: GLI	2000-2002	Cloud properties	oxygen A-band	no CO ₂ channels	250 m-1 km	NASDA
ICESat-1: GLAS	2001-2005	Lidar cloud and boundary layer height	active lidar	nadir only	70 m	GSFC V1 DAAC
EOS AM-2: EOSP	2003-2013	Aerosols, ice cloud microphysics	polarization, calibration	day only, large FOV	10 km	LaRC V1 DAAC

Supporting satellite observations of clouds and radiation in the EOS era. Satellite instruments with special capabilities but limited time sampling. Critical for global validation of primary data (*Wielicki et al. 1995, used with permission from the American Meteorological Society*).

2.2.3.5.1 TOA radiative fluxes

The measurement of TOA fluxes will enter its fourth generation with the CERES instruments on the TRMM (Simpson 1988) and EOS AM-1 and PM-1 spacecraft. The most recent ERBE measurements provide the standard of comparison for global radiation data sets. This success was gained through extensive pre-launch work with a science team to: a) oversee instrument design, development, and testing, b) design data products, and c) design analysis algorithms. A final key element was an integrated data management team to execute two versions of the data system before launch. This is the same overall strategy being used by the EOS project for the EOS data products.

Because there is no “ground truth” to test the accuracy of satellite TOA flux estimates, a comprehensive set of internal consistency checks is required to achieve high-quality data (Barkstrom et al. 1989). As a result of the extensive ERBE, Nimbus-3, and Nimbus-7 experience, there is a good understanding of the sources of error in determining TOA radiative fluxes.

In essence, the measurement of TOA fluxes is a 7-dimensional sampling problem: spectral (1), spatial (2), angular (3), and temporal (1). These sampling requirements lead to a measurement strategy with: a broadband instrument (spectral coverage) with cross-track scanning (spatial coverage) plus a scanner that rotates in azimuth (angular sampling) and six observations per day from two sun-synchronous polar orbiters and one medium-inclination orbiter to sample diurnal variations (spatial, temporal, and angular sampling). Error estimates for such a sampling strategy are developed in Wielicki et al. (1995), and are much better than previously achieved. Overall, the CERES measurement errors are expected to be a factor of 2 to 4 lower than ERBE errors. The improvements are expected from three major sources:

- 1) Factor of 2 improvement in instrument calibration by using more-accurate ground and on-board calibration sources.
- 2) Factors of 2-4 improvement in angular sampling errors by the use of the rotating azimuth plane CERES scanner to fully sample angular space, combined with the use of advanced cloud imagers (VIRS, MODIS) to identify anisotropic targets as a function of cloud and surface properties.
- 3) Factor of 2-3 improvement in time-sampling errors by the use of a three-satellite sampling system and the use of improved shortwave models of the dependence

of scene albedo on varying solar zenith angles throughout the day.

2.2.3.5.2 Surface radiative fluxes

Global satellite estimates of radiative fluxes at the surface (up, down, and net) are now becoming available (Darnell et al. 1992; Li and Leighton 1993). In general, the intervening atmosphere complicates the measurement when compared to the more-straightforward derivation of TOA fluxes. A major advantage, however, is the ability to test satellite-based surface flux estimates directly against surface-based measurements such as those currently provided by the Global Energy Balance Archive (GEBA; Ohmura and Gilgen 1991; Li et al. 1995) and in the future by the BSRN (World Climate Research Program [WCRP] 1991) now being established around the globe. As a result of this ability, two independent approaches are desirable for determining surface radiative fluxes:

- 1) Calculation of surface fluxes using observed cloud and atmosphere parameters, with measured TOA broadband fluxes acting as a constraint on the radiative calculation.
- 2) Parameterized relationships between simultaneously-observed TOA fluxes (or radiances) and surface fluxes. Typically, the form of the parameterization is based on a radiative transfer model, but the final coefficients used are determined by comparisons against actual surface flux observations.

Work is progressing on both of these approaches.

Initial global surface radiation budget estimates of SW up, down, and net fluxes use ISCCP narrowband radiances, along with a narrowband-to-broadband transformation (Darnell et al. 1992; Pinker and Laszlo 1992). Verification against GEBA data and FIRE field experiment data indicates a monthly average of 2.5° regional mean insolation accuracies of about 20 Wm^{-2} (1σ). While this is not as accurate as estimates of TOA fluxes using ERBE data, most of this discrepancy appears to be caused by spatial mismatching of the scales of observations of the satellite (250 km) and surface (30 km) observations, so that actual rms errors may be closer to $5\text{-}10 \text{ Wm}^{-2}$ (Li et al. 1995). In the time frame of the EOS observations, calculated SW surface flux accuracies should increase greatly as more-accurate cloud (VIRS, MODIS), atmospheric (AIRS), and surface properties (MISR, MODIS) become available, and as simultaneous

broadband measurements of TOA fluxes are available to constrain the model calculations, including implicit corrections for 3-D radiative transfer effects. The MISR measurements of bidirectional reflectance of vegetation canopies will provide improved separation of net surface SW flux into upwelling and downwelling components.

The second approach to SW flux estimation is to make use of a direct linear relationship between net SW flux at the top of the atmosphere and net SW flux at the surface (Cess et al. 1991; Li et al. 1993). This relationship is derived theoretically and verified against surface observations as a function of solar zenith angle. The rationale for this method (Davies et al. 1984) is that water vapor absorption and absorption by liquid water and ice occur in the same portion of the spectrum. To first order, then, placing a cloud in the atmosphere simply changes the vertical distribution of solar absorption, but not the total amount. The dependence of absorption on solar zenith angle can be understood as a change in path length. Because cloud particles reflect a significant amount of radiation even at absorbing wavelengths, however, and because reflection depends on particle size and shape, there are still questions about accuracy as a function of cloud type and height. The key to improvements in the empirical algorithm is to obtain more-extensive surface-observed net SW fluxes for validation as a function of varying cloud conditions and climate regimes. FIRE, the ARM program, and BSRN observations will be key to increasing the accuracy and confidence in this empirical approach.

The situation for LW surface fluxes is more complex and difficult, at least for the downward LW flux at the surface. Calibration of surface LW flux pyrgeometer measurements is still undergoing study, and downward flux radiative computations are dominated by low-level water vapor and cloud-base altitude (Gupta 1989; Gupta et al. 1992)—two of the more-difficult measurements to obtain from space. For clear-sky conditions, encouraging progress has been made in developing direct relationships between surface and TOA LW fluxes (Inamdar and Ramanathan 1994; Stephens et al. 1994). In the EOS time frame, improved lower-tropospheric water vapor will be available globally from the AIRS/HSB instruments and over land from MODIS (Kaufman and Gao 1992). Tests are under way using FIRE observations to examine methods to relate satellite measurements of cloud temperature and optical depth to estimated cloud geometrical thickness (Minnis et al. 1990, 1992). Recent sensitivity studies using ISCCP cloud data indicate that cloud overlap may in fact be the largest uncertainty for calculations of downward longwave flux at the surface (Charlock et al. 1994).

Methods to identify multiple cloud layers using satellite data have only recently begun, however, and a great deal of additional work is needed in this area. Two approaches appear promising. For optically-thin high clouds, infrared sounding channels can isolate the high cloud, while visible and infrared window channels are used for the low-level cloud (Baum et al. 1992). For optically-thick high clouds, a combination of optical measurements for the upper (ice) cloud and microwave measurements for the low (water) cloud may help define cloud overlap. In the long term, active systems such as the GLAS lidar for optically-thin cloud and a 94-GHz cloud radar for optically-thick cloud offer the best solution (WCRP 1994).

For surface LW emission, additional work is still required to improve models of land emissivity and directional thermal emission from vegetation canopies (Li and Becker 1993; Sellers and Hall 1992; Slingo and Webb 1992).

2.2.3.5.3 Radiative fluxes within the atmosphere

Determination of profiles of atmospheric radiative fluxes is necessary to estimate radiative heating rates within the atmosphere. Clearly, the most accurate measurement of radiative heating rate will be for the total atmospheric column. The total column heating rate can simply be determined from the difference between the TOA and surface radiative fluxes.

A second level of complexity is the determination of radiative heating rates within the atmosphere. Even for aircraft observations, this is an exceedingly difficult measurement, primarily because of the large spatial and temporal variability of cloud fields. Estimates from space will necessarily be a combination of observed atmospheric properties (temperature, water vapor, aerosols, clouds) used as input to radiative transfer calculations. One of the primary concerns is the accuracy of these radiative models, but an advantage available during the EOS period will be the use of broadband TOA flux observations to constrain the model solution. For example, if SW TOA fluxes calculated for a cloud field disagree with TOA measurements, then the satellite-derived cloud optical depth could be adjusted to get agreement. In this case, the error in both the satellite optical depth estimate and the radiative calculations could be caused by the use of a 1-D radiative transfer model for a 3-D cumulus cloud field. Since the TOA flux measurement can use CERES-measured anisotropic models appropriate for a 3-D cumulus cloud field, the TOA conversion of SW radiance to flux can in fact include the typical 3-D radiative properties of the cloud field, and thereby remove most of the bias in the radiative flux calculations of the effect of the cloud

within the atmosphere. The bias is removed by adjusting the cloud optical depth to one which would give a 1-D equivalent albedo. In this way, the radiative flux profile within the atmosphere will be consistent with TOA observations, and the cloud optical depth estimation can be corrected for first-order 3-D effects as well.

A second possible constraint on radiative fluxes within the atmosphere is the use of satellite-estimated surface radiative fluxes. If direct relationships between TOA and surface-observed radiative fluxes prove to be a more-accurate estimate of surface fluxes than radiative calculations using satellite-observed atmosphere and cloud properties, then the satellite-estimated surface flux estimates can be used as an additional constraint on the calculated radiative fluxes within the atmosphere. The use of the TOA and surface flux constraints would be weighted by the estimated accuracy of each radiative flux component. In this case, TOA fluxes would probably provide a stricter constraint than surface fluxes. Note that, if using radiative modeling proves more accurate in estimating surface radiative fluxes, then the only observational constraint is the TOA flux.

Even with TOA flux constraints, however, the ability to remotely sense cloud thickness, or cloud overlap, is subject to serious question. As a result, the initial strategy for EOS is to phase in progressively-more-advanced estimates of in-atmosphere radiative fluxes, as indicated in the following list:

- *At launch + 6 months:* TOA, surface, tropopause, 2-5 stratospheric levels
- *At launch + 24 months:* Add 500-hPa level
- *At launch + 36 months:* Add 4-12 tropospheric levels, as validation warrants

One of the elements for testing within-atmosphere flux calculations is likely to be the use of remotely-piloted aircraft currently under development, which are capable of gathering statistics over very long flight legs with accurately stacked flight tracks; ARM began test flights in spring 1994. The remote-sensing challenges for within-atmosphere fluxes are similar to those for downward LW flux at the surface: profiles of water vapor, cloud thickness, and cloud overlap.

2.2.3.5.4 Cloud properties

The remote sensing of cloud properties from space is complicated greatly by the rapid changes of clouds in both space and time. To further complicate matters, their radiative properties are a strong function of viewing angle and solar geometry. Where the remote sensing of TOA

fluxes was a 7-dimensional sampling problem, cloud properties add a vertical dimension for a total of 8.

Nevertheless, a great deal of progress has been made in recent years, especially through the work of ISCCP and FIRE. Overall lessons learned include:

- Cloud analysis can often be separated into cloud detection, followed by cloud property determination.
- Lack of accurate calibration of narrowband imaging radiometers remains a major stumbling block in climate work.
- No single cloud algorithm or portion of the spectrum (i.e., solar, infrared, microwave) can handle the diversity of cloud physical properties needed for the cloud/radiation problem.
- Significant improvements in cloud retrievals are still possible with current satellite data, including new estimates of cloud particle size.
- The next jump in quality should be provided by MODIS, the first instrument whose design specifically includes cloud property determination as a requirement.
- Validation of cloud physical properties requires not only tests against field observations, but also consistency between independent satellite methods. For example, very-high-spatial-resolution ASTER data are needed to answer questions about inadequate beam filling within the larger MODIS or VIRS pixels; multi-angle MISR data are needed to provide stereo cloud height confirmation, and confirmation of 3-D cloud radiative effects on retrieved cloud radiative properties; and EOSP measurements are needed to provide independent estimates using polarization of cloud particles, especially for ice particle clouds.
- The final step in cloud remote sensing will be the combination of passive and active remote sensors. EOS will begin this step with MODIS, AMSR-E, and GLAS (active lidar). Ultimately, a 94-GHz radar will also be required. It is clear that active remote sensors will require multiple spectral bands, just like the passive radiometers.

2.2.3.5.4.1 Cloud fraction

The problem of determining cloud fraction has typically been treated as either one of cloud detection (Rossow et

al. 1985) or energy balance (Coakley and Bretherton 1982; Minnis and Harrison 1984a-c; Stowe et al. 1988). Other methods include the use of spectral signatures or spatial textures (Stowe et al. 1991; Saunders and Kriebel 1988).

A cloud-detection method typically defines a threshold reflectance (solar wavelengths) or brightness temperature (thermal infrared) to distinguish between satellite measurement pixels containing clear-sky or cloudy-sky conditions. The major problem with this approach is how to handle partially cloud-filled pixels (i.e., the “beam-filling” problem).

An energy-balance cloud fraction measurement is based on the assumption that many, if not most, of the pixels may be partially cloud-filled. These methods use an estimate of a typical cloud reflectance (Minnis and Harrison 1984a-c; Stowe et al. 1988) or a typical cloud brightness temperature (Coakley and Bretherton 1982) to allow cloud fraction in each pixel to be linearly related to the reflectance or brightness temperature in each pixel.

Wielicki and Parker (1992) showed results of using 30-m-spatial-resolution Landsat data to test the performance of the ISCCP-determined cloud fraction on the spatial resolution of the data. Two things were found to occur. As expected, when the spatial resolution degrades, the beam-filling problem increases cloud fraction, especially for boundary-layer clouds. But unexpectedly, at full resolution, the ISCCP bispectral thresholds underestimate cloud fraction because they miss a significant amount of optically-thin cloud below the threshold. The net effect is a combination of a tendency to underestimate the optically-thin cloud and to overestimate the broken optically-thicker cloud. These results indicate that, for EOS, the 250-m channels on MODIS will greatly reduce the problem of beam-filling, but that further work will be required for the detection of optically-thin cloud.

Several advances in the EOS era that will give key improvements in cloud fraction measurements are:

- higher spatial resolution;
- additional near-infrared channels for thin cloud detection, especially the 1.38- μm channel added for detection of optically thin cirrus (Gao et al. 1992); and
- additional thermal infrared channels (3.7, 8.5, 13.3, 13.6, 13.9 μm) to allow improved detection of optically-thin cloud at night.

A second major concern is the variation of derived cloud fraction, as obtained by ISCCP and other studies as a function of viewing zenith angle (Minnis 1989). This

needs further study using multi-angle MISR and POLDER data for solar-channel cloud detection and the Along Track Scanning Radiometer-1 (ATSR-1) for the thermal infrared detection.

The third major concern is cloud detection in polar regions. In these regions, recourse is often made to a combination of spectral and textural measures to improve cloud detection (Ebert 1987; Welch et al. 1992; Yamanouchi et al. 1987).

2.2.3.5.4.2 Cloud height

The measurement of cloud height has typically been accomplished by one of three different methods:

- set measured brightness temperature equal to cloud top temperature assuming a black cloud (Stowe et al. 1988);
- use 15- μm infrared sounding channels to estimate the pressure level in the atmosphere at which the cloud is radiating (Smith and Woolf 1976; Chahine 1974); or
- use the solar reflectance measurement to estimate visible cloud optical depth (and thereby infer an infrared emittance) and then correct the estimate of cloud temperature if the cloud has emittance less than unity (Rossow et al. 1985).

Additionally, the spatial coherence method (Coakley and Bretherton 1982) has the ability to uniquely distinguish cloud fields with well-defined layers, as exhibited by small spatial variability in the cloud thermal infrared window emission. Several problems with these methods have recently been documented by FIRE:

- Even boundary-layer clouds are often nonblack (Wielicki and Parker 1992; Luo et al. 1994).
- Infrared sounder methods work well for upper-level clouds, but poorly for low-level clouds (Wielicki and Coakley 1981; Wylie and Menzel 1989).
- The ISCCP visible optical depth calculations have traditionally assumed water clouds, a poor assumption for cirrus (Minnis et al. 1990; Wielicki et al. 1990).
- In the presence of boundary-layer inversions over the ocean, conversion of cloud temperature to cloud height can cause large errors (Minnis et al. 1992).

These problems suggest that algorithms must be varied with varying cloud types. For boundary-layer stratus, spatial coherence will work best. For cirrus without lower-level cloud, the ISCCP method using hexagonal ice crystals (Minnis et al. 1990) is sufficient; for cirrus over low-level stratus, the infrared sounder methods work best. For large-scale storm systems, any of the methods should give accurate results.

The largest remaining problems are multi-level cloud situations (almost half of all cloud cases according to surface observations; Hahn et al. 1982; Tian and Curry 1989), and cumulus or altocumulus fields. Key improvements for these cases will come from the increased spectral resolution of MODIS as well as the increased spatial resolution to minimize beam-filling problems in interpreting thermal infrared channel observations. Recent studies have shown progress in cases of cirrus over stratus by using infrared sounder data to determine the upper cloud level, and multispectral thermal infrared window channel data using spatial coherence methods to determine the low cloud (Baum et al. 1994). Key validation data will come from surface lidar and radar, field experiments, and the spaceborne GLAS lidar and MISR stereo cloud-height capabilities. The most difficult area to validate will remain multi-level cloud, especially if both layers are optically thick in the visible and thermal infrared. In this case, the only validation tool will be the use of millimeter wavelength radar (WCRP 1994).

2.2.3.5.4.3 *Cloud visible optical depth and thermal infrared emittance*

The first global satellite estimates of visible cloud optical depth were provided recently by ISCCP. The methodology used was to calculate the expected visible reflectance for a water cloud of 10- μm spheres as a function of surface reflectance, solar zenith angle, and satellite viewing angle using a 1-D multiple scattering radiative transfer model (Rossow et al. 1991). A look-up table then converted reflectance into visible optical depth. The range of optical depths which can be measured is typically between about 0.5 and 100, limited by cloud detection limits on the lower end and lack of further sensitivity on the upper end. FIRE and other validation studies showed that there are three major difficulties with the present data:

- Most of the year-to-year variability in the ISCCP global cloud optical depth is caused by varying calibration of the visible radiometers (Klein and Hartmann 1993a). Improved calibration is critical.

- Nonspherical ice particle scattering differs greatly from the assumed 10- μm spheres, causing an overestimate of ice cloud optical depths (Minnis et al. 1990). The ISCCP data will soon be reprocessed using improved hexagonal crystal scattering for cold clouds (Takano and Liou 1989).
- The cloud-filled-pixel assumption causes substantial underestimates of cloud optical depth for cumulus fields, even when cloud amounts are correct or too small (Harshvardhan et al. 1994).

All of the above concerns should be greatly alleviated by the improved calibration and spatial resolution offered by the VIRS and MODIS instruments in the EOS era. An unresolved problem, however, is whether a 1-D radiative transfer model can be applied to inherently 3-D cloud structures such as cumulus. For boundary-layer clouds over ocean, new evidence implies that the relatively small aspect ratio (v/h) and optical depths of broken cloudiness cause errors due to the 1-D assumption being relatively small for domain-averaged values (Cahalan et al. 1994; Wielicki and Parker 1992; Duda and Stephens 1994). For cumuli over land, however, the larger aspect ratios and larger optical depths require re-examination of this result. In addition, initial observations of non-plane-parallel cirrus clouds during FIRE showed mixed results (Stackhouse and Stephens 1991). One of the key verifications of the importance of 3-D effects is the test for consistency in derived optical depth as a function of satellite viewing angle. POLDER and MISR data will provide key tests of this assumption on a global basis. Regional field experiment data will allow tests using in-cloud measurements combined with fully 3-D radiative transfer models. If 3-D effects are found to be critical, further studies of the remote sensing of cloud field horizontal structure will be required (e.g., Zhu et al. 1992). Continuing work will also be required to understand the effects of ice cloud particle shape and size on satellite-inferred optical depths.

Thermal infrared emittance is related to visible optical depth through cloud particle size and phase. For nighttime observations, estimates are typically made using either infrared sounder data (Smith and Woolf 1976; Chahine 1974) for upper-level clouds, or multiple thermal infrared window channels with varying response to cloud particle size (Luo et al. 1994) for lower-level clouds. Classically, the infrared sounder measurement is actually considered to be ϵA_c , or emittance times cloud fraction. Recent studies indicate, however, that for cirrus clouds, partially cloud-covered fields of view are not a problem for pixel sizes less than about 8 km (Wielicki and Parker

1992). In this case, the MODIS 1-km resolution infrared sounder channels should be able to unambiguously measure infrared cirrus emittance. Multispectral methods for low-cloud emittance need further validation by field experiments, although they appear promising.

2.2.3.5.4.4 *Cloud particle size*

A great deal of progress has been made recently in the remote sensing of cloud particle size. Two approaches have been examined initially; one using solar reflectance channels, and the other using thermal infrared channels. Both approaches make use of the large variation in the imaginary part of the refractive index for water and ice as a function of wavelength. For example, the imaginary part of the refractive index of water varies from about 10^{-8} at $0.6\ \mu\text{m}$ to 10^{-4} at $1.6\ \mu\text{m}$, 10^{-3} at $3.7\ \mu\text{m}$, and 10^{-1} at $11\ \mu\text{m}$. The origins of these approaches date back to Blau et al. (1966), Hansen and Pollack (1970), and Arking and Childs (1985).

Daytime methods use the visible channel to determine cloud optical depth, plus absorbing channels to estimate cloud particle size. In essence, the visible channel estimates the average number of scattering events per reflected photon, while the absorbing channel determines the absorption per scattering event, which is a function of particle size. The first global estimate of low-cloud water droplet size has recently been produced using the AVHRR 0.6-, 3.7-, and 11- μm channels (Han et al. 1994). In addition, aircraft radiometers and Landsat observations have been used in FIRE field experiments to show that for water clouds over ocean, the determination of effective droplet radius using visible, 1.6-, and 2.1- μm channels tracks changes measured by aircraft in situ data with possible offsets of about 30%. The discrepancy has recently been ascribed to either water vapor continuum absorption in the 1.6- and 2.1- μm region bands (Stephens and Tsay 1990; Nakajima et al. 1991), or to problems with the Forward Scattering Spectrometer Probe (FSSP) typically used to measure cloud droplet size distribution from aircraft. Further validation of the 3.7- μm methodology is required using aircraft observations. For both daytime methods, solutions become multivalued for very small particles (less than $5\ \mu\text{m}$) and small optical depths (Nakajima and King 1990; Han et al. 1994). The primary uncertainties in these methodologies would appear to be inaccuracies in handling water vapor absorption in the window channels and in handling the horizontal and vertical inhomogeneities of clouds (Coakley and Davies 1986). The majority of work has been done for water clouds, but initial work on ice clouds has also begun (Wielicki et al. 1990; Stone et al. 1990). The major problem for ice clouds is the uncer-

tain scattering and absorption properties of nonspherical particles. Extensive further theoretical and observational work is needed for ice clouds. In particular, advances in aircraft probes are needed to routinely measure the number of small ice crystals and to measure the scattering phase functions of ice crystals.

Purely infrared methods to infer particle size have evolved more recently (Prabhakara et al. 1988; Ackerman et al. 1990; Luo et al. 1994). These methods rely on the variation in cloud emittance caused by varying particle size. Their primary advantage is the ability to provide night-time observations. Whereas the reflectance methods have greatest sensitivity to particle size at relatively-large optical depths, the thermal infrared methods are most sensitive for optically-thin clouds with optical depths of 1-2. Using the currently available 3.7-, 11-, and 12- μm data, the thermal infrared retrievals are limited, due to the strong ice and water absorption at these wavelengths, to an effective radius of about $30\ \mu\text{m}$. Validation against field experiment data is just beginning for these new methods.

The increased number of spectral channels available on the VIRS and MODIS instruments will allow substantial improvements in cloud particle remote sensing. Key advances are the availability of global 1.6- and 2.1- μm channel data during the day and a new 8.5- μm infrared window channel at night. In the future over ocean regions, water cloud particle sizes should be verified independently by combining the microwave-measured LWP using TRMM Microwave Imager (TMI) data on TRMM and AMSR data on EOS PM-1 and METOP, and the VIRS- or MODIS-derived cloud optical depth using $r_e = 1.5LWP/\tau_c$ (Stephens 1978). A second independent verification can be obtained by using the polarization measurements of POLDER and EOSP, especially for nonspherical particles.

2.2.3.5.4.5 *Cloud liquid/ice water path*

Passive microwave radiometers on the Nimbus-7 Scanning Multifrequency Microwave Radiometer (SMMR) and the Defense Meteorological Satellite Program (DMSP) Special Sensor Microwave/Imager (SSM/I) platforms have demonstrated the ability to observe cloud LWP over ocean backgrounds (Greenwald et al. 1993). Over land, however, these methods are not applicable because of the large variability of surface emission at microwave frequencies. The primary difficulty in this measurement is caused by beam filling for the 10-30-km footprints typical of these measurements. For EOS, the AMSR-E field of view is about a factor of 2 smaller than is available with the current SSM/I data, thereby eliminating some of

the beam-filling concern. For applications where only a grid-box average LWP is required, beam filling is not a concern. Error analyses and verification against surface-based LWP measurements indicate instantaneous accuracies of about 25% for the current SSM/I instrument, with much smaller bias errors for monthly average data (Greenwald et al. 1993).

Over land, LWP estimates will have to be provided using VIRS or MODIS estimates of cloud optical depth and effective droplet radius, using the relation discussed in the previous section. Uncertainties will be larger than for ocean cases, but the magnitudes will require further analysis of FIRE and ASTEX data.

Currently, there is no method to infer ice water path (IWP) using passive microwave observations. Initial estimates of IWP for EOS will be obtained using VIRS- and MODIS-derived cloud optical depth and effective particle size. The key problem here will be lack of a good ground truth source for IWP and the greater uncertainties caused by nonspherical geometry for ice crystals. The nonspherical particles will cause increased errors in both optical depth (uncertain scattering phase function) and effective particle size (uncertain phase function and single scattering albedo), as discussed in previous sections. Much further work is needed in this area, both to provide improved new observational techniques and to gain improved information from current and planned observations. In this regard, the polarization information provided by POLDER or EOSP may provide key information for distinguishing ice particle habits. The most promising technique for remote sensing of IWP and particle size is the use of high-frequency passive microwave at 300-to-650 GHz (Evans and Stephens 1995a, b).

2.2.3.5.4.6 *Cloud mesoscale organization and structure*

The high cloudiness and precipitation in the tropics are dominated by mesoscale convective systems (MCS) (sometimes called “cloud clusters”). MCS occur in a highly-discrete intermittent manner. They have time and space scales much less than those of the large-scale circulation of the tropics. The mean cloudiness derived from satellite imagery, long-period rain accumulations at tropical locations, and the total latent heating of the tropical atmosphere are the net results of these sporadic and small-scale cloud phenomena.

The size spectrum of tropical MCS tends toward being lognormal. A small number of very large MCS account for a large portion of the total high cloudiness and rainfall. If an infrared temperature of 208 K is used to define “high cloud top,” then roughly one-fourth of the area covered by high cloud is accounted for by MCS in

the size ranges $< 7,000 \text{ km}^2$, $7,000\text{-}30,000 \text{ km}^2$, $30,000\text{-}90,000 \text{ km}^2$, and $>90,000 \text{ km}^2$ (Mapes and Houze 1993; Chen et al. 1995).

The cloud dynamical and microphysical processes within an MCS determine the amount of upper-level cloud and precipitation that are generated by the MCS. These processes vary across the size spectrum of MCS. The smallest MCS are dominated by convective processes. The larger develop broad regions of stratiform precipitation, and the large upper-level cloud shields delineating the large MCS are primarily associated with stratiform processes.

The convective and stratiform processes lead to different vertical profiles of latent heating, and they generate different types of ice particles in the upper-level cloud shields (Houze 1982, 1989, 1993). The large-scale tropical atmosphere responds differently to these different profiles of heating (Hartmann et al. 1984; Mapes and Houze 1995).

To understand the physical chain of events involved in the interaction of deep convective cloud systems and the large-scale circulation and climate over the tropical ocean, it is necessary to understand how the MCS in different parts of the size spectrum of the MCS contribute to the production of upper-level cloud and to latent heating. To do this, the individual MCS comprising the spectrum must be identified as must the regions of stratiform and convective precipitation within the MCS.

The EOS MODIS data (high-resolution infrared channel) can be used to identify the individual elements of the MCS spectrum by previously-developed methods (Williams and Houze 1987; Mapes and Houze 1993; Chen et al. 1996). The EOS AMSR-E data (especially the passive microwave channels at 90 and 36.5 GHz) will identify the precipitation within an MCS identified in the MODIS infrared (IR) data. This analysis will identify the regions where latent heat is being imparted to the atmosphere. The AMSR-E data will further indicate the locations of the convective and stratiform regions. This can be done approximately by using an appropriately-calibrated passive microwave threshold separating the higher-intensity convective rain from the lighter stratiform rain. The EOS data set will thus provide global analyses of the location and sizes of an individual MCS and how each member of the overall size spectrum of an MCS contributes to latent heating of the large-scale tropical atmosphere.

2.2.4 *Water vapor and climate*

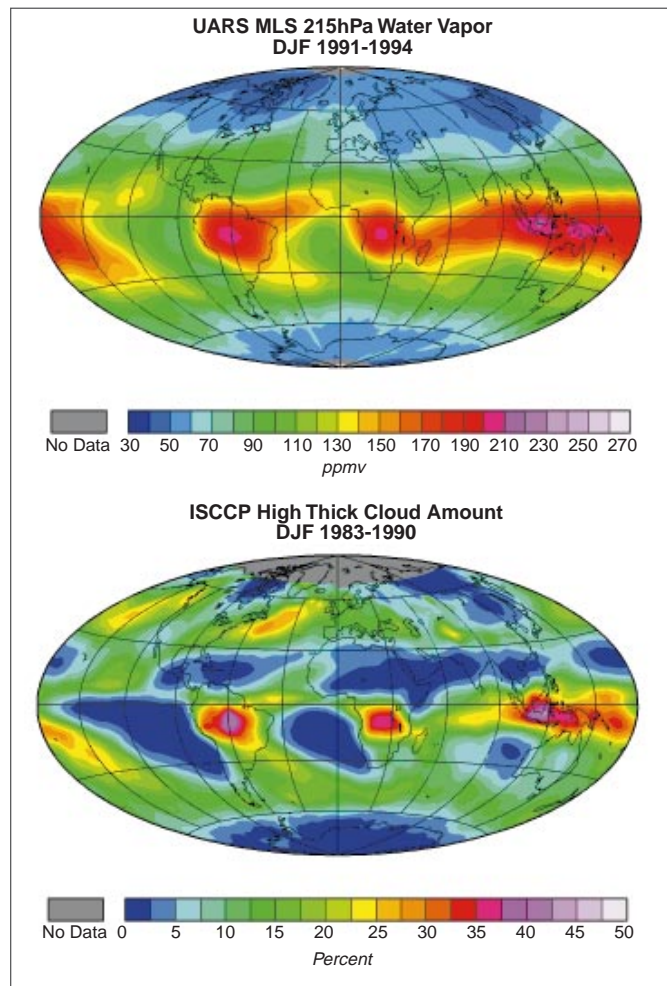
Most of the water in the atmosphere is in the form of vapor, and water vapor plays a critical role in many key processes in the hydrologic and energy cycles. Water va-

por is the most important greenhouse gas, both in terms of its role in maintaining the current climate and in terms of its role in sensitivity through the water vapor feedback process. The supply of moisture for precipitation and runoff in land areas is by lateral transport of water vapor in the atmosphere. River flow from land to ocean must be balanced by an equivalent transport of water vapor from ocean areas to land areas. The abundance and vertical distribution of water vapor in the atmosphere interact very strongly with convection and cloudiness, thereby influencing the albedo of the planet as well as the infrared opacity of the atmosphere.

2.2.4.1 Water vapor feedback and climate sensitivity

Because water vapor is the primary greenhouse gas in the Earth’s atmosphere and the saturation vapor pressure increases exponentially with temperature, the abundance of water vapor in the atmosphere can provide a very strong positive feedback to climate change. The strong positive feedback associated with an assumption of fixed relative humidity was studied in early one-dimensional climate models (Manabe and Wetherald 1967), and its importance has been confirmed by succeeding observational (e.g., Raval and Ramanathan 1989) and modeling studies (e.g., Cess et al. 1990). The assumption of fixed relative humidity in climate sensitivity calculations has been challenged by Lindzen (1990), who called attention to the uncertainties associated with the detrainment of water from cumulus clouds and the associated distribution of water vapor in the middle and upper troposphere. He reasoned that warming in the equatorial region induces stronger and deeper cumulus convection, which would detrain at lower temperatures, and lead to drying in the upper troposphere. Betts (1990) argued that air in the convective regions detrains not only in the upper troposphere, but over a wide region between 150 and 550 mb where a significant fraction of the detrained water is in the form of ice from thick anvil ice clouds that dissipate and leave behind large amounts of water vapor, implying that a more-humid middle and upper troposphere could result from a warmer climate, i.e., a positive water vapor-temperature feedback.

FIGURE 2.11



Top panel shows the 215 hPa MLS water vapor climatology for December-February that uses measurements made from 1991-1993 binned into 4°×4° latitude/longitude boxes. The bottom panel shows the December-February 1983-1990 ISCCP fractional high thick (altitude above 440 hPa and visible optical depth greater than 9.38) cloud cover climatology map (Read et al.).

Water vapor abundance near the ocean surface is most closely linked to the saturation vapor pressure at the surface temperature, and in the upper troposphere is more strongly controlled by mesoscale and large-scale transport processes. The greenhouse effect is about equally sensitive to the relative humidity of the lower and upper troposphere. Climate models indicate that the net feedback is about equally sensitive to variations in the vertical structure of water vapor and temperature (Sinha 1995), and there may be some degree of cancellation between water vapor and lapse rate changes that occur in global climate models (Zhang et al. 1994). For the above rea-

sons it is critically important to understand the vertical distribution of water vapor in the atmosphere, its horizontal variation around the globe, and the processes that maintain this global water vapor distribution.

2.2.4.2 *Water vapor distribution and variability*

Until recently our knowledge of the global water vapor distribution derived primarily from global weather analyses based mostly on radiosonde observations. In the last few years these global analyses have begun to take better advantage of the water vapor information available from conventional polar-orbiting meteorological sounders. In addition, several attempts to make self-consistent water vapor data sets based on satellite sounding data have been initiated, including the TIROS Operational Vertical Sounder (TOVS) Pathfinder project under EOS. Other useful data sets include those derived from geosynchronous satellites that afford high temporal and spatial resolution to follow the influence of MCS on water vapor (Soden and Bretherton 1993; Udelhofen and Hartmann 1995), and high-vertical-resolution observations of water vapor in the upper troposphere from limb-scanning instruments such as the Stratospheric Aerosol and Gas Experiment (SAGE) (Rind et al. 1993) and MLS (Read et al. 1995). Wu et al. (1993) and Bates et al. (1996) also developed an intercalibrated satellite upper tropospheric water vapor data set using the High-Resolution Infrared Radiation Sounder (HIRS) on National Oceanic and Atmospheric Administration (NOAA) polar-orbiting satellites. Figure 2.11 (from Read et al. 1995) shows the strong association between humidity at 200 mb and deep convective cloudiness. These satellite observations provide homogeneous sampled observations of precipitable water and water vapor for the lower, middle, and upper troposphere and stratosphere. The typical accuracy is 20% for specific humidity and 10% for relative humidity. These accuracies are good enough to study the global water vapor climatology and seasonal variation, marginally good enough to study the large-scale features of interannual variation, but not adequate to study the long-term trends of water vapor and water-vapor processes.

Water vapor varies rather smoothly with longitude but decreases rapidly poleward. The annual mean value of the column-integrated water vapor, or total precipitable water, ranges by a factor of 10-20 from $\approx 50 \text{ kg m}^{-2}$ in the equatorial region to $< 5 \text{ kg m}^{-2}$ in the Arctic and to $< 2.5 \text{ kg m}^{-2}$ in the Antarctic (Peixoto and Oort 1992). Longitudinally, the total precipitable water varies by a factor of < 3 and is affected by land-ocean distribution and monsoon circulations. In the equatorial region, the most humid regions are located in the Congo basin, the

Brazilian basin, and the Indonesian region, where the trade winds bring in large amounts of water vapor to support strong convection. At higher latitudes, water vapor is generally more abundant over ocean than over land. Since most of the ocean is in the Southern Hemisphere, the longitudinal distribution of the total precipitable water is smoother in the Southern Hemisphere than in the Northern Hemisphere.

The specific humidity decreases nearly exponentially with height. This is because temperature decreases nearly linearly with height and saturation vapor pressure is an exponential function of temperature. The vertical distribution of specific humidity ranges over several orders of magnitude. More than 50% of the water vapor is contained in the region below the 850-mb level, while more than 90% is confined in the region below the 500-mb level (Peixoto and Oort 1992). The relative humidity also decreases with height. Minimum relative humidity is found in the subtropical regions and land-locked desert regions.

Data from EOS instruments will improve the quality of global measurements of the water vapor distribution. In particular, the combination of AIRS, AMSU, and HSB will provide more-precise simultaneous measurements of temperature and humidity in the troposphere, with better vertical resolution than is currently available. Vertical resolution is particularly important because climate feedbacks are sensitive to the vertical distribution of water vapor and temperature. Also, the vertical structure gives information about the mechanisms that maintain the water vapor distribution. Limb-scanning instruments such as MLS, SAGE III, and HIRDLS will measure the vertical water vapor profiles from middle troposphere to stratosphere with 200-km horizontal and 1-km vertical resolution. They will provide improved vertical resolution in the upper troposphere, and, because it is a microwave sensor, MLS will not be affected by the presence of cirrus clouds in this region. Together with more-accurate observations of thin cirrus clouds, these data can provide critical information on the effects of convection and cirrus clouds on upper-troposphere and lower-stratosphere water vapor.

2.2.4.3 *Maintenance of the global water vapor distribution*

2.2.4.3.1 *Role of convection and clouds*

The source of water vapor is evaporation from the surface. The climate system is in balance to first order, so that the globally-averaged precipitation rate is approximately equal to the evaporation rate. Precipitation occurs

primarily in association with convection and clouds, so that convection and clouds are the sink regions for water vapor in the atmosphere. If one thinks of the vertical distribution of water vapor, however, convection carries water from the lower to the upper troposphere, so that as far as the atmosphere above the planetary boundary layer is concerned, convection is a source of water vapor. This is especially true in the tropics, where large-scale motions mostly dry the troposphere by subsidence, and convection is the only major source of upper-tropospheric water vapor. The mechanisms whereby convection humidifies the upper troposphere have not been well quantified, and the changes in the relative efficiency of the drying and moistening mechanisms for the upper troposphere that would occur in association with a global climate warming are not known at all. These changes may have a profound effect on climate sensitivity and need to be understood.

EOS spaceborne measurements will provide accurate high-spatial-resolution measurements of water vapor and temperature profiles, together with cloud properties such as cloud-top height, visible optical depth, and mean cloud-particle radius. Instruments such as AIRS/AMSU/HSB, MODIS, MISR, EOSP, and GLAS may provide measurements of thin cirrus occurrence with very good height information for cirrus that are too thin to be detected by passive means. These data, combined with wind estimates from data assimilation and in situ measurements from carefully-designed field programs, will provide a much better understanding of the mechanisms whereby the moisture balance of the troposphere is maintained. With this information it will be possible to validate better physical parameterizations for the convective injection of moisture into the upper troposphere and gain more confidence in the simulation of water-vapor feedback in climate models. Investigations underway within the EOS IDS investigations are poised to take advantage of these new data and provide the diagnostic and modeling studies to translate them into improved climate predictions.

2.2.4.3.2 Role of large-scale atmospheric motions

Large-scale atmospheric motions also have a controlling effect on the distribution of water vapor in the atmosphere. In regions of mean descent the water vapor concentration is greatly suppressed. The effect is offset by lateral mixing by large-scale motions from regions where water vapor is injected into the troposphere (e.g., Peixoto and Oort 1992, Chapter 12). In the upper troposphere and lower stratosphere, some aspects of the distribution of water vapor can be understood by considering the important role

of mixing along isentropic surfaces (e.g., Kelly et al. 1991; Yang and Pierrehumbert 1994). Such mixing can play an important role in drying the troposphere because isentropic surfaces slope upward with latitude. Air is thus dehydrated by condensation and precipitation as it moves poleward and upward, and when it returns equatorward it provides a source of very dry air to lower latitudes and altitudes. Offsetting this drying action must be a cross-isentrope flow of water, either through diabatic advection or small-scale cross-isentrope transport of water, such as by penetrative convection.

The effect of large-scale motion on water vapor transport can be examined by studying the interannual changes of global water vapor distribution and transport using satellite observations and 4-D data assimilation. Interannual changes of deep convection in the equatorial Pacific associated with the ENSO dramatically alter the distribution of upper tropospheric moisture (Soden and Fu 1995; Bates et al. 1996) as well as global circulation patterns (e.g., Wallace and Gutzler 1981; Lau and Nath 1994). Since the influence of large changes in temperature and surface fluxes upon the moisture field is small compared to the seasonal changes, the impact of atmospheric motion on the water vapor field is more robust. The analysis of TOVS upper tropospheric relative humidity index and water vapor transport assimilated by the GEOS DAS suggests that the 1987 El Niño affected the tropics-extratropics water vapor transport and thus upper tropospheric humidity in the mid-latitudes (Fu and Soden 1996). Quantifying these changes can provide critical information to assess the effect of large-scale motion on water vapor transport and distribution, but is not possible with the accuracy of the current data sets. The EOS AIRS, AMSU, and HSB will provide specific humidity at 10% accuracy. With a more-accurate atmospheric heating field provided by CERES, MODIS, GLAS, and SAGE III, the assimilated wind fields by the GEOS DAS will be more reliable. Thus, the water vapor transport and distribution can be more-accurately estimated and the impact of large-scale motion on water vapor can be estimated quantitatively.

Measuring the effect of large-scale motions on the water vapor budget of the troposphere and lower stratosphere requires very accurate fields of winds, water vapor, and heating rate. These fields will be obtained through the assimilation of EOS radiances into dynamical models, followed by detailed diagnostic and sensitivity studies. Key EOS instruments include AIRS/AMSU/HSB for temperature and humidity profiles, and AMSR-E for precipitable water.

2.2.4.3.3 Role of surface temperature

The importance of surface temperature for the global distribution of water vapor can be easily appreciated from the high correlation between water vapor over the oceans and SST. The monthly mean precipitable water above the oceans can generally be prescribed from the SST (Stephens 1990). Location and season seem to have little effect on the relationship. This close relationship reflects the fact that SST, atmospheric circulation, and convective activities are highly interactive. Also, most of the total precipitable water is near the surface where it is highly influenced by the saturation vapor pressure associated with the SST.

A key consideration in global climate change research and forecasting is how the humidity distribution will respond to a climate forcing that increases the surface temperature. The first guess has traditionally been that the distribution of relative humidity will remain approximately fixed in some averaged climatological sense, so that increases in surface temperature will result in significant increases in the mixing ratio of water vapor in the atmosphere. These changes have consequences for the climate through the greenhouse effect of water vapor, and also for the hydrological cycle through the increased capability of the atmosphere to both provide moisture in regions of precipitation and also to carry it away from regions of new moisture deficit. The interactions among the water vapor distribution, surface temperature, and the hydrologic cycle over land and ocean are critically important, and the EOS observations and scientific investigations are directed toward a more-integrated understanding of these connections and their role in determining the future climate of the Earth. The combination of detailed information on clouds and more-accurate information on the vertical distribution of water vapor will be used by several EOS IDS investigations to better understand the processes that maintain water vapor in the atmosphere and the potential role of these processes in climate sensitivity and change.

2.2.4.4 *Water vapor in global climate models*

Global climate models contain an explicit atmospheric moisture balance equation, which includes evaporation from the surface, transport through the atmosphere, and precipitation. These models typically produce a strong water vapor feedback when they are forced with doubled carbon dioxide, or some other climate forcing, and this feedback contributes a significant part of the temperature increase (Hansen et al. 1984; Cess et al. 1990). Attempts are currently being made to include explicit cloud water and ice budgets as part of the climate modeling process,

and these interact very strongly with the water vapor distribution.

There are many reasons why simulations of water vapor in climate models are very difficult. The water vapor gradient is large, especially in the vertical where specific humidity varies by several orders of magnitude. To properly compute water vapor transport in the atmosphere requires high spatial resolution in both the horizontal and vertical directions. The spatial resolution of current GCMs is not sufficiently high, and many of the numerical schemes have difficulty conserving the water vapor field (Rasch and Williamson 1990). Parameterizations of sub-grid boundary-layer processes, convection, and soil moisture are difficult. The thick anvil clouds associated with deep cumulus towers contain a huge number of ice particles. These particles detrain away from the convection regions and are the main source of humidity in the middle and upper troposphere of the broad subtropical subsidence region (Sun and Lindzen 1993). Climate models are only beginning to explicitly account for cloud water and ice, their transport, and their evaporation to provide a source of water vapor in the free atmosphere. EOS data will play an important role in validating the new generation of climate models that explicitly include cloud water and ice, both in terms of the cloud simulation and the interaction of the cloud simulation with the water vapor budget.

Despite the difficulties encountered in computing water vapor transport, many climate models simulate the global water vapor field reasonably well. The most reliable element of the water vapor simulation is the total precipitable water. Comparisons of observations and 28 AMIP GCMs show that the models tend to underestimate precipitable water over Northern America, over the zonal band 35°N-50°N, and globally (Gaffen et al. 1995). The mean seasonal cycles are reasonably well simulated, but with a wide range among models. There is a clear tendency for the models to overestimate the poleward transport over much of the globe.

Due to the lack of a global data set, it is very difficult to validate the model simulations of the upper-tropospheric water vapor. Satellite-inferred humidity fields, such as those inferred from SAGE, TOVS, and the Geostationary Operational Environmental Satellite (GOES) radiance measurements, have been used to evaluate the validity of model simulations. There are a few studies addressing the field of relative humidity but none addressing specific humidity. Nevertheless, some GCMs are able to simulate either the seasonal variation of the upper-tropospheric relative humidity (Rind et al. 1991) or the large-scale pattern of the upper-tropospheric rela-

tive humidity as indicated by the brightness temperature in the water vapor absorption band (Salathé et al. 1995).

An important issue is the insertion of the H₂O information from the EOS sensors into research and operational NWP assimilation systems. Water vapor is important for the initialization of weather forecasts, and major centers are directly incorporating radiance information from sounding channels designed to detect the vertical distribution of water vapor in the atmosphere. A data assimilation product to be generated within the EOS program, GEOS-1, can be expected to apply the full complement of EOS H₂O sensors in determining the best water vapor fields. If operational weather prediction centers are given the applicable forward radiative transfer models to compute the observed radiances, given the humidity and temperature profiles, and are then supplied with the observed radiances within 2-3 hours after they are observed, they are likely to incorporate EOS data into their analysis/forecast cycle. This will benefit the forecasts issued and will also help in developing the optimal water vapor fields for use in research and monitoring. Radiation interacts with clouds at all scales.

2.2.4.5 *Needed observations of water vapor*

2.2.4.5.1 Available climatologies

A number of estimates of the climatological water vapor distribution are currently available. These come from operational analyses at the National Centers for Environmental Prediction (NCEP) (formerly the National Meteorological Center [NMC]) and the European Centre for Medium-Range Weather Forecasts (ECMWF), from special satellite data processing studies such as the TOVS Pathfinder, the GEWEX GVAP Project, and from attempts to provide high-spatial-and-temporal-resolution fields from geosynchronous satellites. All of these data sets suffer from one or more deficiencies that make them inadequate for detailed process studies, interannual variability studies, and long-term trends studies. Most are poorly calibrated or are based on an analysis system that changes with time. Most have rather poor vertical resolution, which makes it difficult to diagnose the processes that lead to the vertical distribution of water in the atmosphere.

Three-dimensional and time-continuous global water vapor data sets have been produced from four-dimensional data assimilations (Bengtsson and Shukla 1988; Kalnay and Jenne 1991; Schubert et al. 1995). Water vapor data from radiosonde and satellite measurements are integrated into global climate models. The assimilated field is thus consistent with measurements and modeled

physical processes. Its purpose is to provide research quality data sets suitable for climate studies.

Long-term radiosonde measurements of water vapor have been made routinely at selected locations over land. For temperatures below -40°C and relative humidities below 20%, radiosonde measurements are not accurate. Consequently, few radiosonde measurements are available in the upper troposphere (Peixoto and Oort 1983). The sensitivity of OLR to a given mass of water vapor peaks at the rather cold temperatures and low humidities of the upper troposphere, so that these observational problems are serious. The density of sounding is rather high in North America and Europe but not in other regions. Except for a few island stations, there are practically no upper-air soundings over the oceans. Compared to satellite-retrieved water vapor data, the radiosonde measurements have a high vertical resolution but usually are made only twice a day. Radiosonde measurements of water vapor suffer from various degrees of uncertainties. For the United States, radiosondes using the carbon hygrometer humidity sensor have problems that have been identified. Errors approaching 25% are reported (Wade 1994). Nevertheless, radiosounding of the water vapor in the middle and lower atmosphere is used for the validation of passive remote sensing of water vapor because of its availability and traditional acceptance as the standard of reliability. Validation in the upper troposphere, particularly in the tropics, is sorely lacking. Airborne measurements may make a significant contribution in this area in the near future. Humidity sounders may be placed on commercial aircraft, and additional flights of manned and unmanned research aircraft are needed.

The global distribution of water vapor is also derived from satellite measurements of radiances in the solar, thermal IR, and microwave spectral bands. Operational and research-mode water vapor profiles are derived from TOVS on NOAA satellites (Smith and Woolf 1976; Susskind et al. 1987). The total precipitable water (PW) over the oceans has been successfully retrieved from satellite microwave radiance measurements, such as SMMR and SSM/I (Prabhakara et al. 1985; Wentz 1994). Due to the high variability of land emissivity, microwave radiometry is not used to retrieve PW over land. It is generally believed that the accuracy of PW retrieval is better than 10%.

Water vapor in the stratosphere and the upper troposphere has been routinely retrieved from the SAGE II solar occultation instrument since 1985 (Rind et al. 1993). The SAGE II water vapor has a high vertical resolution of 1 km but a low horizontal resolution of several hundred kilometers. It also has a low sampling rate, with only

a few observations per month in equatorial regions, and it can only detect the humidity in regions that are cloud-free, so its sampling frequency in the upper troposphere is further reduced. The MLS gives a somewhat better spatial coverage in the upper troposphere because it is less sensitive to thin clouds (Read et al. 1995).

2.2.4.5.2 Needed improvements

In every respect, the available water vapor data sets are inadequate for climate studies. Radiosondes are limited to land areas with an uneven geographical distribution, and satellite retrievals suffer from poor vertical resolution and accuracy. It can be anticipated that global data sets with high spatial resolution (both horizontal and vertical) must come from satellite measurements. The areas that need the most improvement are:

- *Vertical resolution of water vapor, especially over oceans.* Most important convection and cloud processes are small scale (Starr and Melfi 1991). Information on high-vertical-resolution water vapor distribution is essential for understanding and parameterizing these processes. Current satellite-retrieval techniques cannot resolve water vapor distribution within a layer of ≈ 3 -4 km thick.
- *Upper-tropospheric specific humidity.* The outgoing longwave radiation and, hence, the greenhouse effect are sensitive to the specific humidity in the upper troposphere. Currently, the upper-tropospheric humidity cannot be obtained from radiosonde measurements. Current satellite retrievals of the upper-tropospheric humidity have either poor vertical resolution (HIRS and GOES/Meteosat), or low data sampling rate (SAGE II). A substantial improvement in vertical resolution, accuracy, and spatial sampling is expected from AIRS/AMSU/HSB on the EOS PM-1 satellite.
- *Water vapor content in the planetary boundary layer.* Convective activities depend critically on the properties of the planetary boundary layer. Due to the effect of surface temperature on the satellite-radiance measurement and the inherent low vertical resolution of the satellite water vapor retrievals, accurate retrievals of water vapor content in the planetary boundary layer are not currently available.
- *High-accuracy, high-vertical-resolution ground-based lidar measurements.* Developments of methodologies for retrieving water vapor from satellite-radiance measurements require high-accuracy and high-vertical-

resolution water vapor measurements for calibration and validation. Even radiosondes cannot provide such measurements, especially in the upper troposphere.

The EOS instruments, particularly AIRS/AMSU/HSB, seek to provide better vertical resolution and better calibration for tropospheric water vapor measurements. Improved horizontal- and vertical-resolution measurements in the stratosphere will be provided by HIRDLS and MLS. SAGE III will provide very accurate monitoring of water vapor trends in the stratosphere. High-vertical-resolution measurements in the upper troposphere in the presence of thin clouds will be provided by MLS. Assimilation of all of these data into a global analysis using a high-quality assimilation system will provide data sets necessary for studying and monitoring atmospheric water vapor.

2.2.5 Precipitation

2.2.5.1 Role and importance of precipitation

Rainfall is essential for the existence of the Earth's population. It determines the distribution of vegetation, food supply, and habitats of the diverse living species of plants and animals. Rainfall maintains life, but excessive as well as deficient rainfall may cause loss of life, property damage, and failure of crops, resulting in widespread socio-economic hardships. Tropical or midlatitude cyclones, thunderstorms, typhoons, or hurricanes that produce excessive rainfall become major natural disasters and afflict many nations. While flash floods can occur in a relatively short time, from a few hours to a few days, the effect of drought is often more widespread and lasts much longer and may produce even more-disastrous effects. During severe drought, crops fail and topsoils are blown away, often forcing massive migration, starvation, and death of people and animals. The severe drought of the Sahel in the 1980s, which lasted for close to a decade, is a grim example.

In addition to having a direct impact on human society, rainfall plays a central role in governing the climate of the Earth. The latent-heat release in convection is the main source of energy that drives the general circulation of the atmosphere, since much of the solar radiation absorbed by the Earth is used to evaporate water, which later condenses to release latent heat in the atmosphere during precipitation. It is responsible for many scales of tropical motions ranging from hurricanes, tropical cyclones, and monsoon depressions, to the much-larger-scale intraseasonal oscillation, Walker circulation, and Hadley circulation. Not only is tropical rainfall essential in main-

taining atmospheric motions in the tropics, it is known to have strong influence on weather and climate in the extratropics. Latent-heat release in tropical convection forces atmospheric motions that disperse heat and moisture into the extratropics, diverting subtropical jetstreams, and altering rainfall patterns in midlatitudes.

2.2.5.1.1 Role in climate system operation

From a climate system point of view, rainfall is a key agent that connects the Earth's oceans, atmosphere, land, and the biosphere through the global hydrologic cycle. Water vapor evaporated over the tropical and subtropical oceans is partially released locally in the form of rainfall in convection and partially transported away from the place of origin. The continental land surface receives its moisture supply via surface precipitation through a combination of local recycling processes and import of moisture from the adjacent oceans. The water received by the land is given up in part to the atmosphere by evaporation from the land surface or evapotranspiration from plants and trees. Except for a fraction of the water that is stored as underground water or as snow cover, most of the net fresh water input on the land surface is returned to the ocean through river run-off, thus completing the hydrologic cycle. The global precipitation rate determines the average "residence time" of water substance in the atmosphere, ocean, and land, which sets the internal clocks within these different components of the climate system. It is estimated that the replacement time scale (the reservoir size divided by the precipitation rate) is on the order of 10 days for the atmosphere (the fast component), 10^2 - 10^3 days for the land (the intermediate component), and 10^3 - 10^5 days for the upper ocean (the slow component). The Earth climate system evolves as a complex interplay among processes partaking in the fast, intermediate, and slow components giving rise to a myriad of fundamental climatic spatial and temporal time scales.

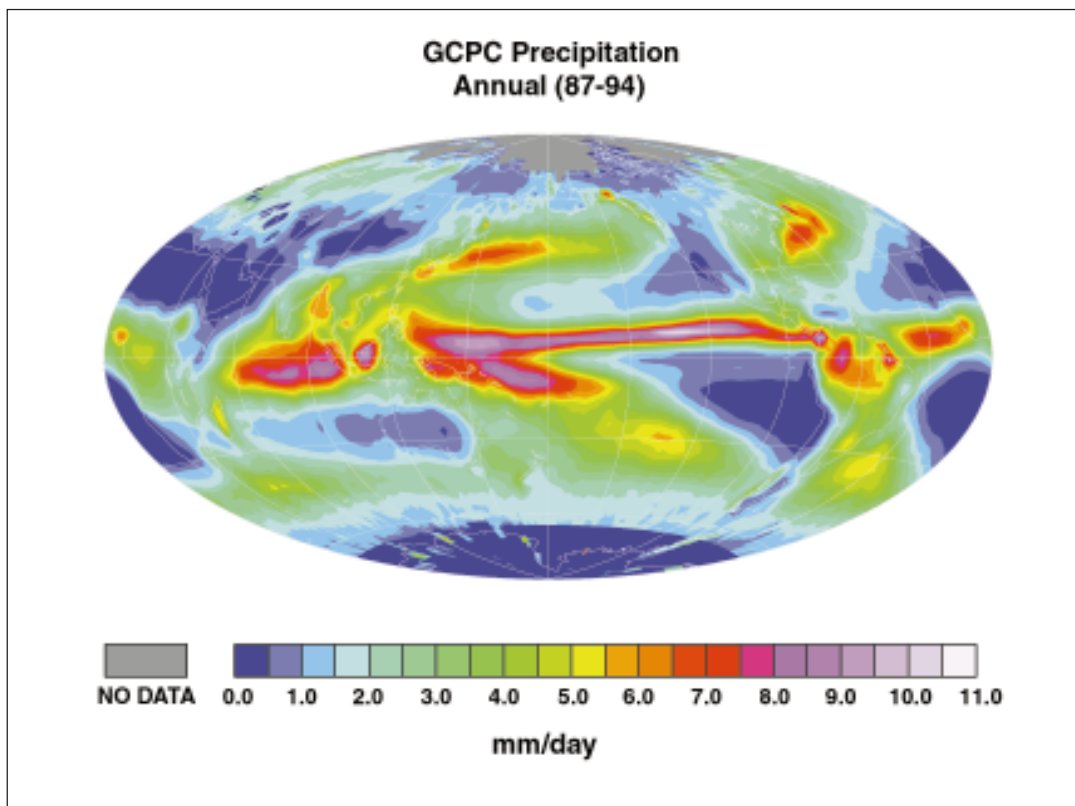
On the intermediate-to-slow time scale, clouds and water vapor are two of the most important factors that determine the Earth's climate, by virtue of their ability to reflect or absorb solar radiation and to re-emit longwave radiation. Both clouds and water vapor are intimately related to precipitation. Water vapor is transported from the surface to the upper troposphere by strong updrafts in moist convection, while cool, dry air is brought down by convectively induced downdrafts. The amount of water vapor that remains in the atmosphere and the amount of water substance in clouds in the atmosphere are therefore dependent on how much atmospheric water is depleted by precipitation. Measurements of precipitation are therefore central to a better understanding of the maintenance

of cloud populations. The interaction between the latent heating from precipitation and the radiation heating due to clouds and water sets up a large spatial gradient in total heating in the interior of the atmosphere and at the Earth's surface. This heating gradient is key to driving atmospheric large-scale mean motions in the tropics, such as the Walker and Hadley circulations, and the transient eddies in the extratropics. These motions produce the mean meridional transport of heat which is required to maintain the equilibrium equator-to-pole temperature difference of the present climate. It has been estimated that between the clear and cloudy region, such as the ITCZ and the subtropical subsidence region, the horizontal latent-heating gradient due to precipitation is about twice as large as the radiation heating set up by clouds and water vapor (Stephens and Webster 1984). While latent heating due to deep convection tends to be concentrated in the midtroposphere, cooling from cloud shielding of shortwave tends to occur most strongly at the surface. Consequently, the net heating gradient in the vertical is altered, leading to either enhanced stability (reduced precipitation) or reduced stability (increased precipitation).

Precipitation also plays an important role in the Earth's climate control through its influence on ocean temperature and circulation. Input of fresh water from precipitation on the ocean surface may alter the salinity and hence the density gradient in the ocean, resulting in alterations of ocean dynamics. Examples of regions where the precipitation-induced salinity changes may have an effect on ocean dynamics, which may have an impact on global climate, are the tropical western Pacific warm pool and the North Atlantic region. The former is the region for the TOGA COARE field experiment, which is aimed at providing a better understanding of the coupling between atmospheric hydrologic processes, in particular precipitation, and surface fluxes over the warm pool region (Webster and Lukas 1992). Fresh water input in the tropical western Pacific may have an influence on the timing and duration of major El Niño events. Similarly, the fresh water input at high latitudes may alter the large-scale ocean circulation and impact climate in the North Atlantic region (see discussion in Section 2.2.5.1.2).

Finally, it is common knowledge that precipitation is essential for the survival of the biosphere. Without precipitation, vegetation disappears and land turns into desert. Recent modeling studies have established that the land-surface vegetation may provide a positive feedback on rainfall through its ability to: (a) evapotranspire, (b) trap solar radiation within leaf organizations, (c) regulate evapotranspiration by stomatal control, and (d) modify (generally increase) the surface roughness on the scale of

FIGURE 2.12



Annual average (1987-1994) precipitation measurements from the Global Precipitation Climatology Project (GPCP).

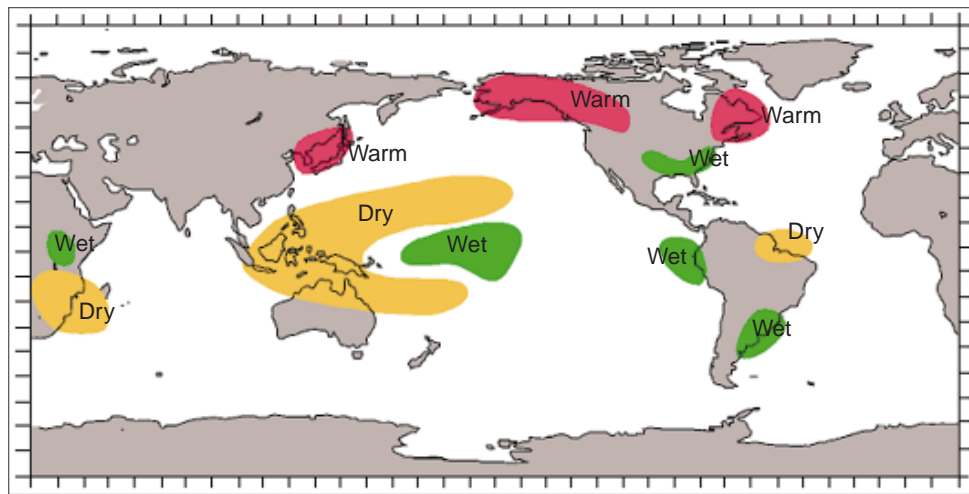
turbulent eddies. Model sensitivity studies have shown that the above biogeophysical effects, both individually and jointly, have produced increased rainfall over different regions of the world. Model experiments on deforestation areas such as the Amazon have shown a significant impact of precipitation on the regional scale. From a synthesis of modeling results of the last decade, it has been shown that the biosphere-atmosphere interactions play an important role in redistributing continental precipitation to fulfill the survival and growth requirements of different biomes: forests, pasture, agricultural lands, and deserts. However, studies of the scale dependence of the vegetation influence on global precipitation patterns are still rudimentary and have many uncertainties. For a better understanding of precipitation-biosphere interaction, improved representation of hydrologic processes, systematic investigations, and observational collaborations are essential.

2.2.5.1.2 Importance in global change scenarios

Because of the lack of long-term global data, the possible effects of global warming on precipitation rely mainly on

projections from climate models. Given the uncertainties of precipitation prediction in climate models (see Section 2.2.5.5), these projections should be considered extremely tentative. Based on the IPCC report (Houghton et al. 1996), the following scenarios for precipitation are possible due to global warming. Due to doubling of CO_2 , there will be an increase in global precipitation from 3-15%, mostly in the higher latitudes during the boreal winter. This increase is related to the dependence of saturation vapor pressure on temperature and to the poleward movement of the midlatitude oceanic storm tracks. In a warmed climate the drying season commences earlier and the soil moisture content in mid-to-late summer may be decreased. This warming and drying may be amplified through the summer by enhanced solar heating because of the drier surface and associated reduction in cloudiness. Climate models show reasonable agreement in terms of the occurrence of the summer land warming and drying in midlatitudes due to global warming. Changes in the monsoon circulation can also be expected. Model results from IPCC suggested that the East Asian monsoon may be strengthened because of the increased thermal

FIGURE 2.13



Summary of large-scale climate anomalies associated with the warm phase of the ENSO cycle during the Northern Hemisphere winter (Ropelewski and Halpert 1987, used with permission from the American Meteorological Society).

contrast between the Eurasian landmass and the tropical oceans, which are least sensitive to global warming (Held 1993).

The before-mentioned possible global change scenarios are for equilibrium climate, which may take hundreds of years to reach. The real impact of global change depends upon the way the Earth's climate evolves from the present to the future equilibrium climate. Hence the transient response to anthropogenic forcing over the next 50-to-100 years is most important. Here, the effect of the ocean is paramount, and changes of precipitation may play a critical role. Coupled models suggest that the increase in precipitation at high latitudes may result in a deceleration of the Atlantic oceanic meridional circulation, causing a reduction in the oceanic transport of heat from tropics to extratropics. This reduction in heat transport may lead to a delayed warming or even a temporarily cooler climate over the North Atlantic region as global warming progresses. A similar mechanism will cause a delayed warming in the southern oceanic regions (Held 1993; Manabe et al. 1991). Monitoring precipitation over the oceans will put us in a better position to detect the fingerprints of global warming and to develop sound policies for global change.

2.2.5.2 Spatial and temporal distribution of precipitation

The distribution of precipitation is highly inhomogeneous in space and time. The spatial and temporal scales range

from thundershowers that last from several minutes over a distance of less than a kilometer to displacements of major precipitation systems that cover distances of thousands of kilometers and last over several years. Because of the wide range of variability, the long-term, accurate mapping of global precipitation is a daunting task. To obtain a global rainfall map, land-based rain gauge, satellite-derived oceanic rainfall, and sometimes model-generated rainfalls are often blended in an optimal way to minimize the bias from each individual estimate. Figure 2.12 shows a typical annual distribution of rainfall from the Global Precipitation Climatology Project (GPCP) (Huffman et al. 1995). The major rainy zones include the eastern Pacific Intertropical Convergence Zone (ITCZ), the South Pacific Convergence Zone (SPCZ), the Asian monsoon, and the rainbelt over the Amazon and central Africa.

These rainfall patterns undergo large annual cycle variations (not shown). Most important, there is strong year-to-year variability in the precipitation pattern. Figure 2.13 shows the composite changes in precipitation patterns associated with an ENSO event including the timing of the extreme over different regions. Widespread drought conditions can be found over the maritime continent, northern and central Australia, northern India, northern Brazil, Central America, and southeast Africa. Flood conditions are found over the equatorial central Pacific, the west coast and southeast coasts of South America, and the southeast and southwest United States.

In the tropics, the precipitation pattern shifts are very robust and are directly related to the changes in tropical SST due to ENSO. In the extratropics, the changes in precipitation result from alteration of the subtropical jetstreams and wintertime storm tracks, and have much larger variability. There are also other observed trends and large interannual and possibly interdecadal changes in precipitation that are not related to ENSO. An example is the dramatic and prolonged decrease in rainfall in the Sahel region from the early 1970s to the late 1980s. There are speculations that desertification induced by overgrazing may have been responsible for the prolonged drought (Charney 1975). Another plausible explanation is that the observed precipitation “trend” is a part of the natural decadal or bi-decadal oscillation in SST in the coupled ocean-atmosphere system. At present, there is no generally-accepted explanation for the occurrence of such a prolonged drought, much less a method to predict its occurrence.

2.2.5.3 Integration of ground data

Surface observations of precipitation play an important role in the validation and calibration of remote sensing and model-based estimates of large-scale precipitation patterns. Rainfall measurements from rain gauge networks have been traditionally regarded as the “ground truth” of precipitation. Recently, ground-based radar data have also been used to improve sparse rain gauge-derived precipitation data. However, it should be mentioned that, for both oceans and remote areas of the globe, precipitation is poorly observed and almost no ground data are available for these locations.

In order to serve the needs of climate study, great efforts have been made to collect ground precipitation data over the globe. In the United States, the National Climatic Data Center (NCDC) routinely archives hourly and 15-minute precipitation data from over 5,000 stations nationwide. Legates and Willmott (1990) published a mean seasonal variability in gauge-corrected global precipitation. Recently, Legates has created a global-mean monthly precipitation archive based on surface and ship observations. In addition, the database of the Global Historical Climatology Network (GHCN) contains monthly total precipitation from 7533 stations throughout the world. Both of these databases are now accessible through EOSDIS. The GPCP seeks to construct an optimal global data set from microwave, IR, and in situ data. A global, two-year, 2.5-degree data set for 1987-1988 is currently available (<http://orbit-net.nesdis.noaa.gov/gpcp/>).

The Next Generation Weather Radar (NEXRAD) program of the United States has made great efforts to develop, procure, and deploy an advanced Weather Sur-

veillance Radar-1988 Doppler (WSR-88D) system that will replace the current meteorological radar system. The first WSR-88D system was installed near Oklahoma City, Oklahoma, in 1990. When the last installation is completed during 1996, a NEXRAD network consisting of at least 136 operational WSR-88D systems will cover most of the contiguous United States and provide quality high-resolution, real-time-processed precipitation data. Weather radar systems have been developed in Europe (European Communities COST-73 Weather Radar Network), Japan (the Japanese Weather Radar Network), Australia, and many other countries; however, there is no worldwide radar database yet.

Because rain gauge observations are point values, it is necessary to apply interpolations, such as distance weighting and Kriging, to render the spatial distribution of precipitation. However, highly-inhomogeneous characteristics of precipitation distribution (described in Section 2.2.5.2) require an unmanageably high-density gauge network. On the other hand, because radar images provide the high-resolution, real-time precipitation distribution, compositing techniques have been developed that use high-quality gauge measurements within the radar image to calibrate the precipitation quantity. These composite gauge-radar data are considered more reliable for climate studies. Climate statistics also offer alternative means to integrate precipitation.

2.2.5.4 Precipitation in climate models

Because precipitation is a noisy field, it is one of the most difficult hydrologic parameters for which to validate simulations. At present the reliability of precipitation estimates in climate models is not very high. Yet it should be noted that uncertainties in global rainfall estimation, especially over the oceans, are as large if not larger than those among climate models. Recently, an intercomparison study of precipitation processes in over 30 state-of-the-art global-climate models has been carried out under the AMIP. The result of AMIP should provide a snapshot of the current capability of global-climate models in precipitation simulation. The following is a summary of the results for the AMIP global-climate models (Lau et al. 1995).

- Most models are able to produce a global precipitation rate to within 10-20% of the observed, which is comparable to the standard deviation among “observations.”
- Most models show a conservation of water substance, to within 5-10%. Because of the possible large errors in regional water balance associated with a 5% error in global water balance, it is not clear that climate

models with that level of deficiency can be tolerated for global-change regional precipitation assessment. Models that have Evaporation-Precipitation (E-P) imbalance over 10% are clearly not suited for long-term climate water resource assessments.

- While most models can simulate the annual cycle reasonably well, compared with the observations in a region with strong annual cycles, models generally have problems in simulating the annual cycle in a region of strong dynamical control, i.e., $P-E > 0$.
- Models differ substantially in regional- and subcontinental-scale rainfall variability. Model rainfall estimates disagree most in the eastern Pacific ITCZ, the South and Southeast Asian monsoon, and the Mexican region. All models underestimate the northward advance and the intensity of the East Asian summer rainbelt. The extratropical wintertime rain belts are also underestimated in most models.
- All models underestimate the frequency of occurrence of the light-rain category ($< 1 \text{ mm day}^{-1}$). This may be related to the poor treatment of shallow clouds and stratocumulus in all climate models.
- Over 90% of the models show enhanced skill in prediction of precipitation pattern changes due to SST-anomaly forcing from the ENSO. However, all models show no skill in extratropical interannual rainfall prediction.
- More than 30% of the models seem to have unrealistically strong land-lock convection and excessive rainfall over steep terrain. These may be due to the deficiency in the vertical coordinates over steep terrain. Spurious, small-scale rainfall, likely due to truncations and other basic numerical problems, is still present in a number of the climate models.

Given the above assessment, it is clear that climate models still have a long way to go before their precipitation projections for climate change can be trusted with any reasonable level of reliability.

2.2.5.5 Needed satellite measurements and algorithms

To better understand the role of precipitation in driving the Earth's climate and to validate global climate models, quantitative information regarding the global distribution of precipitation is essential. For understanding the physics of precipitation processes and its interaction with land surfaces, daily sampling over the globe and sampling at

shorter time intervals over selected target regions are both desirable. Because it is impossible to set up uniform networks of rain gauges over the entire globe, satellite rainfall retrieval algorithms will play a vital role in producing realistic global rainfall distributions. The synergistic use of remote-sensing, ground-based, and model-based rainfall information is of paramount importance.

Satellite retrieval of rainfall has a heritage beginning with the passive microwave measurements made by the Electrically Scanning Microwave Radiometer (ESMR) on board Nimbus-5, SMMR on Nimbus-7, and SSM/I on the Defense Department satellites and the Microwave Sounding Unit (MSU) on NOAA polar-orbiting satellites. In addition, AVHRR on NOAA operational satellites and similar IR sensors on geostationary weather satellites, GOES and the Japanese Geostationary Meteorological Satellite (GMS), have provided extremely useful estimates of rainfall. Both the microwave and the IR measurements have their inherent drawbacks. For example, microwave measurements are reliable over the oceans but not over land because of the large variation of background emissivity over land. IR measurements rely on relationships between cloud top temperature and rainfall, which may vary greatly in different rainfall regimes and are indirect at best. TRMM employs a suite of sensors including one passive TMI, one VIS/IR scanner (VIRS), and one active precipitation radar (PR), and aims at producing the best rainfall estimation from space, which is based on algorithms that combine measurements from all the sensors.

Within the EOS measurement system, the key instruments for precipitation measurement are the AMSR-E and the HSB on the EOS PM-1 platform. While there may be an inherent sampling problem with precipitation measurements based on a single satellite, because of the strong diurnal cycle in rainfall, it is expected to be eased by coordinated measurements by microwave and IR sensors flown by Europe and Japan. It is important that different equator crossing times are maintained for these different satellites, so that different parts of the diurnal cycle can be sampled. It is expected that knowledge gained from TRMM will be used for guidance to improve the rainfall estimates from combined satellites and sensors. The use of hybrid algorithms, which combine IR and microwave information, will be pursued. While TRMM is uniquely equipped to make measurements of precipitation over the tropical regions, through a combination of passive and active microwave instruments, it falls short of providing global coverage. Hence, the TRMM capability should be extended to higher latitudes with AMSR-class passive microwave sensors from sun-synchronous polar orbits with morning and afternoon crossing times. The Advanced Earth Observing Satellite II (ADEOS-II) and METOP mis-

sions will carry AMSR and the Multi-frequency Imaging Microwave Radiometer (MIMR), respectively. Both missions are suitable for sampling precipitation at high latitudes; however, they will both be in midmorning orbits. The SSM/I and SSM/IS passive microwave radiometers on the DMSP series can provide precipitation measurements, but these have less precision and coarser spatial resolution than those from either AMSR or MIMR. Moreover, the DMSP measurements continue to be at dawn and dusk, which limits their utility for capturing the diurnal dynamics of precipitation processes. There is a need for sampling precipitation globally in an early afternoon crossing orbit to complement the morning measurements from the ESA and the National Space Development Agency of Japan (NASDA) platforms. AMSR-E on the EOS PM-1 satellite is intended to achieve this objective. Without AMSR-E or a similar passive microwave imager, a significant portion of the science supported by the EOS PM-1 mission will be seriously compromised. Without an AMSR or MIMR, placement of a modified TMI would at least accomplish the desired diurnal sampling, although not at the desired spatial resolution.

2.2.6 Atmospheric circulation, hydrologic processes, and climate

2.2.6.1 Hydrologic processes and the tropospheric circulation

As discussed in the previous chapters, hydrologic processes due to clouds, water vapor, and precipitation are critically important in determining the Earth's climate. The presence of these hydrologic parameters in the atmosphere significantly alters the Earth's radiation budget, in particular in generating differential heating between the tropics and the polar regions, between the ocean and the land, and between clear and cloudy regions. This differential heating is the main driver of the atmospheric large-scale circulation. The essential component of the circulation is wind.

The continuity equation of water vapor for the atmospheric branch of the hydrologic cycle can be written in the following form:

$$\frac{\partial W_a}{\partial \tau} = \nabla \cdot \sum \langle q \vec{V}_a \rangle = E - P$$

This equation shows the linking among the total atmospheric columnar water vapor, W_a , the divergence of vertically-integrated moisture by wind $\nabla \cdot \sum \langle q \vec{V}_a \rangle$, evaporation E , and precipitation P . It is clear from this equation that moisture transport plays an important role

in determining the amount and the distribution of water vapor in the atmosphere. The dynamics of atmospheric motions also determine the amount and types of clouds in the atmosphere. The rising motions in the tropics and the subsidence in the subtropics associated with the Hadley circulation are closely linked to the meridional distribution of E-P. Climatologically, the subtropics is a source of atmospheric moisture (E-P>0) and the equatorial and midlatitude regions are sinks (E-P<0). Within the tropics, the eastern Pacific is a source and western Pacific a sink of atmospheric moisture, connected via the Walker circulation. On a more-regional scale, the land regions of the Asian monsoon act as a sink, and the adjacent oceans are sources of moisture during the boreal summer monsoon (Lau et al. 1995). The annual reversal of the surface wind and associated low-level moisture convergence play an important role in determining the distribution of precipitation and evaporation over the monsoon region.

In addition, many weather and climate anomalies in the extratropics have been attributed to climate anomalies in the tropics, e.g., the Pacific-North American teleconnection pattern (Horel and Wallace 1981; Wallace and Gutzler 1981). This kind of remote response to local forcing is effected by transport and energy dispersion via the atmospheric circulation. Hence consideration of the atmospheric wind circulation is indispensable in order to understand the role of the global hydrologic cycle, clouds, water, and precipitation on regional and global climate fluctuations.

2.2.6.2 Large-scale circulation and climate feedback processes

For long-term climate changes resulting from natural and anthropogenic causes, knowledge of the changes in the radiative forcing of the planet is of foremost importance. It is now recognized that, while the radiative forcings such as that due to doubling of CO_2 may be small, feedback processes in the climate system may amplify the initial response to the radiative forcing, thus making it more detectable. These feedback processes involve the interaction of clouds, radiation, and dynamics and in many cases, especially for seasonal-to-interannual time scales, the large-scale circulation plays a fundamental role. To fully understand climate feedback mechanisms, it is important to keep in mind that physical processes from cloud-scale radiation to global circulation interactions are taking place simultaneously at all time scales. In the recent debate regarding the thermostat mechanisms for tropical SST (Ramanathan and Collins 1991), many authors (Fu et al. 1992; Hartmann and Michelsen 1993; Lau et al. 1994; and others) have pointed to the importance of the large-scale circulation vs. that due to local feedback as the

fundamental mechanism for regulating tropical SST. Pierrehumbert (1994) argued that radiative cooling from the dry atmosphere of the subsiding branch of the large-scale circulation may be needed to balance the heat accumulated by the warm tropical ocean. Bony et al. (1995) have shown that the sensitivity of the greenhouse effect to SST is much larger for seasonal and interannual variations compared to climate-change estimates. It is quite obvious that for seasonal-to-interannual changes, it is the change in large-scale circulation, not local cloud-radiative processes, that is causing the large sensitivity. This is confirmed by the recent work of Lau et al. (1997), which shows that the sensitivity of outgoing longwave radiation to SST is reduced by a factor of three when the effect of the large-scale divergence is removed. Thus it is extremely important to consider the contribution of the large-scale circulation when using seasonal and interannual variability as surrogates for climate change.

Atmospheric transport of energy and water by large-scale motions may also play a critical role in determining the amount of polar amplification associated with climate change. Atmospheric motions carry more than half of the poleward transport of energy at most latitudes, and all of the transport into polar latitudes.

2.2.6.3 *Need for satellite measurements of wind*

EOS will provide some very important measurements of surface wind speed and direction over the oceans from scatterometry (NASA SeaWinds scatterometer on QuikSCAT and also on ADEOS II) and passive microwave remote sensing. These data will be particularly critical for estimating air-sea exchanges of heat, momentum, and moisture.

For a proper description of the global tropospheric circulation useful for climate studies, a global wind measurement accuracy of 2-3 m s⁻¹ with a horizontal resolution of 100 km and a vertical resolution of about 1 km in the vertical, preferably higher resolution (0.5 km) in the planetary boundary layer, with a temporal coverage of 6 hours is required (Baker et al. 1995). The current global radiosonde network for tropospheric wind measurements is grossly inadequate to provide this coverage, especially over the tropical and southern oceans and for the remote continental and desert regions. Yet these regions, such as the central equatorial Pacific, the Indian Ocean, and the midcontinental desert region, are the most important climatic regions because they encompass the sources and sinks of atmospheric heat and moisture, where potential and kinetic energy are exchanged through the large-scale circulation. The network of radiosonde wind observations is not expected to be significantly upgraded in the next several decades because of the budget constraints of world

governments. Currently, a reliable mapping of the global wind distribution has relied mainly on four-dimensional data assimilation systems. However, in the absence of real data input over large regions, 4DDA data are mostly model climatologies. That is why the largest differences between wind products for the major 4DDA systems, e.g., ECMWF and NMC (Trenberth and Olsen 1988) are found over the southern oceans. Similarly, observation system simulation experiments with lidar winds are found to have the largest impact over the tropical and southern oceans (Baker et al. 1995). In the current EOS payloads for AM-1 and PM-1, there is no consideration for tropospheric wind-measuring instruments. In the new EOS/ESE era, we should seriously consider a satellite wind-measurement system, such as a lidar, which depends on aerosol backscatter, to provide uniform, global, and continuous wind coverage. These satellite winds will then be assimilated into state-of-the-art 4DDA systems to provide a global wind measuring system in the troposphere. Improved tropospheric wind measurements will also allow trajectory computations for atmospheric chemical species that will have an impact on global change.

2.2.7 *Strategy for combining observations and modeling*

To solve many of the scientific problems described in preceding sections requires a thoughtful and careful integration of improved observations with improved theory and models. Figure 2.14 illustrates a strategy for combining EOS global satellite observations with critical modeling and correlative observational efforts. None of these efforts alone can provide a high degree of confidence in climate predictions, such as those used to study global-warming scenarios. At the largest time and space scales, climate models must be tested against global satellite observations of temperature, humidity, precipitation, clouds, radiation, and large-scale wind fields. Current global models do not perform adequately on this test, diminishing our confidence in their predictions. Direct tuning of climate models to satellite observations must be avoided, however, as it invalidates the independence of the data, and provides no new or improved physics to the model. Instead, cloud-scale and regional-scale models with more-advanced cloud physics and radiation physics must be tested against both field experiment data and satellite data. Once the models pass these tests, they can be reduced to simpler forms for inclusion in global climate models. In addition, field experiment and surface data must be used to verify the accuracy of the global satellite remote-sensing observations, and provide additional information not accessible from space.

Confidence in climate predictions will require, as a minimum, the achievement of four basic elements:

- detailed dynamical, physical, and radiative cloud models verified against field and laboratory experiments for a wide range of cloud types and conditions;
- successful construction of simplified climate model parameterizations derived from more-detailed models and theories and validated against observations;
- availability and verification of the accuracy of global satellite observations of key variables; and
- agreement of climate models with satellite observations on a range of space and time scales (global, synoptic, regional, yearly, seasonal, monthly, and diurnal).

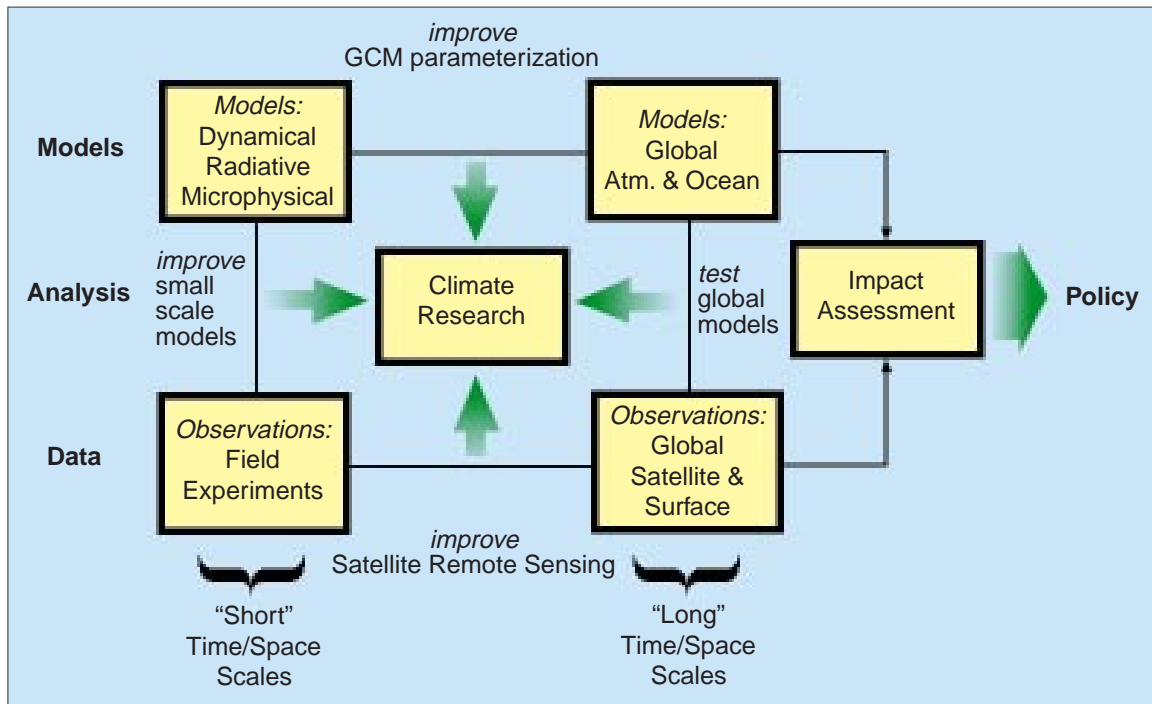
In fact, this process is iterative, and all four tasks should be pursued simultaneously.

Satellite data useful for climate studies have historically been collected by both operational satellite systems (NOAA, Department of Defense [DoD]) as well

as NASA research satellites. Some operational systems such as GOES and AVHRR are designed for an operational weather forecasting mission and therefore lack the high-quality calibration required for climate research instruments such as ERBE and SAGE II (McCormick et al. 1992). This accurate and stable calibration is critical to providing climate data that will improve GCMs as well as monitor climate change. An advantage of the operational systems, however, is a well-developed and stable data-processing and distribution system, as well as the commitment to long-term data collection that results in climate records with long time coverage and minimal data gaps. A critical problem for national and international efforts in remote sensing of climate is to bring together high calibration and characterization of remote-sensing instruments with a commitment to collect homogeneous measurements over a long period of time.

EOS will attempt to describe the radiative effects of clouds on fluxes at the large scale for climate monitoring and for validation of GCMs, mesoscale models, and cloud-scale models. A profitable interaction between EOS and the new generation of models will be fostered by the participation of EOS teams in small-scale, intensive measurement programs such as ARM and the GEWEX-WCRP

FIGURE 2.14



Observational strategy for the determination of the role of clouds and radiation in climate. Confidence in climate model predictions of global warming requires iterative improvements in global climate modeling, global satellite observations, and cloud/regional-scale modeling of cloud dynamical and radiative processes (Wielicki et al. 1995, used with permission from the American Meteorological Society).

TABLE 2.5

<i>PARAMETER NAME</i>	<i>UNITS</i>	<i>ACCURACY Abs.:REL</i>	<i>TEMPORAL RESOLUTION</i>	<i>COMMENTS</i>
Irradiance, Solar, Total	Wm ⁻²	0.1% :: 0.001%	1/(2 min)	ACRIM

Total solar irradiance

BSRN. ARM and the BSRN function continuously and can provide much data to EOS researchers, in some cases at no cost. Through GCIP, the ARM Southern Great Plains (SGP) site is already targeted for the validation of operational tools such as the NMC Eta mesoscale model. A surface-based CPR will soon be deployed at the ARM SGP site. The same sites can be used as a focal point for the development and validation of EOS remote sensing.

Concentration on a limited number of well-instrumented sites will foster interactions even within EOS. Strong interaction between detailed surface-based observations and high-quality global remote sensing by EOS is critical to gaining increased understanding of the radiative effects of clouds and the proper simulation of cloud effects in climate models.

2.3 Required satellite measurements and data sets

2.3.1 Summary of required satellite observations

We present here an abbreviated description of some key EOS observations related to radiation, clouds, water vapor, precipitation, and atmospheric circulation. More-complete descriptions of the EOS instruments and detailed descriptions of data products can be found in the EOS Data Products Catalog.

2.3.1.1 Total solar irradiance

The total solar irradiance at the Earth is about 1370 Wm⁻² and was observed to vary peak to peak by about 1.5 Wm⁻² or 0.1% during solar cycle 21. If this amount of total solar irradiance change were applied continuously to a relatively sensitive climate model [$\Delta T = 1.0 \text{ K}/(\text{Wm}^{-2})$], a surface temperature response of about 0.26 K would be induced. This temperature change is small compared to those that might result from a doubling of CO₂, but it is significant compared to the estimated 0.5 K warming during the last century, and would be significant in the problem of early detection and assessment of global climate change. By using overlapping flights of ACRIM instruments (0.1% absolute accuracy), it is believed that a relative precision of 0.001% can be achieved. This relative precision would be sufficient to detect any climatically-significant changes in total solar irradiance on time scales of up to a century (see Table 2.5).

2.3.1.2 Radiative fluxes

All of the energy exchange between the Earth and space is achieved by radiative transfer, as is much of the impor-

tant energy exchange within the climate system. To provide points of reference for required accuracies, consider that observed changes in climate forcing associated with total-solar-irradiance changes are about 0.25 Wm⁻², and the expected climate forcing from doubling CO₂ is about 4 Wm⁻². Variations of radiative fluxes within the climate system that are associated with season, location, weather, or natural interannual variability are much larger, often on the order of 100 Wm⁻². While it seems beyond current capability to measure the small changes in fluxes within the climate system that are directly associated with total solar irradiance or atmospheric CO₂ variability, useful measurements can be made of the magnitude and variability of radiative fluxes in the climate system, and these can be used to both understand climate and validate climate models. Current climate models appear to be in error by tens of Wm⁻², so that an achievable accuracy of 5 Wm⁻² is very useful, despite being larger than the expected climate forcings.

In planning to make observations of radiative fluxes within the climate system it is helpful to consider the general requirements for resolution of the frequency spectrum, spatial resolution, temporal resolution, and calibration. To accurately estimate the total radiative energy flux, the measurements must span the range of frequencies that contribute significantly to the flux. In instruments such as CERES, which are specifically designed to measure total solar or longwave energy flux, a thermal detector is used. In order to understand what causes a change in radiative flux it is useful to separate contributions from

different wavelength intervals that respond differently to changes in temperature, clouds, aerosols, water vapor, or other greenhouse gases. MODIS provides both high spectral and spatial resolution.

In order to measure the gross energy balance of the Earth, global coverage is required; global coverage is achievable from a single polar-orbiting satellite. In order to measure fluxes in the atmosphere and at the surface, and to evaluate the role of clouds in the radiation balance, it is necessary to have sufficient spatial resolution in the basic observations to have a high probability of obtaining measurements for which the instrument field of view contains no clouds. A reasonable frequency of such clear scenes is obtained for pixels of about 25 km across, though much higher spatial resolution can be required for other purposes such as cloud detection. For example, to adequately reduce the effect of partially-filled pixels on the determination of cloud properties, it has been estimated from Landsat data that the size of pixels should be no larger than 250 m. This resolution has been provided for two of the channels on MODIS.

In addition to wavelength dependencies, the dependence of outgoing radiance on satellite viewing angle can be used to retrieve physical properties such as aerosol abundance or type. In many retrieval problems using solar radiation, knowledge of the bidirectional reflectance distribution function (BRDF: the dependence of the radiance on the solar and satellite viewing angles at the point of interest for a particular scene type) is critically important. MISR, which can view a pixel as small as 275 m in 4 frequencies from 9 angles during a single overpass, was designed to provide accurate BRDFs and exploit the potential of angular sampling for remote sensing. CERES has been provided with two scanning instruments on early platforms so that the angular and diurnal sampling errors can be minimized. One scanner is intended to operate in the cross-track direction to provide global coverage, while the other rotates in azimuth to provide better angular sampling.

Temporal sampling is also an issue. Radiation fluxes respond strongly to changes in clouds, humidity, and temperature, which evolve on time scales of hours. It is not possible to follow these high-frequency developments from polar-orbiting satellites, although the aggregate effect of these phenomena can be captured in spatial and temporal averages of data from polar-orbiting satellites. An important systematic variability of radiative fluxes occurs on the diurnal time scale. At most points on the globe a strong 24-hour rhythm in insolation drives corresponding variations in clouds, temperature, and radiative fluxes. The diurnal variation is important because it represents a known forcing which can be used as a probe

to understand the response of certain facets of the climate system. It is also important to remove any systematic effects of the diurnal cycle on our sampling of radiative fluxes and clouds. For this reason, it is necessary to fly radiation and cloud instruments in at least two sun-synchronous orbits simultaneously, usually an AM (~10:30) and PM (~13:30) equator crossing time, plus either one precessing orbit or a third sun-synchronous orbit. Current planning is for TRMM and TRMM follow-on to provide the precessing orbit to complement the two EOS sun-synchronous orbits. This provides observations of most points at six local times each day, sampling which is sufficient to resolve the diurnal cycle and to reduce monthly mean time sampling errors to values similar to errors expected for calibration and angular sampling (Wielicki et al. 1996). An important complement to these global diurnal-resolving radiation measurements will be the planned launch of a Geostationary Earth Radiation Budget (GERB) broadband radiometer on the Meteosat Second Generation (MSG) spacecraft scheduled for launch in 2000.

2.3.1.2.1 TOA fluxes

Fluxes of solar and longwave radiation at the TOA are the energy exchange of the Earth with space. These fluxes are modulated by clouds, temperature, humidity, aerosols, and greenhouse gases, and the relationship between these fluxes and the surface temperature is a fundamental measure of climate sensitivity. The natural variability of TOA fluxes on decadal time scales can be observed with highly-calibrated instruments in properly maintained orbits (e.g., Cess 1990). With a combination of highly-accurate broadband radiance measurements from CERES and higher-spatial and spectral-resolution radiances from cloud imagers (VIRS on TRMM, MODIS on EOS AM-1 and PM-1), each flown in two sun-synchronous orbits with different equator crossing times (CERES, MODIS), as well as a precessing orbit (CERES, VIRS), it will be possible to provide TOA flux measurements with an estimated absolute accuracy of 2.5 Wm^{-2} for LW and 5 Wm^{-2} for SW. These absolute accuracies are specified as the absolute error of a large ensemble of instantaneous observations with a mean emitted TOA LW flux of 240 Wm^{-2} and a mean reflected SW flux of 300 Wm^{-2} , typical of the EOS AM-1 or EOS PM-1 orbit solar illumination conditions. Instantaneous relative errors (1 standard deviation) for the same ensemble of instantaneous observations are expected to be about 5 Wm^{-2} for LW and about 15 Wm^{-2} for SW TOA fluxes for CERES pixels of about 20 km in diameter (see Table 2.6). These instantaneous satellite swath data will be useful for many scientific investigations.

For global-scale diagnostic studies and model validation, spatially-gridded and time-averaged data will more commonly be used. Spatial gridding will start at $1^\circ \times 1^\circ$ latitude-longitude resolution and be nest-able to coarser grids. Two important products for use in analysis and model validation are planned. Global synoptic maps at three-hour intervals are planned for use in validating weather prediction models. Daily and monthly mean maps also will be generated and made available for modeling and diagnostic studies. For monthly averages it is planned to also produce mean monthly diurnal variations of flux quantities at three-hourly intervals and also to use scene identification information to produce separate clear-sky and total-sky fluxes, so that the role of clouds in modifying these fluxes is isolated. Because averaging reduces random errors associated with sampling and inversion, the expected accuracies of the monthly-mean, spatially-averaged data are greater than those of corresponding instantaneous observations. The error estimates assume a three-satellite system (see Table 2.7).

2.3.1.2.2 Surface and internal atmospheric fluxes

Using measurements of temperature, water vapor, and clouds from EOS instruments as input to a model calculation, and constraining these models further with TOA flux measurements, it is possible to produce estimates of radiative fluxes at the surface and at several levels within the atmosphere, for example, at 500 mb and at the tropopause. A similar suite of instantaneous, synoptic, and diurnally- and monthly-averaged products is planned. The accuracies of the surface and internal atmospheric radiative fluxes that will be achieved are less certain than for fluxes at the TOA, since more modeling is required and the experience base with this type of flux estimate is less developed than for the TOA problem.

2.3.1.3 Cloud properties

Because of the critical importance of cloud properties to many of the outstanding global climate questions (Section 2.4), and because of the extreme difficulty in deriving accurate cloud data, cloud properties are derived by many

TABLE 2.6

PARAMETER NAME	UNITS	ACCURACY ABS::REL	TEMPORAL RESOLUTION	HORIZONTAL RESOL::COVER	COMMENTS
Radiative Fluxes, SW, TOA	Wm^{-2}	15 Wm^{-2} :: 15 Wm^{-2}	100 Hz	20 km :: G	CERES/MODIS
Radiative Fluxes, LW, TOA	Wm^{-2}	5 Wm^{-2} :: 5 Wm^{-2}	100 Hz	20 km :: G	CERES/MODIS

Top-of-atmosphere radiative fluxes: Instantaneous pixels

TABLE 2.7

PARAMETER NAME	UNITS	ACCURACY ABS::REL	TEMPORAL RESOLUTION	HORIZONTAL RESOL::COVER	COMMENTS
Radiative Flux, LW, Statistics, TOA, Clear_sky and Total_sky	Wm^{-2}	TBD	1/(3hr) [avg]	$1.0^\circ \times 1.0^\circ$:: G	Synoptic OLR at 3-hour intervals
Radiative Flux, SW, Statistics, TOA, Clear_sky and Total_sky	Wm^{-2}	TBD	1/(3hr) [avg]	$1.0^\circ \times 1.0^\circ$:: G	Synoptic solar radiation at 3-hour intervals
Radiative Flux, LW, Statistics, TOA, Clear_sky, Total_sky, Monthly_Avg	Wm^{-2}	3 Wm^{-2} :: 2 Wm^{-2}	1/mon	$1.0^\circ \times 1.0^\circ$:: G	Monthly averages of longwave radiation
Radiative Flux, SW, Statistics, TOA, Clear_sky, Total_sky, Monthly_Avg	Wm^{-2}	4 Wm^{-2} :: 3 Wm^{-2}	1/mon	$1.0^\circ \times 1.0^\circ$:: G	Monthly averages of shortwave radiation

Top-of-atmosphere radiative fluxes: Gridded data

of the EOS instruments. Clouds affect almost all of the EOS observations, and, as a result, the different measurement strategies used by each instrument provide fundamentally different information on cloud properties:

- **MODIS:** Provides high-spatial-resolution, global, cloud-property measurements. This instrument represents a major improvement in global cloud measurements for a wide range of cloud properties. MODIS is the prime instrument for EOS cloud-property measurements. Roughly 12 cloud spectral channels, 0.25- to 1-km fields of view.
- **ASTER:** Extremely high-spatial-resolution regional data used to verify the effect of sub-pixel cloud variability on MODIS global cloud retrievals. Eight cloud spectral channels, 15-m-to-90-m spatial resolution for selected 60-km regions.
- **MISR:** Multi-angle views (9 along-track views from nadir to 70° fore and aft) with high spatial resolution (275 m to 1.1 km) in 4 solar spectral channels. Used for narrowband cloud anisotropy measurements as well as stereo cloud heights for broken cloud fields. Especially useful for studies of the anisotropy of non-plane-parallel broken cloud fields, and non-spherical ice particles (Kahn et al. 1996).
- **AIRS:** High-spectral-resolution but coarse-spatial-resolution infrared data used to measure the spectral variation of cloud emittance and confirm the interpretation of cloud particle phase and size determined using higher-spatial-resolution but coarser-spectral-resolution MODIS data. Up to 2300 spectral channels in a 14-km field of view.
- **EOSP:** Unique solar-reflected radiation polarization measurements at coarse spatial resolution (10 km). Useful at small optical depths and for cloud particle size and phase estimation. EOSP and MISR are the instruments most likely to have information on ice crystal shape.
- **GLAS:** Active lidar useful for remotely sensing cloud height and base of optically-thin clouds. Only nadir viewing. Offers the most accurate cloud screening and cloud-height checks of MODIS global cloud retrievals.
- **SAGE III, HIRDLS:** Height measurement and detection of extremely thin cloud in the upper troposphere or stratosphere (i.e., polar stratospheric clouds and thin

cirrus). Spatial resolution is very coarse (200 km) but these instruments give unique measurements of sub-visible clouds.

- **CERES:** Broadband, highly-calibrated coarse-spatial-resolution radiation-budget measurements. CERES data are used to constrain cloud-property retrievals in the CERES data products by providing a broadband TOA flux constraint. The objective of CERES cloud products for matched CERES/MODIS and CERES/VIRS fields of view is a radiatively consistent set of cloud and radiation data.
- **VIRS:** Provides an advance over current AVHRR for TRMM cloud measurements with 5 spectral channels, a 2-km nadir field of view, and on-board solar calibration. Data will be analyzed as part of CERES cloud/radiation data products.

Tables 2.8-2.17 summarize accuracies and space/time characteristics of the key cloud data products planned for EOS. The tables are presented individually for each major cloud property. Since accurate tools to objectively validate global cloud measurements have only recently become available, all estimates of global cloud property accuracies are very preliminary. The combination of multiple EOS sensors and new ground-based and aircraft-based instrumentation will provide a great improvement in the knowledge of the accuracy of cloud property measurements and their dependence on cloud type and climate region. As a minimum, accuracies will differ for clouds over ocean and land, for optically-thick versus thin clouds, and for low versus high clouds. The validation of these cloud properties will be a major effort within EOS and will require both dedicated field campaigns (e.g., FIRE) as well as long-term surface site data (e.g., ARM).

2.3.1.3.1 Cloud fractional area coverage

The fractional-area coverage of clouds over the globe should be monitored with the precision necessary to measure changes of a few percent in $2.5^\circ \times 2.5^\circ$ regions over a period of decades.

Our ability to measure the global distribution of tropospheric clouds from space will be greatly enhanced by MODIS, because of enhanced spatial resolution (250 m, 1 km) in the traditional visible and thermal infrared spectral channels, because of new spectral channels which will enhance the detection, cloud height, and particle size determination of thin cloud (1.38, 8.5, 13.3, 13.6, and 13.9 μm), and, finally, because of its greatly improved solar calibration using both on-board sources and lunar stabil-

TABLE 2.8

PARAMETER NAME	ACCURACY Abs::REL	TEMPORAL RESOLUTION	HORIZONTAL RESOL::COVER	VERTICAL RESOL::COVER	COMMENTS
MODIS Cloud Cover	0.05 :: 0.05	2/day [d,n]	5 km :: G	N/A :: Cloud	
MISR Cloud Fraction, Altitude-Binned (Nadir)	TBD :: TBD	1/(2-9 day) [d]	17.6 km :: G	4 km :: Atmos	

Cloud fractional area coverage

TABLE 2.9

PARAMETER NAME	ACCURACY Abs::REL	TEMPORAL RESOLUTION	HORIZONTAL RESOL::COVER	VERTICAL RESOL::COVER	COMMENTS
MODIS Cloud Height, Top	50 hPa :: 50 hPa	2/day	0.5° :: G	N/A :: Cloud	
AIRS Cloud Height, Top	0.5 km :: 0.25 km	2/day [d,n]	50x50 km :: G	N/A :: Cloud	
GLAS Cloud Height, Top	:: 75m	25 ms	70 km ::	75 m ::	
EOSP Cloud Pressure, Top	30 hPa :: 30 hPa	1/day [d]	40 km :: G	30 hPa :: Cloud_top	
HIRDLS Cloud Height, Top	0.4 km :: 0.4 km	2/day [d,n]	400x400 km :: G	0.4 km :: Trop	
SAGE-III Cloud Height, Top	0.2 km :: 5%	1/(2 min), 30/day	<2°x<1° :: G	0.5 km :: Strat/Trop	

Cloud height

TABLE 2.10

PARAMETER NAME	ACCURACY Abs::REL	TEMPORAL RESOLUTION	HORIZONTAL RESOL::COVER	VERTICAL RESOL::COVER	COMMENTS
MODIS Cloud Optical Depth	10% :: 20%	1/day [d]	5 km :: G	N/A :: Cloud	
MODIS Cloud Emissivity, Top	::	2/day	0.5° :: G	N/A :: Cloud	
AIRS Cloud Emissivity, IR Spectral (3-14 μm)	0.05 :: 0.025	2/day [d,n]	50x50 km :: G	N/A :: Cloud	
EOSP Cloud Optical Thickness	20% :: 10%	1/day [d]	40 km :: G	Column :: Cloud	
GLAS Thin Cloud /Aerosol Optical Depth	20% ::	1/(2-16 day)	2-100 km :: G	N/A :: Atmos	For thin clouds only

Cloud optical depth and IR emissivity

TABLE 2.11

PARAMETER NAME	UNITS	ACCURACY Abs::REL	TEMPORAL RESOLUTION	HORIZONTAL RESOL::COVER	VERTICAL RESOL::COVER	COMMENTS
MODIS Cloud Particle Phase	water/ice	90% Conf :: 90% Conf	2/day [d,n]	5 km :: G	N/A :: Cloud	
MODIS Cloud Particle Size (Effective Radius)	μm	0.4 :: 2.0	1/day [d]	5 km :: G	N/A :: Cloud	
EOSP Cloud Particle Phase	water/ice	:: 95% Corr	1/day [d]	100 km :: G	N/A :: Cloud_top	
EOSP Cloud Particle Size	μm	25% :: 25%	1/day [d]	100 km :: G	N/A :: Cloud_top	

Cloud particle size and phase

TABLE 2.12

PARAMETER NAME	ACCURACY Abs::REL	TEMPORAL RESOLUTION	HORIZONTAL RESOL::COVER	VERTICAL RESOL::COVER	COMMENTS
AMSR-E Cloud Liquid_Water Content	3 mg cm ⁻²		14 km :: Ocean	N/A :: Trop	Pixel-scale observations
AMSR-E Cloud Liquid_Water Content	1 mg cm ⁻²	1/day	1.0° ::	N/A :: Trop	Spatial averages for daily maps

Cloud liquid water path

ity checks. Multi-angle observations in shortwave channels from MISR will provide improved angular directional models for use in cloud detection. ASTER will provide data to verify the effect of beam filling on MODIS cloud detection, especially for small cumulus clouds over land.

2.3.1.3.2 Cloud height

In order to understand the role of clouds in the longwave radiation balance and to monitor interannual variability in the distribution of cloud top height, it is desirable to obtain cloud top height measurements with an accuracy of about 0.3 km for monthly means. This gives an uncertainty in the cloud top temperature for tropospheric clouds of about 2 K, and an uncertainty in blackbody emission of about 3 Wm⁻² for low clouds in the tropics, and less for colder clouds. The spatial resolution of the basic measurements should be close to 250 m, in order to avoid errors associated with partially-filled scenes.

A variety of instruments will give information on cloud top heights or pressures. The best combination of

spatial resolution and global coverage will be provided by MODIS, but other instruments will provide cloud height data based on other techniques, which will add value to the cloud top height data set. AIRS cloud data sets can be determined in conjunction with high-quality determinations of the temperature and humidity fields. GLAS will provide very precise and sensitive data on cloud top from lidar measurements, but only along the satellite ground track. These data will be very useful for validating other methods of cloud height determination and also for detecting cloud tops in polar darkness and above snow where other methods may have large uncertainties. EOSP makes use of polarization information, which other instruments do not. HIRDLS, MLS, and SAGE III use limb measurements of the atmospheric emissivity in different wavelength regions and can give information on thin clouds in the stratosphere and upper troposphere.

TABLE 2.13

PARAMETER NAME	ACCURACY Abs::REL	TEMPORAL RESOLUTION	HORIZONTAL RESOL::COVER	VERTICAL RESOL::COVER	COMMENTS
AIRS/AMSU Temperature Profile	1.0 K :: 0.4 K	2/day [d,n]	50 × 50 km :: G	1 km :: Atmos	
MODIS Temperature Profile	0.5 K :: 0.5 K	2/day	5 km :: G (clear)	:: Atmos (20 levels)	
HIRDLS Temperature Profile	1 K < 50 km; 2 K > 50 km :: 0.3 K < 50 km; 1 K > 50 km	2/day [d,n]	400 × 400 km :: G	1 km :: 5-130 km	
MLS Temperature Profile	< 2 K :: 0.2-1 K	2/day [d,n]	1.3° × 2.5° :: 82°N-82°S	2 km :: 5-80 km	
SAGE-III Temperature Profile (O ₂ Conc.), Solar	2 K :: 2K	1/(2 min), 30/day	< 2° × < 1° :: G	1 km :: 6-70 km	
TES Temperature Profile	2 K :: 0.2 K	1 (4-day survey) /mon	53 × 169 km :: G	4-6 km :: 0-33 km	

Atmospheric temperature profile

2.3.1.3.3 Cloud visible optical depth and infrared emissivity

Cloud visible optical depth is an integrated measure of the reflecting power of a cloud at visible wavelengths, which accounts for reflection by both liquid water and ice. The relationship between visible optical depth and reflected solar radiation depends on the solar zenith angle, the albedo of the underlying surface, and a number of variables of lesser importance. Radiative fluxes are most sensitive to changes in cloud optical depth when the optical depth is relatively small where the most precision in measurement is therefore required. Global remote measurements of cloud optical depth should have a detection threshold of 0.05 and an accuracy of about 20%.

2.3.1.3.4 Cloud particle size and phase

Cloud particle size has importance for the formation of clouds and precipitation, and also for the radiative effects of clouds. For water clouds the optical depth is approximately proportional to LWP divided by cloud particle radius, so percentage errors in LWP and cloud radius are about equally important for deducing the relationship between cloud substance and cloud optical depth. For a fixed LWP, the albedo of a water cloud varies by about 0.2 as the effective droplet radius is changed from 5 μm to 25 μm . If the insolation is 400 Wm^{-2} , then an albedo accuracy of about 0.01 is required to give an accuracy in absorbed solar radiation of 5 Wm^{-2} . In order to obtain this accuracy in computing albedo from observations of LWP and effective radius, the effective radius should be known to an accuracy of 1.25 μm . It is anticipated that the effective radius of clouds may be obtainable with this accuracy from MODIS, MISR, and EOSP measurements. These instruments may also be used to distinguish ice clouds from water clouds with a certainty of 95%.

2.3.1.3.5 Cloud liquid/ice water path

Cloud liquid/ice amounts can be inferred from visible optical depth using a model, if the effective particle radius and phase are known. Observations of LWP over water surfaces can be obtained in a different way, from microwave measurements (e.g., MIMR or AMSR). Albedo increases most rapidly with liquid water content when the liquid water content is small; albedo becomes only weakly sensitive to liquid water amount changes when the liquid water amount is large. From the perspective of its effect on planetary albedo then, precision in the measurement of relatively small values of liquid water below about 5 mg cm^{-2} is required. A precision of about one part in fifty within this range, or 0.1 mg cm^{-2} is necessary to give the required accuracy of 5 Wm^{-2} for fluxes

of solar radiation. This accuracy in LWP is much higher than that offered by the methods available for inferring it.

2.3.1.3.6 Lightning

Lightning flashes associated with electrical discharges in clouds can be detected from space. These observations provide a global survey of thunderstorm occurrence and cloud electrification processes. LIS will detect such occurrences with a relatively inexpensive instrument on TRMM and succeeding satellites. LIS will provide a wide variety of data on the number, location, and intensity of lightning flashes as observed by a spaceborne camera.

2.3.1.4 Atmospheric temperature profiles

In order that temperature profile measurements from satellites can provide a significant benefit to current weather forecasting efforts, it has been determined that profiles with an accuracy of 1 K for vertical scales on the order of 1 km are required. In addition, horizontal spatial resolution of 50 km or less is desirable to better define the positions of fronts and other thermal features. The AIRS instrument was designed with these requirements in mind. High spatial resolution and scanning capability are required so that the effects of clouds on the infrared radiances used for sounding can be minimized. The addition of AMSU microwave channels improves the capability of the AIRS instrument to provide accurate temperature profiles under partly cloudy conditions.

MODIS provides a backup temperature profile retrieval capability about equal to that of current operational instruments. Other instruments provide measurements of temperature with lower horizontal resolution either by limb-viewing in the stratosphere (HIRDLS, MLS, SAGE III) or as a required adjunct to retrievals of atmospheric chemical constituents (TES).

Most modern data assimilation systems for use in numerical weather prediction assimilate radiances from satellite temperature sounders rather than inverted temperatures. This is because the inversion process is underdetermined for the high vertical resolution used in weather prediction models, so that the inversion is often an optimal modification of an a priori profile. The model forecasts often contain realistic temperature variations of small vertical scale that cannot be resolved with nadir sounding channels, and the assimilation of remote sounding data should not corrupt this information. It is better to modify the model temperature profile optimally to conform to the radiances, than to make the model temperatures conform to an inverted temperature profile based on some other a priori temperature profile. This process can be incorporated into the data assimilation system with all

TABLE 2.14

PARAMETER NAME	UNITS	ACCURACY ABS::REL	TEMPORAL RESOLUTION	HORIZONTAL RESOL::COVER	COMMENTS
AIRS Level-1B Radiance	$Wm^{-2} sr^{-1} \mu m^{-1}$	0.2° NEdT :: 0.2° NEdT	2/day [d,n]	15 × 15 km :: G	
AMSU Level-1B Radiance	K	0.2° NEdT :: 0.2° NEdT	2/day [d,n]	15 × 15 km :: G	
HSB Level-1B Radiance	K	0.2° NEdT :: 0.2° NEdT	2/day [d,n]	15 × 15 km :: G	

Radiances for temperature profiling

TABLE 2.15

PARAMETER NAME	ACCURACY ABS::REL	TEMPORAL RESOLUTION	HORIZONTAL RESOL::COVER	VERTICAL RESOL::COVER	COMMENTS
AIRS/AMSU/HSB Humidity Profile g/kg	10% (goal) :: 5%	2/day [d,n]	50 × 50 km :: G	2 km :: Atmos	
AIRS/AMSU/HSB Precipitable Water (mm)	5% :: 3%	2/day [d,n]	50 × 50 km :: G	N/A :: Atmos	
AMSR-E Precipitable Water (g/cm ²)	0.2 g cm ⁻² ::		14 km :: Ocean	Column :: Trop	MIMR also planned for METOP-1.
AMSR-E Precipitable Water - gridded	<0.1 g cm ⁻² ::	1/day	1.0° ::	Column :: Trop	MIMR also planned for METOP-1.
HIRDLS H ₂ O Concentration	5-10% :: 1-10%	2/day [d,n]	400 × 400 km :: G	1 km :: 5-70 km (given accuracies for 7-70 km)	
HIRDLS H ₂ O Concentration - gridded	5-10% :: 1-10%	2/day [d,n]	4° × 4° :: G	1 km :: 5-70 km	
MLS H ₂ O Concentration	<5% :: 1-10%	2/day [d,n]	1.3° × 2.5° :: 82°N-82°S	2 km :: 5-80 km	
MODIS Water Vapor Profile	5-50% :: 6-50%	2/day	5 km :: G (clear)	:: Atmos (15 levels)	
SAGE-III H ₂ O Conc & Mixing Ratio, Solar	10% :: 15%	1/(2 min), 30/day	<2° × <1° :: G	1 km :: 3-50 km	
SAGE-III H ₂ O Conc & Mixing Ratio, Lunar	10% :: 15%	1/(2 min), 30/day	<2° × <1° :: G	1 km :: 3-50 km	
TES H ₂ O/HDO Mixing Ratio	:: 0.5-50 ppmv	1 (4-day survey) /mon	53 × 169 km :: G	2-6 km :: 0-33 km	

Water vapor profiles and precipitable water vapor column

other data types if a forward radiative transfer model for the sounding channels is available. For these reasons radiances for the frequency intervals required for sounding temperature and humidity must be made available to operational weather prediction centers within two-to-three hours of collection, so that they may be assimilated and contribute to timely forecasts. For the desired precision of 1 K in temperature sounding, these radiances must have an accuracy corresponding to 0.2 K noise equivalent temperature difference. AMSU and HSB provide microwave radiances that improve soundings of temperature and humidity in the presence of clouds.

2.3.1.5 Water vapor

Water vapor measurements in the atmosphere are critically important for many purposes. Water vapor mass mixing ratios vary from about 20 g/kg in the tropical boundary layer to less than 1 g/kg in the Arctic winter. Humidities vary between about 10% and 100% of the saturation value for a particular location. Water vapor decreases upward because of the decrease of temperature with altitude and reaches values around 2 ppm near the tropical tropopause. From the perspective of its effect on the energy balance of the Earth, about the same fractional precision at all levels of the atmosphere is required because a molecule of water at the tropopause is much more effective in reducing emitted energy than a molecule of water vapor in the tropical boundary layer. This precision is required for layers of about equal thickness in height at all levels. An accuracy of 5-10% is very useful. Such accuracy is difficult to achieve at all levels with a single instrument. AIRS/AMSU/HSB provide good spatial resolution and adequate vertical resolution in the lower troposphere, while limb-viewing instruments such as SAGE III, HIRDLS, and MLS provide good vertical resolution and precision in the upper troposphere and lower stratosphere. Profiles of somewhat less accuracy and resolution can also be obtained from IR channels on MODIS, when AIRS/AMSU/HSB are not available.

2.3.1.6 Precipitation

Measurement of precipitation by passive remote sensing from space is a developing science. Requirements for spatial and temporal resolution and accuracy vary widely depending on the application. For global-scale studies and climate model validation, averages over 100-km \times 100-km regions with accuracies of 10% would be extremely useful. The primary technology for estimating precipitation globally during the EOS period will be passive remote sensing from microwave imagers such as MIMR and AMSR-E, which have comparable capabilities. The ac-

curacies for these measurements will likely be less than required, but will represent an improvement over current estimates. In the tropical regions precipitation estimates will also be available from the precipitation radar on TRMM.

2.3.1.7 Winds and circulation

Direct wind measurements with an accuracy of 10% for wind speed and a 20° random error would be very useful. Such measurements for near-surface winds over the ocean are attainable with scatterometers such as SeaWinds. Wind speed estimates with comparable accuracy are also available from passive microwave radiometers, and the along-track data from the Dual-Frequency radar Altimeter (DFA). Sea-surface wind velocity measurements are very useful for calculating air-sea exchange of heat, momentum, and moisture between the ocean and the atmosphere, and are also useful in validating surface wind simulations in climate models and numerical weather prediction models.

No direct measurements of wind speed in the free troposphere or in the boundary layer over land will be included in the planned phases of EOS. Wind vectors in the free troposphere will be derived indirectly by assimilating data into a global model. Direct measurement of tropospheric winds with lidar would be very useful for both weather forecasting and climate modeling, but this capability was eliminated from the EOS program for cost reasons. New technologies that would make direct wind measurements economically and reliably from space should be pursued.

2.3.2 Critical surface observations and field experiments

A vital component of any Earth observing system aimed at obtaining long-term global observations of multiple components of the Earth-atmosphere-ocean system is a well-coordinated ground-based monitoring network together with periodic field experiments. The importance of this part of any integrated global climate observing system cannot be underestimated. This component is vital for the purposes of: 1) assessing the accuracy of satellite-derived geophysical parameters, such as aerosol optical thickness, surface radiation budget components, cloud top altitude, sea surface temperature, total ozone content, etc.; 2) evaluating the precision and accuracy of the satellite sensor calibration through intercomparison of satellite measurements with calculations based on radiative transfer computations using surface and aircraft measurements of atmospheric composition; and 3) providing enhanced information on the characteristics of

TABLE 2.16

PARAMETER NAME	ACCURACY ABS::REL	TEMPORAL RESOLUTION	HORIZONTAL RESOL::COVER	VERTICAL RESOL::COVER	COMMENTS
AMSR-E Precipitation (Land)	100% ::		6 km :: Land		MIMR also planned for METOP-1.
AMSR-E Precipitation (Ocean, 2 layers)	50% ::		14 km :: Ocean		MIMR also planned for METOP-1.
AMSR-E Precipitation (Land) mapped	20% ::	1/day	1.0° ::		MIMR also planned for METOP-1.
AMSR-E Precipitation (Ocean) mapped	10% ::	1/day	1.0° ::		MIMR also planned for METOP-1.

Precipitation

TABLE 2.17

PARAMETER NAME	UNITS	ACCURACY ABS::REL	TEMPORAL RESOLUTION	HORIZONTAL RESOL::COVER	COMMENTS
SeaWinds Wind Vectors, Near-Surface	m s ⁻¹ , dg	> of 2 m s ⁻¹ or 10% rms (speed); 20° rms (direction) ::	90% of oceans every 2 days	50 km :: Ocean (1600 km swaths)	
AMSR Wind Speed, Sea_sfc	m s ⁻¹	1.5 m s ⁻¹ ::		14, 25 km :: Ocean	MIMR also planned for METOP-1.
AMSR-E Wind Speed, Sea_sfc-averaged	m s ⁻¹	<0.5 m s ⁻¹ ::	1/day	1.0° ::	MIMR also planned for METOP-1.
Radar Altimeter Wind Speed, Along-track	m s ⁻¹	2 m s ⁻¹ ::		7 km :: Ocean	

Wind speed and direction near the ocean surface

surface and atmospheric constituents assumed in the remote-sensing retrievals using satellite observations. Space, surface, and aircraft approaches are all required to observe the range of critical physical processes that occur from the microscale (e.g., microphysical properties of clouds) to the macroscale (e.g., basin-wide SST variations associated with El Niño). To this end, many surface observational networks and airborne field experiments have been established. Highlighted below is a selection of these extremely important programs, emphasizing their role in improving the understanding of the role of clouds and radiation in climate.

2.3.2.1 FIRE

FIRE is an ongoing multi-agency, international program to support the development of improved cloud radiation parameterization schemes for use in climate models, to provide an assessment of the accuracy of ISCCP-derived

cloud products, and to test and develop new remote-sensing methods for future spaceborne missions and to assess their accuracy through intercomparisons with in situ microphysical measurements. FIRE has been conducted in two phases, the first from 1985-1990 and the second from 1991-1995, and has thus far concentrated on two cloud types: marine stratocumulus and cirrus.

Marine stratocumulus clouds exert a large influence on the radiation balance of the Earth-atmosphere-ocean system through their large areal extent, temporal persistence, and high reflectivity to solar radiation. Cirrus clouds, on the other hand, exert their greatest radiative influence on the Earth's climate through their effects on longwave radiation emitted to space. Both of these cloud types are spatially and temporally persistent in the Earth's atmosphere, and both create difficulty in the remote sensing of cloud properties from spaceborne sensors. As a direct consequence of the need to determine

the optical and microphysical properties of clouds from present and future spaceborne systems, such as MODIS, a need arose to conduct intensive field observations (IFOs) of marine stratocumulus and cirrus clouds. These two field campaigns, conducted as major components of FIRE (Cox et al. 1987), have focused exclusively on these two cloud types. Largely as a result of these four field experiments (conducted in 1986 and 1987; repeated and enhanced in 1991 and 1992), the radiative and microphysical properties of these cloud systems have been more extensively studied than others.

In all of these intensive field campaigns, emphasis has been placed on coordination between aircraft-, spacecraft-, and ground-based observing systems, and has led to a number of important insights. For marine stratocumulus clouds, outstanding problems include the discrepancy between observations and theory of the absorption of solar radiation by clouds, the discrepancy between remote sensing and in situ estimates of the effective droplet radius derived from spectral reflectance measurements, and the variability and spatial structure of stratocumulus clouds derived both from reflection and transmission measurements. For cirrus clouds, the thermal emission characteristics of these clouds suggest that the effective radius of ice crystals is much smaller than previously believed and, in addition, the thermal emittance of cirrus clouds is generally less than theoretically predicted for a given value of the visible albedo. These important results, described in detail by King (1993), lead immediately to the conclusion that carefully planned airborne field campaigns, together with coincident ground-based observations, are essential for assessing the accuracy and validity of satellite-derived geophysical cloud properties. Plans are currently being developed for FIRE phase III, which will likely include campaigns in complex environments such as Arctic stratus clouds overlying sea ice, a regime for which remote sensing of cloud properties from space is especially difficult.

2.3.2.2 *GEWEX*

GEWEX is an international program of the WCRP that focuses on observing and modeling the hydrologic cycle and energy fluxes in the atmosphere, at the land surface, and in the upper layers of the oceans. This enormous program plans to compare results from ongoing process studies aimed at improving the parameterization of clouds, radiation, and surface processes with coincident satellite observations and modeling studies (Chahine 1992). As such, it has a considerable validation component that will prove a valuable source of data to assess the accuracy of satellite retrieval schemes such as the remote sensing of

atmospheric temperature and moisture profiles, vertically integrated water vapor (precipitable water), cloud base altitude, surface longwave flux, and cloud optical and microphysical properties. Since passive satellite observations are especially sensitive to cloud top properties, a valuable role of GEWEX is assessing the longwave radiation flux reaching the Earth's surface under cloudy conditions in both a dry and humid environment. Here again a combination of surface observations, temperature and moisture soundings, focused airborne observations, and modeling studies will provide an opportunity to assess the accuracy of satellite-derived geophysical properties and to translate the results of process studies to the global scale.

The GEWEX program will focus on five main components of the hydrologic cycle: clouds and radiation, atmospheric moisture, precipitation, ocean fluxes, and land surface processes. Since current satellite-derived moisture data are accurate to ~10-20% over the oceans and 20-30% over the land, since water vapor is the most important greenhouse gas, and since clouds and their radiative properties play a major role in cloud feedback processes, process studies such as GEWEX are vital to enhancing the value of the spaceborne observations to be provided as part of the Earth Science Enterprise (ESE) program (TRMM, EOS AM-1, EOS PM-1). Over the oceans, two current experiments are providing valuable data on ocean fluxes, including cloud radiative properties, TOGA and the World Ocean Circulation Experiment (WOCE). In late 1992 and early 1993 COARE was conducted in the western tropical Pacific as part of the TOGA program, and this large multinational and multiagency program obtained numerous data sets on cloud radiative and microphysical properties as well as passive and active microwave measurements of precipitation patterns. This valuable data set will provide much needed information that will enable algorithms to be tested and evaluated for both the EOS (MODIS, GLAS, AMSR) and TRMM programs.

2.3.2.3 *Climate Variability (CLIVAR) Project*

The CLIVAR Project of the WCRP (WCRP 1995) seeks to understand and predict climate variability on interannual-to-centennial time scales. It is initially organized into three component programs. CLIVAR-Global Ocean Atmosphere Land System (GOALS) will study seasonal-to-interannual variability and prediction, CLIVAR-DecCen will study decadal-to-centennial variability and predictability, and CLIVAR-ACC will study modeling and detection of anthropogenic climate change. The science goals of EOS intersect strongly with the goals

of CLIVAR in the areas of radiation, clouds, water vapor, precipitation, and atmospheric circulation, as well as in other areas.

2.3.2.4 ARM

The ARM Program (Stokes and Schwartz 1994) is a research program of the U. S. Department of Energy (DoE) and is the largest component of DoE's contribution to the USGCRP. This program is aimed at assessing the radiative properties of the atmosphere under both clear and cloudy conditions, and thus consists of a sophisticated measurement program from ground-based facilities as well as from remotely-piloted aircraft. ARM is therefore complementary to NASA's Earth Science Enterprise in that it provides an intensive ground-based component that emphasizes process studies focused on two related scientific issues in the development of models to assess human impact on climate: 1) radiative energy transport and 2) cloud formation, maintenance, and dissipation.

The measurement program will focus on Cloud and Radiation Testbed (CART) sites consisting of facilities at three key locales around the world: 1) the SGP of the U. S., 2) the western tropical Pacific, and 3) the north slope of Alaska. Each of these sites will characterize the broadband and spectral components of both longwave and shortwave radiation reaching the Earth's surface, as well as measure the water vapor, temperature, and wind profiles throughout the lower atmosphere. These measurements will aid both in improving parameterization of the radiative properties of the atmosphere for use in GCMs and as ground and airborne calibration/validation sites for EOS sensors such as CERES, MODIS, AIRS, MISR, and EOSP. All three of these distinct climatological regimes will be well characterized by the time of the launch of the first EOS AM-1 platform in 1998, and can thus be used as prime locations for intercomparisons of clear sky, aerosol, and cloud properties (including cloud base altitude). Finally, in addition to the CART sites, the ARM program has an aggressive modeling component, including radiative transfer, cloud formation, and data assimilation.

2.3.2.5 BSRN

The BSRN (WCRP 1991) is an international program of the WCRP designed to improve the accuracy and sampling rate of surface-measured shortwave and, especially, longwave radiative fluxes. Data collection has recently begun at a few sites, and should increase to about 30 sites within the next few years. A key element of these data is the provision of downward longwave flux at the surface at all BSRN stations, since most observational records at the surface cover shortwave fluxes only. The recom-

mended BSRN instrument complement includes: shortwave total, direct, and diffuse downward fluxes, longwave downward fluxes, and synoptic and upper-air observations. Expanded measurements at some sites will include lidar for cloud base altitude and direct solar spectral irradiance at specified wavelengths for aerosol optical properties. These data will provide a critical database for validation of satellite-inferred downward shortwave and longwave radiative fluxes and for monitoring long-term trends.

2.3.2.6 ECLIPS

Another key international experiment is the Experimental Cloud Lidar Pilot Study (ECLIPS) (Platt et al. 1994). ECLIPS is designed to obtain observations of cloud backscattering profiles (including cloud base altitude and cloud top altitude for optically-thin cloud) from about 10 participating ground-based lidar sites around the world. About half of these sites provide lidar depolarization measurements to distinguish water and ice clouds, and several use uplooking 11- μm radiometers to provide improved estimates of cloud optical depth. The ECLIPS lidar systems have derived nearly continuous cloud observations for two experiment months, and conducted a third experiment in conjunction with Lidar In-space Technology Experiment (LITE), a lidar system successfully flown on space shuttle Discovery in September 1994 (STS-64). These lidar systems provide a unique and objective data set for cloud base altitude for all cloud types, including cirrus. For cloud base altitudes below 4 km, the NOAA ceilometer database will also be a critical data source.

2.3.2.7 Ties to other research areas

2.3.2.7.1 Oceanic processes

The storage and transport of heat by the ocean are strongly affected by surface forcing of momentum, heat, and moisture through interaction with the atmosphere. The surface thermal forcing of the ocean is composed of radiative (shortwave and longwave) and turbulent (sensible and latent) heat fluxes. The most viable method of monitoring these fluxes over adequate temporal and spatial scales is by spaceborne sensors. Scatterometry and passive microwave imaging can give surface wind stress over the ocean, which is key to momentum, heat, and moisture exchange rates.

The relative accuracy of surface solar irradiance derived from satellite data has been found to be sufficient in monitoring the seasonal cycle over most of the ocean and the interannual anomalies over the tropical oceans. The surface flux derived from satellite data has been used to study the evolution of major climate signals, such as

the ENSO (e.g., Liu and Gautier 1990; Chertock et al. 1991). It has also been used to examine the feedback of cloud and atmospheric circulation on SST changes over the global ocean (Liu et al. 1994). Cloud and moisture feedbacks are important for the seasonal-to-interannual predictability associated with ENSO.

The surface heat flux could be integrated to give the mean meridional heat transport by the ocean. In the past, only meteorological reports from volunteer ships were used (Tally 1984), but satellite data have the potential of providing better coverage. To adequately resolve the meridional heat transport, an absolute accuracy of better than 10 Wm^{-2} in the total heat flux is required (WCRP 1982). While surface shortwave radiation estimates from satellite data approach this accuracy, the estimation of other components needs improvement. Such improvement is expected in the next decade with the launching of advanced sensors for surface wind and atmospheric temperature and humidity soundings.

The radiation that penetrates the ocean surface, particularly within the photosynthetically-active range (0.4-0.7 μm), is important to ocean biological productivity and the distribution of chemical species in the ocean (Platt et al. 1988). The monitoring of ocean surface solar irradiance, together with observations from future ocean color sensors, will also advance our understanding of the biogeochemical cycle in the ocean.

2.3.2.7.2 Land processes

Clearly radiation, clouds, water vapor, and precipitation interact strongly with land surface processes. Information on all components of the surface radiation budget is vital for land surface studies, covering the gamut from land surface climatology to ecology. Precipitation and

evaporation control the availability of surface moisture for plants, animals, and people. Large-scale circulations provide a supply of moisture to the land and exchange other gaseous compounds of importance between land areas and the rest of the globe.

It is clear that currently the surface radiation balance is not modeled well in climate or numerical weather prediction models (Nobre et al. 1991; Shuttleworth and Dickinson 1989). It is also clear that realistic changes in land surface albedo, brought about by land use change, could have a large influence on continental climatologies (Nobre et al. 1991; Lean and Warrilow 1989). Lastly, increasing evidence of the linkages between a region's cloud climatology and its surface hydrometeorology is being seen. The role of vertical water recycling in Amazonia in maintaining the "protective" cloud layer over the region is just beginning to be understood. A detailed, reliable global data set on the surface radiation budget and surface albedo is urgently needed if the models are to be improved.

Global carbon cycle (fast component): Global photosynthesis and fast cycle respiration are closely tied to the energy and water cycles, and so in large part they depend on the terms discussed above. In addition, the incoming flux of photosynthetically-active radiation (0.4-0.7 μm) is a critical forcing of photosynthesis (Sellers and Schimel 1993).

Ecology and global carbon cycle (slow component): The biogeography of the world's vegetation is closely coupled to the physical climate system. Key drivers are water availability and temperature that determine the rate of soil respiration and litter turnover. These factors are in turn linked to the surface radiation climatology, precipitation, and evaporation.

2.4 Summary of EOS contributions

2.4.1 Observation and monitoring of key climate variables

2.4.1.1 Total solar irradiance

The EOS/ACRIM experiment was selected to provide the total solar irradiance database during the EOS mission. The ACRIM measurement approach, capable of providing the maximum precision for the long-term TSI database with current measurement technology, employs an "overlap strategy" in which successive ambient temperature TSI satellite experiments are compared in flight, transferring their operational precision to the database. ACRIM

flight instrumentation has demonstrated a capability of providing annual precision smaller than 10 ppm of the TSI.

A successful deployment of ACRIM using the mission overlap strategy will provide a high-quality, continuous record of total solar irradiance variability that may be linked with prior measurements and continued into the foreseeable future. This would provide a basis for evaluating the role of variability in solar energy output in climate variability, and allow a clear separation between solar-caused climate change and other causes,

including greenhouse gases released by human industrial activity. Such a clear separation of causes is critical to the assessment of the causes of climate change and predictions of future changes.

2.4.1.2 Radiative energy fluxes—TOA, surface, atmospheric

Satellite remote sensing, in situ data, and models will be brought together under EOS to provide a global, homogeneous data set of observations of radiative fluxes at the TOA, at the surface, at the tropopause, and at intervening layers of the atmosphere (in order of priority). Because of both improved instrumentation and improved techniques for estimating radiative energy fluxes, the radiative flux estimates produced by EOS will be useful in understanding climate and in validating models to predict future climate variability and change. Key contributions will come from improved calibration, improved spatial and spectral resolution of the MODIS solar and IR imager, improved directional information from MISR, improved sampling in space, time, and angle and greater accuracy from CERES, and better methods to incorporate cloud information in flux estimates.

2.4.1.3 Cloud properties

Cloud property detection and monitoring are essential both for understanding the maintenance of the current climate and for observing seasonal and interannual shifts in cloud distributions that may be related to natural or anthropogenic climate variability. Instruments to be flown as part of EOS provide unprecedented capabilities for monitoring the properties of clouds with detail and precision not previously possible. Critical instruments include MODIS, CERES, MISR, and EOSP. They will provide not only improved technology for determining critical cloud properties from space, but also better calibration for determining long-term trends.

2.4.1.4 Precipitation

Global precipitation measurements, currently in a rather unsatisfactory state, will be greatly improved during the EOS era. The combination of visible/infrared imaging, microwave imaging, and rain radar on the TRMM mission will provide a revolutionary data set of precipitation observations in the tropics, and will also lead to improvement in algorithms for precipitation estimation from combined VIS/IR and microwave imaging. Adequate temporal and spatial sampling by better quality microwave imagers such as MIMR and AMSR will improve precipitation estimates over the oceans, and provide a high-quality, long-term data set of the type required for

seasonal-to-interannual and longer-term prediction research and testing.

2.4.2 Understanding of the processes that relate clouds and water vapor to global climate and their effect on climate sensitivity

Critical climate sensitivity mechanisms involve radiation, clouds, and water vapor. The global coverage, high-spatial-resolution, and high-spectral-resolution data from EOS can be used to better understand the processes that lie at the core of these sensitivity mechanisms. EOS will provide accurate global measurements of the exchange of energy between the Earth and space with sufficient spatial resolution and detail so that, when combined with observations of temperature, clouds, and water vapor, also to be provided by EOS, the role of clouds and water vapor in climate can be accurately assessed. The spatial resolution of some of the key instruments will be fine enough that the phenomena (e.g., convective cloud complexes in the tropics) involved in these processes can be resolved and their interactions with the larger-scale environment depicted, particularly those relating to the distribution of water vapor. These observations can be used to test explicit simulations of these phenomena using regional and cloud-scale models, and the observations and regional models together can be used to test and improve the parameterizations required in global climate models. This end-to-end validation of key processes involving clouds and water vapor in global climate models will greatly increase confidence in the validity of seasonal forecasts and predictions of global climate change.

2.4.3 More-accurate treatment of cloud and water vapor and their radiative effects in global climate models

Processes that control cloud properties and the distribution of atmospheric water vapor are critical to climate sensitivity and accurate climate forecasts. Current efforts to include more-explicit treatments of cloud water and ice in global climate models are hampered by insufficient understanding of the key physical processes and lack of adequate data for validation. The observations and associated scientific investigations to be provided by EOS are designed to improve this situation. Key contributions will be made in the areas of tropical mesoscale anvil clouds that accompany deep convection in the tropics. EOS will provide key microphysical and radiative properties of these clouds that will be helpful in determining how to represent the detrainment of ice from cumulus updrafts into anvil clouds. New observations of the ubiquitous and poorly understood thin cirrus that exists at all latitudes

will help to define the source of this cloud and its climatic importance.

Upper troposphere water vapor is maintained by some combination of detrainment from cumulus and synoptic-scale eddy fluxes. The SAGE III, MLS, and HIRDLS instruments that are part of EOS will provide greatly improved sampling of upper tropospheric water vapor, while AIRS will have the capability to derive a water vapor product analogous to that available from the operational satellites, but with greatly improved accuracy and vertical resolution.

Subtropical marine stratus and trade cumulus are important to climate models not only as a source of cloud feedback but also as a key deficiency that causes climate drift in coupled ocean-atmosphere GCMs. EOS will also allow improved analysis of observed relationships between the liquid water content of warm clouds and ambient temperature, a potentially powerful climate feedback mechanism.

A related question for GCMs is how to translate grid-scale predicted cloud water content into cloud albedo, given small-scale inhomogeneities. The 250-m resolution of MODIS is sufficient to capture the most important scales of inhomogeneity, permitting optical thickness probability density functions to be characterized for different cloud types. This combined with MODIS particle size estimates will help define parameterizations for albedo as a function of LWP.

Another particle size issue is the poorly defined indirect effects of aerosols on clouds, both the radiative effect of smaller droplets and the suppression of drizzle. EOSP and MISR will define the tropospheric aerosol distribution, which can be combined with MODIS optical thickness and particle size to isolate the indirect radiative effect. In principle, AMSR can complement this by measuring drizzle rates for stratus, but current microwave algorithms are insensitive to light precipitation.

A key to reducing uncertainty in climate model forecasts is to efficiently incorporate the new observations from EOS into the understanding and methodology that underlie cloud and precipitation parameterizations in climate models. The EOS interdisciplinary investigations will help catalyze a more-effective and productive interaction between theory, observation, and modeling.

2.4.4 Better measurement of precipitation and understanding of the role of precipitation in connecting atmospheric and surface processes, and more-accurate modeling of precipitation in global climate models

With improved measurements of global precipitation from TRMM and advanced microwave imagers such as MIMR

and AMSR, cloud properties from MODIS/MISR/EOSP, temperature and humidity from AIRS/AMSU/HSB, and surface wind patterns from scatterometry, it will be possible to more closely relate precipitation to the large-scale environment. This will enable much more rigorous testing of precipitation simulations in global weather prediction models, seasonal-to-interannual forecast models, and climate models.

2.4.5 Synergism with oceanic and land-surface processes

Radiation, clouds, water vapor, and precipitation are all closely related to important processes at the land surface and in the ocean. Improvements in these areas will interact very positively to improve understanding and simulation of land surface and oceanic processes. The ocean is driven by heat, momentum, and water fluxes at its surface, and these are all closely related to the water and energy budgets of the atmosphere and the processes that maintain them. The character of the land surface and its suitability for habitation are shaped by precipitation and the supply of radiant energy to warm the surface and evaporate water.

2.4.6 Enhanced assessment of global change: Monitoring and trend detection

The long-term (>15 years), accurate, global data sets for total solar irradiance, TOA, surface, and atmospheric radiation fluxes, temperature, humidity, cloud properties, precipitation, and winds that EOS will develop, will provide an unprecedented view of the global climate system that will be essential in developing assessments of climate variability and change. The diurnal, intraseasonal, seasonal, and year-to-year variability within this database will give a needed perspective on the natural variability on these time scales, and the relationships between the variables will provide insight into how the climate system operates. This perspective on the decadal variability of the climate system will be essential in reaching a consensus about what aspects of global change can be attributed to human activities, and what this information implies about future changes and their effects on humanity. In addition, variability on time scales from seasons to a decade is of great practical importance to humanity, and the global, homogeneous, long-term measurements of the climate system to be provided by EOS, together with the associated scientific research efforts, will result in improved ability to predict seasonal and interannual variability.

2.4.7 Improved predictions of future climates and the influence of climate change on humanity

The database to be assembled under the EOS program will provide a global picture of the Earth system from the relatively small scales of convection to the much larger scales of planetary circulation systems. This database will be critical in understanding climate sensitivity processes and assuring that they are adequately treated in global climate models used to predict future climates. Total solar irradiance, exchanges of energy between the Earth and

space, upper-tropospheric humidity, and global precipitation can all be measured very effectively from space and are all central to important climate maintenance and sensitivity mechanisms. These measurements, when combined with in situ measurements, models, and a well-directed program of scientific research, will lead to great enhancements in our ability to understand and predict global climate changes and their effects on human activities.

References

- Ackerman, S. A., W. L. Smith, J. D. Spinhirne, and H. E. Revercomb, 1990: The 28 October 1986 FIRE IFO case study: Spectral properties of cirrus clouds in the 8-12 micrometer window. *Mon. Wea. Rev.*, **118**, 2377-2388.
- Arking, A., and J. D. Childs, 1985: Retrieval of cloud cover parameters from multispectral satellite images. *J. Climate Appl. Meteor.*, **24**, 322-333.
- Arrhenius, S., 1896: On the influence of carbonic acid in the air upon the temperature of the ground. *Phil. Mag.*, **41**, 237-276.
- Baker, G. D. W., F. R. Emmitt, R. M. Robertson, J. E. Atlas, D. A. Molinari, J. Bowdle, R. M. Paegle, R. Hardesty, R. T. Menzies, T. N. Krishnamurti, R. A. Brown, M. J. Post, J. R. Anderson, A. C. Lorenc, and N. McElroy, 1995: Lidar-measured winds from space: A key component for weather and climate prediction. *Bull. Amer. Meteor. Soc.*, **76**, 869-888.
- Ballard, S. P., B. W. Golding, and R. N. B. Smith, 1991: Mesoscale model experimental forecasts of the Haar of northeast Scotland. *Mon. Wea. Rev.*, **119**, 2107-2123.
- Barkstrom, B., E. Harrison, G. Smith, R. Green, J. Kibler, and R. Cess, 1989: Earth Radiation Budget Experiment (ERBE) archival and April 1985 results. *Bull. Amer. Meteor. Soc.*, **70**, 1254-1262.
- Bates, J. J., X. Wu, and D. L. Jackson, 1996: Interannual variability of upper-troposphere water vapor band brightness temperature. *J. Climate*, **9**, 427-438.
- Baum, B. A., B. A. Wielicki, P. Minnis, and L. Parker, 1992: Cloud-property retrieval using merged HIRS and AVHRR data. *J. Appl. Meteor.*, **31**, 351-369.
- Baum, B. A., R. F. Arduini, B. A. Wielicki, P. Minnis, and C. T. Si, 1994: Multilevel cloud retrieval using multispectral HIRS and AVHRR data: nighttime oceanic analysis. *J. Geophys. Res.*, **99**, 5499-5514.
- Bengtsson, L., and J. Shukla, 1988: Integration of space and in situ observations to study global climate change. *Bull. Amer. Meteor. Soc.*, **69**, 1130-1143.
- Betts, A. K., 1990: Greenhouse warming and the tropical water budget. *Bull. Amer. Meteor. Soc.*, **71**, 1464-1465.
- Betts, A. K., and Harshvardhan, 1987: Thermodynamic constraint on the cloud liquid water feedback in climate models. *J. Geophys. Res.*, **92**, 8483-8485.
- Blau, H. H., R. D. Espinosa, and E. C. Reifenstein, 1966: Near-infrared scattering by sunlit terrestrial clouds. *Appl. Opt.*, **5**, 555.
- Bony, S., J. P. Duvel, and H. Le Treut, 1995: Observed dependence of water vapor and clear-sky greenhouse effect on sea surface temperature: comparison with climate warming experiments. *Climate Dynamics*, **11**, 307-320.
- Braun, S. A., and R. A. Houze, Jr., 1994: The transition zone and secondary maximum of radar reflectivity behind a midlatitude squall line: Results retrieved from Doppler radar data. *J. Atmos. Sci.*, **51**, 2733-2755.
- Budyko, M. I., 1969: The effects of solar radiation on the climate of the Earth. *Tellus*, **21**, 611-619.
- Cahalan, R. F., W. Ridgway, W. J. Wiscombe, S. Gollmer, and Harshvardhan, 1994: Independent pixel and Monte Carlo estimates of stratocumulus albedo. *J. Atmos. Sci.*, **51**, 3776-3790.
- Cahalan, R. F., D. Silberstein, and J. B. Snider, 1995: Liquid water path and plane-parallel albedo bias during ASTEX. *J. Atmos. Sci.*, **52**, 3002-3012.
- Cess, R. D., G. L. Potter, J. P. Blanchet, G. J. Boer, A. D. Del Genio, M. Deque, V. Dymnikov, V. Galin, W. L. Gates, S. J. Ghan, J. T. Kiehl, A. A. Lacis, H. Le Treut, Z.-X. Li, X.-Z. Liang, B. J. McAvaney, V. P. Meleshko, J. F. B. Mitchell, J. J. Morcrette, D. A. Randall, L. Rikus, E. Roeckner, J. F. Royer, U. Schlese, D. A. Sheinin, A. Slingo, A. P. Sokolov, K. E. Taylor, W. M. Washington, R. T. Wetherald, I. Yaga, and M.-H. Zhang, 1990: Intercomparison and interpretation of climate feedback processes in nineteen atmospheric general circulation models. *J. Geophys. Res.*, **95**, 16,601-16,615.
- Cess, R. D., G. L. Potter, M.-H. Zhang, J. P. Blanchet, S. Chalita, R. Colman, D. A. Dazlich, A. D. Del Genio, V. Dymnikov, V. Galin, D. Jerrett, E. Keup, A. A. Lacis, H. Le Treut, X.-Z. Liang, J. F. Mahfouf, B. J. McAvaney, V. P. Meleshko, J. F. B. Mitchell, J. J. Morcrette, P. M. Norris, D. A. Randall, L. Rikus, E. Roeckner, J. F. Royer, U. Schlese, D. A. Sheinin, J. M. Slingo, A. P. Sokolov, K. E. Taylor, W. M. Washington, R. T. Wetherald, and I. Yagai, 1991: Interpretation of snow-climate feedback as produced by 17 general circulation models. *Science*, **253**, 888-892.
- Cess, R. D., M. H. Zhang, G. L. Potter, H. W. Barker, R. A. Colman, D. A. Dazlich, A. D. Del Genio, M. Esch, J. R. Fraser, V. Galin, W. L. Gates, J. J. Hack, W. J. Ingram, J. T. Kiehl, A. A. Lacis, H. Le Treut, Z.-X. Li, X.-Z. Liang, J. F. Mahfouf, B. J. McAvaney, V. P. Meleshko, J. J. Morcrette, D. A. Randall, E. Roeckner, J. F. Royer, A. P. Sokolov, P. V. Sporyshev, K. E. Taylor, W. C. Wang, and R. T. Wetherald, 1993: Uncertainties in carbon dioxide radiative forcing in atmospheric general circulation models. *Science*, **262**, 1252-1255.
- Cess, R. D., and 33 co-authors, 1996: Cloud feedback in atmospheric general circulation models: An update. *J. Geophys. Res.*, **101**, 12,791-12,794.
- Chahine, M. T., 1974: Remote sounding of cloudy atmospheres. I. The single cloud layer. *J. Atmos. Sci.*, **31**, 233-243.

- Chahine, M. T., 1992: The hydrological cycle and its influence on climate. *Nature*, **359**, 373–380.
- Charlock, T. P., 1981: Cloud optics as a possible stabilizing factor in climate. *J. Atmos. Sci.*, **38**, 661–663.
- Charlock, T. P., 1982: Cloud optical feedback and climate stability in a radiative-convective model. *Tellus*, **34**, 245–254.
- Charlock, T., and F. Rose 1994: WMO/TD #593.
- Charlock, T., F. Rose, T. Alberta, G. L. Smith, D. Rutan, N. Manal-Smith, P. Minnis, and B. Wielicki, 1994: Cloud profiling radar requirements: Perspective from retrievals of the surface and atmospheric radiation budget and studies of atmospheric energetics. *Utility and Feasibility of a Cloud Profiling Radar*, WCRP-84, IGPO Publication Series No. 10, Jan. 1994. B10–B21.
- Charlson, R. J., J. Langner, H. Rodhe, C. B. Leovy, and S. G. Warren, 1991: Perturbation of the Northern Hemisphere radiation balance by backscattering from anthropogenic sulfate aerosols. *Tellus*, **43AB**, 152–163.
- Charlson, R. J., S. E. Schwartz, J. M. Hales, R. D. Cess, J. A. Coakley, J. E. Hansen, and D. J. Hofmann, 1992: Climate forcing by anthropogenic aerosols. *Science*, **255**, 423–430.
- Charney, J. G., 1975: Dynamics of deserts and droughts in Sahel. *Quart. J. Roy. Meteor. Soc.*, **101**, 193–202.
- Chen, S. S., 1996: Tropical convection in the active and suppressed phases of TOGA-COARE ISO simulated by a three-dimensional mesoscale model, in prep.
- Chen, S. S., R. A. Houze, Jr., and B. E. Mapes, 1995: Multiscale variability of deep convection in relation to large-scale circulation in TOGA COARE. *J. Atmos. Sci.*, **53**, 1380–1409.
- Chertock, B., R. Frouin, and R. C. J. Somerville, 1991: Global monitoring of net solar irradiance at the ocean surface; climatological variability and the 1982–1983 El Niño. *J. Climate*, **4**, 639–650.
- Chou, M. D., 1991: The derivation of cloud parameters from satellite-measured radiances for use in surface radiation calculations. *J. Atmos. Sci.*, **48**, 1549–1559.
- Chou, M. D., A. Arking, J. Otterman, and W. L. Ridgway, 1995: The effect of clouds on atmospheric absorption of solar radiation. *Geophys. Res. Lett.*, **22**, 1885–1888.
- Coakley, J. A., Jr., and F. P. Bretherton, 1982: Cloud cover from high-resolution scanner data: Detecting and allowing for partially filled fields of view. *J. Geophys. Res.*, **87**, 4917–4932.
- Coakley, J. A., Jr., and R. Davies, 1986: The effect of cloud sides on reflected solar radiation as deduced from satellite observations. *J. Atmos. Sci.*, **43**, 1025–1035.
- Cox, S. K., D. S. McDougal, D. A. Randall, and R. A. Schiffer, 1987: FIRE—The First ISCCP Regional Experiment. *Bull. Amer. Meteor. Soc.*, **68**, 114–118.
- Crommelynck, D., V. Domingo, A. Fichot, and R. Lee, 1994: Total solar irradiance observations from the EURECA and ATLAS experiments. *The Sun as a Variable Star*, IAU Col. 143 proc., J. Pap, C. Frohlich, H. Hudson, and K. Saliency, Eds. Cambridge University Press, 63–69.
- Darnell, W. L., W. F. Staylor, S. K. Gupta, N. A. Ritchey, and A. C. Wilber, 1992: Seasonal variation of surface radiation budget derived from International Satellite Cloud Climatology Project C1 data. *J. Geophys. Res.*, **97**, 15,741–15,760.
- Davies, R., W. L. Ridgway, and K. E. Kim, 1984: Spectral absorption of solar radiation in cloudy atmosphere: A 20 cm⁻¹ model. *J. Atmos. Sci.*, **41**, 2126–2137.
- Del Genio, A. D., M. S. Yao, W. Kovari, and K. K. W. Lo, 1996: A prognostic cloud water parameterization for global climate models. *J. Climate*, **9**, 270–304.
- DeMott, P. J., M. P. Meyers, and W. R. Cotton, 1994: Parameterization and impact of ice initiation processes relevant to numerical model simulations of cirrus clouds. *J. Atmos. Sci.*, **51**, 77–90.
- Deser, C., and M. L. Blackmon, 1993: Surface climate variations over the North Atlantic Ocean during winter: 1900–1989. *J. Climate*, **6**, 1743–1753.
- Duda, D. P., and G. L. Stephens, 1994: Macrophysical and microphysical influences on radiative transfer in two-dimensional marine stratus. Atmos. Sci. Paper 565, Colorado State University, 202 pp.
- Duncan, C. H., R. G. Harrison, J. R. Hickey, J. M. Kendall Sr., M. P. Thekaekara, and R. C. Willson, 1977: Rocket calibration of the Nimbus 6 solar constant measurements, *Applied Optics*, **16**, 2690–2697.
- Ebert, E. E., 1987: A pattern-recognition technique for distinguishing surface and cloud types in the polar regions. *J. Clim. Appl. Meteor.*, **26**, 1412–1427.
- Eddy, J. A., 1977: Historical evidence for the existence of the solar cycle. *Solar Output and Its Variation*. (O.R. White, Ed.), Univ. of Colo. Press, Boulder, CO, 51–71.
- Ellingson, R. G., J. Ellis, and S. Fels, 1991: The intercomparison of radiation codes used in climate models: Long wave results. *J. Geophys. Res. D*, **96**, 8929–8953.
- Evans, K. F., and G. L. Stephens, 1995a: Microwave radiative transfer through clouds composed of realistically shaped ice crystals. Part I: Single scattering properties. *J. Atmos. Sci.*, **52**, 2041–2057.
- Evans, K. F., and G. L. Stephens, 1995b: Microwave radiative transfer through clouds composed of realistically shaped ice crystals. Part II: Remote sensing of ice clouds. *J. Atmos. Sci.*, **52**, 2058–2072.
- Feigelson, E. M., 1978: Preliminary radiation model of a cloudy atmosphere. Part I - Structure of clouds and solar radiation. *Beitr. Phys. Atmos.*, **51**, 203–229.
- Foukal, P., and J. Lean, 1986, The influence of faculae on total solar irradiance and luminosity, *Astrophys. J.*, **302**, 826–835.
- Foukal, P., and J. Lean, 1988: Magnetic modulation of solar luminosity by photospheric activity. *Astrophys. J.*, **328**, 347–357.
- Foukal, P., and J. Lean, 1990: An empirical model of total solar irradiance variations between 1874 and 1988. *Science*, **247**, 556–558.
- Fowler, L. D., D. A. Randall, and S. A. Rutledge, 1996: Liquid and ice cloud microphysics in the CSU general circulation model. Part I: Model description and simulated microphysical processes. *J. Climate*, **9**, 489–529.
- Frohlich, C., 1987: Solar oscillations and helioseismology from ACRIM/SMM irradiance data. *New and Exotic Phenomena*, (O. Fackler and J.T.T. Van, Eds.), Gif-sur-Yvette: Editions Frontieres, 395–402.
- Frohlich, C., 1994: Irradiance observations of the sun. *The Sun as a Variable Star*, IAU Col. **143**, (C. Frohlich, H. Hudson, and K. Saliency, Eds.), Cambridge University Press, 28–36.
- Fu, R., and B. J. Soden, 1996: Changes of upper tropospheric humidity in the global midlatitudes forced by deep convection in the tropical atmosphere. *Nature*, submitted.
- Fu, R., A. D. Del Genio, W. B. Rossow, and W. T. Liu, 1992: Cirrus-cloud thermostat for tropical sea surface temperature tested using satellite data. *Nature*, **358**, 394–397.
- Fujita, T. T., 1984: Review of the history of mesoscale meteorology and forecasting. Satellite and Mesometeorology Research Paper 208, University of Chicago, 42 pp.
- Gaffen, D. J., R. D. Rosen, D. A. Salstein, and J. S. Boyle, 1995: Validation of humidity, moisture fluxes, and soil moisture in GCMS: Report of AMIP diagnostic subproject 11. Part 2: Humidity and moisture flux fields. Atmospheric Model Intercomparison Project, DoE.
- Gao, B. C., A. F. H. Goetz, and W. J. Wiscombe, 1992: Cirrus cloud detection from airborne imaging spectrometer data using the 1.375 μm water vapor band. *Geophys. Res. Lett.*, **20**, 301–304.
- Gates W. L., 1993: AMIP: The Atmospheric Model Intercomparison Project. *Bull. Amer. Meteor. Soc.*, **73**, 1962–1970.
- Gleckler, P. J., D. A. Randall, G. Boer, R. Colman, M. Dix, V. Galin, M. Helfand, J. Kiehl, A. Kitoh, W. Lau, X.-Y. Liang, V. Lykossov, B. McAvaney, K. Miyakoda, S. Planton, and W. Stern, 1995: Cloud-radiative effects on implied oceanic energy transports as simulated by atmospheric general circulation models. *Geophys. Res. Lett.*, **22**, 791–794.

- Green, R. N., and P. O'R. Hinton, 1996: Estimation of angular distribution models from radiance pairs. *J. Geophys. Res.*, **101**, 16,951–16,959.
- Greenwald, T. J., G. L. Stephens, H. T. H. Vonder and D. L. Jackson, 1993: A physical retrieval of cloud liquid water over the global oceans using Special Sensor Microwave/Imager (SSM/I) observations. *J. Geophys. Res.*, **98**, 18,471–18,488.
- Grell, G. A., J. Dudhia, and D. R. Stauffer, 1993: A Description of the Fifth-Generation Penn State/NCAR Mesoscale Model (MM5). NCAR Tech. Note -398+IA, October 1993.
- Groisman, P. Y., T. R. Karl, and R. W. Knight, 1994: Observed impact of snow cover on the heat balance and the rise of continental spring temperatures. *Science*, **263**, 198–200.
- Gupta, S. K., 1989: A parameterization for longwave surface radiation from sun-synchronous satellite data. *J. Climate*, **2**, 305–320.
- Gupta, S. K., W. L. Darnell, and A. C. Wilber, 1992: A parameterization for surface longwave radiation from satellite data: Recent improvements. *J. Appl. Meteor.*, **31**, 1361–1367.
- Gupta, S. K., C. H. Whitlock, N. A. Ritchey, A. C. Wilber, W. L. Darnell, and W. F. Staylor, 1996: A climatology of surface radiation budget derived from satellite data. International Radiation Symposium, Fairbanks, Alaska, August 19–24.
- Hahn, C. J., S. G. Warren, J. London, R. M. Chervin, and R. Jenne, 1982: *Atlas of simultaneous occurrence of different cloud types over the ocean*. NCAR Technical Note, NCAR/TN-201+STR, NTIS PB83-152074, 212 pp.
- Han, Q., W. B. Rossow, and A. A. Lacis, 1994: Near global survey of effective droplet radii in liquid water clouds using ISCCP data. *J. Climate*, **7**, 465–497.
- Hansen, J. E., and J. B. Pollack, 1970: Infrared light scattering by terrestrial clouds. *J. Atmos. Sci.*, **27**, 265–281.
- Hansen, J. E., W.-C. Wang, and A. A. Lacis, 1978: Mount Agung eruption provides test of a global climate perturbation. *Science*, **199**, 1065–1068.
- Hansen, J., A. Lacis, D. Rind, G. Russell, P. Stone, I. Fung, J. Lerner, and R. Ruedy, 1984: Climate sensitivity: Analysis of feedback mechanisms. *Climate Processes and Climate Sensitivity*, J. E. Hansen and T. Takahashi, Eds., AGU, Washington DC, 130–163.
- Hansen, J. E., M. Sato, R. Reudy, A. Lacis, K. Asamoah, S. Borenstein, E. Brown, B. Cairns, G. Caliri, M. Campbell, B. Curran, S. deCastro, L. Druyan, M. Fox, C. Johnson, J. Lerner, M. P. McCormick, R. Miller, P. Minnis, A. Morrison, L. Pandolfo, L. Ramberran, F. Zaucker, M. Robinson, P. Russell, K. Shah, P. Stone, I. Tegen, L. Thomason, J. Wilder, and H. Wilson, 1994: A Pinatubo climate modelling investigation. *The Effects of the Mt. Pinatubo Eruption on the Atmosphere and Climate*, (G. Fiocco, D. Fua, and G. Visconti, Eds.), Springer-Verlag.
- Harrington, J. Y., M. P. Meyers, R. L. Walko, and W. R. Cotton, 1995: Parameterization of ice crystal conversion processes due to vapor deposition for mesoscale models using double-moment basis functions. Part I: Basic formulation and parcel model results. *J. Atmos. Sci.*, **52**, 4344–4366.
- Harrison, E. F., P. Minnis, B. R. Barkstrom, V. Ramanathan, R. D. Cess and G. G. Gibson, 1990: Seasonal variation of cloud radiative forcing derived from the Earth Radiation Budget Experiment. *J. Geophys. Res.*, **95**, 18,687–18,703.
- Harrison, E. F., P. Minnis, G. G. Gibson, and F. M. Denn, 1992: Orbital analysis and instrument viewing considerations for the Earth Observing System (EOS) satellite. *Astrodynamics 1991, Advances in the Astronautical Sciences*, **76**, (B. Kaufman, Ed.), 1215–1228.
- Harshvardhan, B. A. Wielicki, and K. M. Ginger, 1994: The interpretation of remotely sensed cloud properties from a model parameterization perspective. *J. Climate*, **7**, 1987–1998.
- Hartmann, D.L., 1994: *Global Physical Climatology*, Academic Press, 411 pp.
- Hartmann, D. L., and M. L. Michelsen, 1993: Large-scale effects on the regulation of tropical sea surface temperature. *J. Climate*, **6**, 2049–2062.
- Hartmann, D. L., H. H. Hendon, and R. J. Houze, 1984: Some implications of mesoscale circulations in tropical cloud clusters for large-scale dynamics and climate. *J. Atmos. Sci.*, **41**, 113–121.
- Hartmann, D. L., M. E. Ockert-Bell, and M. L. Michelsen, 1992: The effect of cloud type on Earth's energy balance: Global analysis. *J. Climate*, **5**, 1281–1304.
- Hayasaka, T., N. Kikuchi, and M. Tanaka, 1995: Absorption of solar radiation by stratocumulus clouds: Aircraft measurements and theoretical calculations. *J. Appl. Meteor.*, **34**, 1047–1055.
- Held, I. M., 1993: Large-scale dynamics and global warming. *Bull. Amer. Meteor. Soc.*, **74**, 228–241.
- Held, I. M., R. S. Hemler, and V. Ramaswamy, 1993: Radiative-convective equilibrium with explicit two-dimensional moist convection. *J. Atmos. Sci.*, **23**, 3909–3925.
- Heymsfield, A. J., and L. J. Donner, 1990: A scheme for parameterizing ice-cloud water content in general circulation models. *J. Atmos. Sci.*, **47**, 1865–1877.
- Hickey, J. R., L. L. Stowe, H. Jacobowitz, R. H. Maschhoff, F. House, and T. H. Vonder Haar, 1980: Initial solar irradiance determination from Nimbus-7 cavity radiometer measurements. *Science*, **208**, 281–283.
- Horel, J. D., and J. M. Wallace, 1981: Planetary-scale atmospheric phenomena associated with the Southern Oscillation. *Mon. Wea. Rev.*, **109**, 814–829.
- Houghton, J. T., G. J. Jenkins, and J. J. Ephraums, Eds., 1990: *Climate Change: The IPCC Scientific Assessment*. Cambridge University Press, Cambridge, 365 pp.
- Houghton, J. T., L. G. Meira Filho, B. A. Callander, N. Harris, A. Kattenberg, and K. Maskell, Eds., 1996: *Climate Change 1995: The Science of Climate Change*. Intergovernmental Panel on Climate Change, Cambridge, 572 pp.
- Houze, R. A., Jr., 1982: Cloud clusters and large-scale vertical motions in the tropics. *J. Met. Soc. Japan*, **60**, 396–410.
- Houze, R. A., Jr., 1989: Observed structure of mesoscale convective systems and implications for large-scale heating. *Quart. J. Roy. Meteor. Soc.*, **115**, 425–461.
- Houze, R. A., Jr., 1993: *Cloud Dynamics*. Academic Press, 573 pp.
- Hoyt, D. V., H. L. Kyle, J. R. Hickey, and R. H. Maschhoff, 1992: The Nimbus 7 solar total irradiance: A new algorithm for its derivation. *J. Geophys. Res.*, **97**, 51–63.
- Hudson, H. S., and R. C. Willson, 1982: Sunspots and solar variability. Conference on Sunspots, Sacramento Peak Observatory, Sunspot, AZ, Sacramento Peak Observatory.
- Huffman, G. J., R. F. Adler, and P. R. Keehn, 1995: Experiments with a technique for combining satellite-based precipitation estimates with gauge and model estimates. Proceedings, *Seventh Conf. on Sat. Meteor. and Oceanogr.* 6–10 June, 1994, Monterey, Amer. Meteor. Soc.
- Inamdar, A. K., and V. Ramanathan, 1994: Physics of greenhouse effect and convection in warm oceans. *J. Climate*, **7**, 715–731.
- Intergovernmental Panel on Climate Change, 1990: *Climate Change: The IPCC scientific assessment*. Cambridge Univ. Press, 365 pp.
- Kahn, R., R. West, D. McDonald, B. Rheingans, and M. I. Mishchenko, 1996: Sensitivity of multi-angle remote sensing observations to aerosol sphericity. *J. Geophys. Res.*, in press.
- Kalnay, E., and R. Jenne, 1991: Summary of the NMC/NCAR reanalysis workshop of April 1991. *Bull. Amer. Meteor. Soc.*, **72**, 1897–1904.
- Kaufman, Y. J., and B. C. Gao, 1992: Remote sensing of water vapor in the near IR from EOS/MODIS. *IEEE Transactions on Geoscience and Remote Sensing*, **30**, 871–884.
- Kelly, K. K., A. F. Tuck, and T. Davies, 1991: Wintertime asymmetry of upper-tropospheric water between the Northern and Southern Hemisphere. *Nature*, **353**, 244–247.

- Kiehl, J. T., and K. E. Trenberth, 1997: Earth's annual global mean energy budget. *Bull. Amer. Meteor. Soc.*, **74**, 21–34.
- King, M. D., 1993: Radiative properties of clouds. *Aerosol-Cloud-Climate Interactions*, **54**, (P. V. Hobbs, Ed.), Academic Press, 123–149.
- Klein, S. A., and D. L. Hartmann, 1993a: Spurious changes in the ISCCP dataset. *Geophys. Res. Lett.*, **20**, 455–458.
- Klein, S. A., and D. L. Hartmann, 1993b: The seasonal cycle of low stratiform clouds. *J. Climate*, **6**, 1587–1606.
- Klein, S. A., D. L. Hartmann, and J. R. Norris, 1995: On the relationships among low-cloud structure, sea surface temperature, and atmospheric circulation in the summertime northeast Pacific. *J. Climate*, **8**, 1140–1155.
- Krueger, S. K., 1988: Numerical simulation of tropical cumulus clouds and their interaction with the subcloud layer. *J. Atmos. Sci.*, **45**, 2221–2250.
- Lau, K. -M., and H. -T. Wu, and S. Bony, 1997: The role of the large-scale atmospheric circulation in the relationship between tropical convection and sea surface temperature. *J. Climate*, **10**, 381–392.
- Lau, K. -M., Y. S. Sud, and J. H. Kim, 1995: Intercomparison of hydrologic processes in global climate models. NASA Tech. Memo. 104617, 161 pp.
- Lau, K. -M., C. H. Sui, M. -D. Chou, and W.-K. Tao, 1994: An inquiry into the cirrus cloud thermostat effect for tropical sea surface temperature. *Geophys. Res. Lett.*, **21**, 1157–1160.
- Lau, K. -M., C. -H. Sui, and W. -K. Tao, 1993: A preliminary study of the tropical water cycle and its sensitivity to surface warming. *Bull. Amer. Meteor. Soc.*, **74**, 1313–1321.
- Lau, N. -C., and M. J. Nath, 1994: A modeling study of the relative roles of tropical and extratropical SST anomalies in the variability of the global atmosphere-ocean system. *J. Climate*, **7**, 1184–1207.
- Lean, J., and D. A. Warrilow, 1989: Climate impact of Amazon deforestation. *Nature*, **342**, 311–313.
- Lean, J., J. Beer, and R. Bradley, 1995: Reconstruction of solar irradiance since 1610: Implications for climate change. *Geophys. Res. Lett.*, **22** (23), 3195–3198.
- Lee, R. B. I., M. A. Gibson, R. S. Wilson, and S. Thomas, 1995: Long-term total solar irradiance variability during sunspot cycle 22. *J. Geophys. Res.*, **100**, 1667–1675.
- Legates, D. R., and C. J. Wilmott, 1990: Mean seasonal and spatial variability in gauge-corrected global precipitation. *Int. J. Climatol.*, **10**, 111–127.
- LeTreut, H., and Z.-X. Li, 1991: Sensitivity of an atmospheric general circulation model to prescribed SST changes: feedback effects associated with the simulation of cloud optical properties. *Clim. Dyn.*, **5**, 175–187.
- Li, Z., and H. LeTreut, 1992: Cloud-radiation feedbacks in a general circulation model and their dependence on cloud modeling assumptions. *Clim. Dyn.*, **7**, 133–139.
- Li, Z., and H. G. Leighton, 1993: Global climatologies of solar radiation budgets at the surface and in the atmosphere from 5 years of ERBE data. *J. Geophys. Res.*, **98**, 4919–4930.
- Li, Z., and F. Becker, 1993: Feasibility of land surface temperature and emissivity determination from AVHRR data. *Remote Sens. Env.*, **43**, 67–85.
- Li, Z., H. G. Leighton, K. Masuda, and T. Takashima, 1993: Estimation of SW flux absorbed at the surface from TOA reflected flux. *J. Climate*, **6**, 317–330.
- Li, Z., C. H. Whitlock, and T. P. Charlock, 1995: Assessment of the global monthly mean surface insolation estimated from satellite measurements using Global Energy Balance Archive data. *J. Climate*, **8**, 315–328.
- Lilly, D. K., 1968: Models of cloud-topped mixed layers under a strong inversion. *Quart. J. Roy Meteor. Soc.*, **94**, 292–309.
- Lindzen, R. S., 1990: Some coolness concerning global warming. *Bull. Amer. Meteor. Soc.*, **71**, 288–299.
- Lipps, F. B., and R. S. Hemler, 1986: Numerical simulation of deep tropical convection associated with large-scale convergence. *J. Atmos. Sci.*, **43**, 1796–1816.
- Liu, W. T., and C. Gautier, 1990: Thermal forcing of the tropical Pacific from satellite data. *J. Geophys. Res.*, **95**, 13,209–13,217.
- Liu, W. T., A. Zhang, and J. K. B. Bishop, 1994: Evaporation and solar irradiance as regulators of sea surface temperature in annual and interannual changes. *J. Geophys. Res.*, **99**, 12,623–12,637.
- Livingston, W., L. Wallace, and O. R. White, 1988: Spectrum line intensity as a surrogate for solar irradiance variation. *Science*, **240**, 1765–1767.
- Luo, G., X. Lin, and J. A. Coakley, Jr., 1994: 11- μm emissivities and droplet radii for marine stratocumulus. *J. Geophys. Res.*, **99**, 3685–3698.
- Manabe, S., and R. T. Wetherald, 1967: Thermal equilibrium of the atmosphere with a given distribution of relative humidity. *J. Atmos. Sci.*, **24**, 241–259.
- Manabe, S., R. J. Stouffer, M. J. Spelman, and K. Bryan, 1991: Transient response of a coupled ocean-atmosphere model to gradual changes in atmospheric CO₂. Part I: annual mean response. *J. Climate*, **4**, 785–818.
- Mapes, B. E., and R. A. Houze, Jr., 1993: Cloud clusters and superclusters over the oceanic warm pool. *Mon. Wea. Rev.*, **121**, 1398–1415.
- Mapes, B. E., and R. A. Houze, Jr., 1995: Diabatic divergence profiles in western Pacific mesoscale convective systems. *J. Atmos. Sci.*, **52**, 1807–1828.
- McCormick, M. P., R. E. Viega, and W. P. Chu, 1992: Stratospheric ozone profile and total ozone trends derived from the SAGE I and SAGE II data. *J. Geophys. Res.*, **19**, 269–272.
- Minnis, P., 1989: Viewing zenith angle dependence of cloudiness determined from coincident GOES East and GOES West data. *J. Geophys. Res.*, **94**, 2303–2320.
- Minnis, P., and E. F. Harrison, 1984a: Diurnal variability of regional cloud and clear-sky radiative parameters derived from GOES data. Part I: Analysis method. *J. Clim. Appl. Meteor.*, **23**, 993–1011.
- Minnis, P., and E. F. Harrison, 1984b: Diurnal variability of regional cloud and clear sky radiative parameters derived from GOES data. Part II: Cloud distributions. *J. Clim. Appl. Meteor.*, **23**, 1012–1031.
- Minnis, P., and E. F. Harrison, 1984c: Diurnal variability of regional cloud and clear-sky radiative parameters derived from GOES data, Part III: November 1978 radiative parameters. *J. Clim. Appl. Meteor.*, **23**, 1032–1051.
- Minnis, P., D. F. Young, K. Sassen, J. M. Alvarez, and C. J. Grund, 1990: The 27–28 October 1986 FIRE IFO Cirrus Case Study: cirrus parameter relationships derived from satellite and lidar data. *Mon. Wea. Rev.*, **118**, 2402–25.
- Minnis, P., P. W. Heck, D. F. Young, C. W. Fairall, and J. B. Snider, 1992: Stratocumulus cloud properties derived from simultaneous satellite and island-based instrumentation during FIRE. *J. Appl. Meteor.*, **31**, 317–39.
- Mitchell, J. F. B., 1993a: Simulation of climate. *Renewable Energy*, **3**, 421–432.
- Mitchell, J. F. B., 1993b: Simulation of climate change. *Renewable Energy*, **3**, 433–445.
- Mitchell, J. F. B., C. A. Senior, and W. J. Ingram, 1989: CO₂ and climate: A missing feedback? *Nature*, **341**, 132–134.
- Nakajima, T., and M. D. King, 1990: Determination of the optical thickness and effective particle radius of clouds from reflected solar radiation measurements. Part I: Theory. *J. Atmos. Sci.*, **47**, 1878–1893.

- Nakajima, T., M. D. King, J. D. Spinhirne, and L. F. Radke, 1991: Determination of the optical thickness and effective particle radius of clouds from reflected solar radiation measurements. Part II: Marine stratocumulus observations. *J. Atmos. Sci.*, **48**, 728–750.
- National Research Council, 1994: *Solar Influences on Global Change*. National Academy Press, p. 10.
- Nobre, C., P. J. Sellers, and J. Shukla, 1991: Amazonian deforestation and regional climate change. *J. Climate*, **4**, 957–988.
- Norris, J. R., and C. B. Leovy, 1994: Interannual variability in strati-form cloudiness and sea surface temperature. *J. Climate*, **7**, 1915–1925.
- Ohmura, A., and H. Gilgen, 1991: Global Energy Balance Archive GEBA. *The GEBA Database, Interactive Applications, Retrieving Data*, World Climate Program Water Project A7, Report 2, Züricher Geographische Schriften Nr. 44, Geographisches Institut ETH, Zürich.
- Paltridge, G. W., 1980: Cloud-radiation feedback to climate. *Quart. J. Roy. Meteor. Soc.*, **106**, 367–380.
- Peixoto, J. P., and A. H. Oort, 1992: *Physics of Climate*. American Institute of Physics, New York, 520 pp.
- Peixoto, J. P., and A. H. Oort, 1983: The atmospheric branch of the hydrologic cycle and climate. *Variations in the Global Hydrologic Cycle and Climate*. (A. Street-Perott, M. Beran, and R. Radcliffe, Eds.), Reidel Publ. Co., Holland, 5–65.
- Penner, J. E., R. J. Charlson, J. M. Hales, N. S. Laulainen, R. Leifer, T. Novakov, J. Ogren, L. F. Radke, S. E. Schwartz, and L. Travis, 1994: Quantifying and minimizing uncertainty of climate forcing by anthropogenic aerosols. *Bull. Amer. Meteor. Soc.*, **75**, 375–400.
- Pierrehumbert, R., 1994: Thermostats, radiator fins, and the local runaway greenhouse. *J. Atmos. Sci.*, **52**, 1784–1806.
- Pilewskie, P., and F. P. Valero, 1995: Direct observations of excess solar absorption by clouds. *Science*, **267**, 1626–1629.
- Pinker, R., and I. Laszlo, 1992: Modeling surface solar irradiance for satellite applications on a global scale. *J. Appl. Meteor.*, **31**, 194–211.
- Platt, T., S. Sathyendranath, C. M. Caverhill, and M. R. Lewis, 1988: Ocean primary production and available light: Further algorithms for remote sensing. *Deep Sea Res.*, **35**, 855–879.
- Platt, C. M., S. A. Young, A. I. Carswell, S. R. Pal, M. P. McCormick, D. M. Winker, M. DelGuastra, L. Stefanutti, W. L. Eberhard, M. Hardesty, P. H. Flamant, R. Valentin, B. Forgan, G. G. Gimmestad, H. Jäger, S. S. Khmelevtsov, I. Kolev, B. Kaprieolev, Da-ren Lu, K. Sassen, V. S. Shamaev, O. Uchino, Y. Mizuno, U. Wandinger, C. Weitkamp, A. Ansmann, and C. Wooldridge, 1994: The Experimental Cloud Lidar Pilot Study (ECLIPS) for cloud-radiation research. *Bull. Amer. Meteor. Soc.*, **75**, 1635–1654.
- Prabhakara, C., D. A. Short, and B. E. Vollmer, 1985: El Niño and atmospheric water vapor: Observation from Nimbus 7 SMMR. *J. Climate Appl. Meteor.*, **24**, 1311–1324.
- Prabhakara, C., R. S. Fraser, G. Dalu, M. L. C. Wu, and R. J. Curran, 1988: Thin cirrus clouds: Seasonal distribution over oceans deduced from Nimbus-4 IRIS. *J. Climate Appl. Meteor.*, **27**, 279–299.
- Ramanathan, V., and W. Collins, 1991: Thermodynamic regulation of ocean warming by cirrus clouds deduced from observations of the 1987 El Niño. *Nature*, **351**, 27–32.
- Ramanathan, V., R. D. Cess, E. F. Harrison, P. Minnis, B. R. Barkstrom, E. Ahmad, and D. L. Hartmann, 1989: Cloud-radiative forcing and climate: Results from the Earth Radiation Budget Experiment. *Science*, **243**, 57–63.
- Ramanathan, V., B. Subasilar, G. J. Zhang, W. Conant, R. D. Cess, J. T. Kiehl, H. Grassl, and L. Shi, 1995: Warm pool heat budget and shortwave cloud forcing: A missing physics? *Science*, **267**, 499–503.
- Rasch, P. J., and D. L. Williamson, 1990: Computational aspects of moisture transport in global models of the atmosphere. *Quart. J. Roy. Meteor. Soc.*, **116**, 1071–1090.
- Rasmusson, E. M., and J. M. Wallace, 1983: Meteorological aspects of the El Niño-Southern Oscillation. *Science*, **222**, 1195–1202.
- Raval, A., and V. Ramanathan, 1989: Observational determination of the greenhouse effect. *Nature*, **342**, 758–761.
- Read, W. G., J. W. Waters, D. A. Flower, L. Froidevaux, R. F. Jarnot, D. L. Hartmann, R. S. Harwood, and R. B. Rood, 1995: Upper-tropospheric water vapor from UARS MLS. *Bull. Amer. Meteor. Soc.*, **76**, 2381–2389.
- Rind, D., E. W. Chiou, W. Chu, J. Larsen, O. Oltmans, J. Lerner, M. P. McCormick, and L. McMaster, 1991: Positive water vapour feedback in climate models confirmed by satellite data. *Nature*, **349**, 500–503.
- Rind, D., E. W. Chiou, W. Chu, J. Larsen, S. Oltmans, J. Lerner, M. P. McCormick, and L. McMaster, 1993: Overview of the Stratospheric Aerosol and Gas Experiment II water vapor observations: Method, validation, and data characteristics. *J. Geophys. Res.*, **98**, 4835–4856.
- Roeckner, E., U. Schlese, J. Biercamp, and P. Loewe, 1987: Cloud optical depth feedbacks and climate modeling. *Nature*, **329**, 138–140.
- Ropelewski, C. F., and M. S. Halpert, 1989: Precipitation patterns associated with the high index phase of the Southern Oscillation. *J. Climate*, **2**, 268–284.
- Rossow, W. B., and R. A. Schiffer, 1991: ISCCP cloud data products. *Bull. Amer. Meteor. Soc.*, **72**, 2–20.
- Rossow, W. B., F. Mosher, E. Kinsella, A. Arking, M. Desbois, E. Harrison, P. Minnis, E. Ruprecht, G. Seze, C. Simmer, and E. Smith, 1985: ISCCP cloud algorithm intercomparison. *J. Climate Appl. Meteor.*, **24**, 877–903.
- Rossow, W. B., L. C. Garder, P. J. Lu, and A. Walker, 1991: International Satellite Cloud Climatology Project (ISCCP) documentation of cloud data. *WMO/TD-No. 266 (Revised)*, World Meteorological Organization, Geneva, 76 pp.
- Salathe, E. P., Jr., D. Chester, and Y. C. Sud, 1995: Evaluation of the upper-tropospheric moisture climatology in a general circulation model using TOVS radiance observations. *J. Climate*, in press.
- Saunders, R. W., and K. T. Kriebel, 1988: An improved method for detecting clear sky and cloudy radiances from AVHRR data. *Int. J. Remote Sens.*, **9**, 123–150.
- Schubert, S., C. K. Park, C. Y. Wu, Y. Higgins, Y. Kondratyeva, A. Molod, L. Takacs, M. Seablom, and R. Rood, 1995: A multilayer assimilation with the GEOS-1 system: Overview and results. NASA Technical Memorandum 104606, Vol. 6, 183 pp.
- Sellers, P. J., and F. G. Hall, 1992: FIFE in 1992: Results, scientific gains, and future research directions. *J. Geophys. Res.*, **97**, 19,091–19,109.
- Sellers, P. J., and D. S. Schimel, 1993: Remote sensing of the land biosphere and biogeochemistry in the EOS era. *Global and Planetary Change*, **7**, 279–297.
- Sellers, W. D., 1969: A climate model based on the energy balance of the Earth-atmosphere system. *J. Appl. Meteor.*, **8**, 392–400.
- Senior, C. A., and J. F. B. Mitchell, 1993: Carbon dioxide and climate: The impact of cloud parameterization. *J. Climate*, **6**, 393–418.
- Shuttleworth, W. J., and R. E. Dickinson, 1989: Comments on “Modeling tropical deforestation: A study of GCM land-surface parameterizations.” *Quart. J. Roy. Meteor. Soc.*, **115**, 1177–1179.
- Simpson, J., Ed., 1988: TRMM: A satellite mission to measure tropical rainfall: Report of the steering group. National Aeronautics and Space Administration, Goddard Space Flight Center, Greenbelt, MD 20771, 94 pp.
- Sinha, A., 1995: Relative influence of lapse rate and water vapor on the greenhouse effect. *J. Geophys. Res.*, **100** (D3), 5095–5103.
- Slingo, A., and M. J. Webb, 1992: Simulation of clear-sky outgoing longwave radiation over the oceans using operational analyses. *Quart. J. Roy. Meteor. Soc.*, **118**, 1117–1144.

- Smith, R. N. B., 1990: A scheme for predicting layer clouds and their water content in a general circulation model. *Quart. J. Roy. Meteor. Soc.*, **116**, 435–460.
- Smith, W. L., and H. M. Woolf, 1976: The use of eigenvectors of statistical covariance matrices for interpreting satellite sounding radiometer observations. *J. Atmos. Sci.*, **33**, 1177–1187.
- Soden, B. J., and F. P. Bretherton, 1993: Upper-tropospheric relative humidity from the GOES 6.7 micron channel: Method and climatology for July 1987. *J. Geophys. Res.*, **98**, 16,669–16,688.
- Soden, B. J., and R. Fu, 1995: A satellite analysis of deep convection, upper-tropospheric humidity and the greenhouse effect. *J. Climate*, **8**, 2333–2351.
- Somerville, R. C. J., and L. A. Remer, 1984: Cloud optical thickness feedbacks in the CO₂ climate problem. *J. Geophys. Res.*, **89**, 9668–9673.
- Stackhouse, P. W., Jr., and G. L. Stephens, 1991: A theoretical and observational study of the radiative properties of cirrus: results from FIRE 1986. *J. Atmos. Sci.*, **48**, 2044–2059.
- Starr, D. O'C., and S. H. Melfi, 1991: The role of water vapor in climate: A strategic plan for the proposed GEWEX Water Vapor Project (GVaP), NASA Conf. Publ. 3120, 50 pp.
- Stephens, G. L., 1990: On the relationship between water vapor over the oceans and sea surface temperature. *J. Climate*, **3**, 634–645.
- Stephens, G. L., and P. J. Webster, 1984: Cloud decoupling of the surface and planetary radiative budgets. *J. Atmos. Sci.*, **41**, 681–686.
- Stephens, G. L., and S. Tsay, 1990: On the cloud absorption anomaly. *Quart. J. Roy. Meteor. Soc.*, **116**, 671–704.
- Stephens, G. L., A. Slingo, M. J. Webb, P. J. Minnett, P. H. Daum, L. Kleinman, I. Wittmeyer, and D. A. Randall, 1994: Observations of the Earth's Radiation Budget in relation to atmospheric hydrology. 4. Atmospheric column radiative cooling over the world's oceans. *J. Geophys. Res.*, **99**, 18,585–18,604.
- Stokes, G. M., and S. E. Schwartz, 1994: The Atmospheric Radiation Measurement (ARM) program: Programmatic background and design of the cloud and radiation test bed. *Bull. Amer. Meteor. Soc.*, **75**, 1201–1221.
- Stone, R. S., G. L. Stephens, C. M. R. Platt, and S. Banks, 1990: The remote sensing of thin cirrus clouds using satellites, lidar, and radiative transfer theory. *J. Appl. Meteor.*, **29**, 353–366.
- Stowe, L. L., C. G. Wellemeyer, T. F. Eck, H. Y. M. Yeh, and the N. C. D. P. Team, 1988: Nimbus-7 global cloud climatology, Part I, Algorithm and validation. *J. Climate*, **1**, 445–470.
- Stowe, L. L., E. P. McClain, R. Carey, P. Pellegrino, G. G. Gutman, P. Davis, C. Long, and S. Hart, 1991: Global distribution of cloud cover derived from NOAA/AVHRR operational satellite data. *Advances in Space Research*, **11**, 51–54.
- Sui, C. H., K. M. Lau, W. K. Tao, and J. Simpson, 1993: The tropical water and energy cycles in a cumulus ensemble model. Part I: equilibrium climate. *J. Atmos. Sci.*, **51**, 711–728.
- Sun, D. Z., and R. S. Lindzen, 1993: Distribution of tropical tropospheric water vapor. *J. Atmos. Sci.*, **50**, 1644–1660.
- Sundqvist, H., 1978: A parameterization scheme for nonconvective condensation including prediction of cloud water content. *Quart. J. Roy. Meteor. Soc.*, **104**, 677–690.
- Susskind, J., D. Reuter, and M. T. Chahine, 1987: Cloud fields retrieved from HIRS2/MSU. *J. Geophys. Res.*, **90**, 11,602–11,608.
- Takano, Y., and K. N. Liou, 1989: Radiative transfer in cirrus clouds. I. Single scattering and optical properties of oriented hexagonal ice crystals. *J. Atmos. Sci.*, **46**, 3–20.
- Tally, L. D., 1984: Meridional heat transport in the Pacific Ocean. *J. Phys. Oceanogr.*, **14**, 231–241.
- Tian, L., and J. A. Curry, 1989: Cloud overlap statistics. *J. Geophys. Res.*, **94**, 9925–9935.
- Tao, W. K., and S. T. Soong, 1986: A study of the response of deep tropical clouds to mesoscale processes: Three-dimensional numerical experiments. *J. Atmos. Sci.*, **43**, 2653–2676.
- Tao, W. K., and J. Simpson, 1993: The Goddard Cumulus Ensemble Model. Part I: Model description. *Terrestrial, Atmospheric and Oceanic Sciences*, **4**, 35–72.
- Tiedtke, M., 1993: Representations of clouds in large-scale models. *Mon. Wea. Rev.*, **121**, 3040–3061.
- Trenberth, K. E., and J. G. Olson, 1988: Evaluation of NMC global analyses: 1979–1987, National Center for Atmospheric Research. NCAR/TN-299+STR, 82 pp.
- Tselioudis, G., W. B. Rossow, and D. Rind, 1992: Global patterns of cloud optical thickness variation with temperature. *J. Climate*, **5**, 1484–1495.
- Udelhofen, P., and D. L. Hartmann, 1995: The influence of tropical cloud systems on the relative humidity in the upper troposphere. *J. Geophys. Res.*, **100**, 423–440.
- Wade, C. G., 1994: Problems with radiosonde humidity in the United States and their effect on climate analysis. *AGU Chapman Conference on Water Vapor in the Climate System*, October 25–28, Jekyll Island, Georgia.
- Wallace, J. M., 1992: Effect of deep convection on the regulation of tropical sea surface temperature. *Nature*, **357**, 230–231.
- Wallace, J. M., and D. Gutzler, 1981: Teleconnections in the geopotential height field during the Northern Hemisphere winter. *Mon. Wea. Rev.*, **109**, 784–812.
- Wang, W. C., R. B. Rossow, M. S. Yao, and M. Wolfson, 1981: Climate sensitivity of a one-dimensional radiative-convective model with cloud feedback. *J. Atmos. Sci.*, **38**, 1167–1178.
- Wang, W. C., G. Y. Shi, and J. T. Kiehl, 1991: Incorporation of the thermal radiative effect of CH₄, N₂O, CFC₁₃, and CF₂C₁₂ into the NCAR community climate model. *J. Geophys. Res.*, **96**, 9097–9103.
- Warren, S. G., C. J. Hahn, J. London, R. M. Chervin, and R. J. Jenne, 1986: *Global distribution of total cloud cover and cloud type amounts over land*. Technical Note, TN-273+STR, National Center for Atmospheric Research, Boulder.
- Warren, S. G., C. J. Hahn, J. London, R. M. Chervin, and R. J. Jenne, 1988: *Global distribution of total cloud cover and cloud type amounts over ocean*. Technical Note, TN-317+STR, National Center for Atmospheric Research, Boulder.
- Washington, W. M., and G. A. Meehl, 1984: Seasonal cycle experiment on the climate sensitivity due to a doubling of CO₂ with an atmospheric general circulation model coupled to a simple mixed-layer ocean model. *J. Geophys. Res.*, **89**, 9475–9503.
- WCRP (World Climate Research Programme), 1982: Cage Experiment: A feasibility study. WCRP-22, Geneva, 95 pp.
- WCRP (World Climate Research Programme), 1991: Radiation and Climate. *Second Workshop on Implementation of the Baseline Surface Radiation Network*. WCRP-64, WMO/TD-No. 453.
- WCRP (World Climate Research Programme), 1994: Utility and feasibility of a cloud profiling radar. WCRP-84, IGPO Publication Series No. 10, 46 pp.
- WCRP (World Climate Research Programme), 1995: CLIVAR: A study of climate variability and predictability: Geneva, World Meteorological Organization.
- Webster, P. J., and R. Lukas, 1992: TOGA-COARE: The Coupled Ocean Atmosphere Response Experiment. *Bull. Amer. Meteor. Soc.*, **73**, 1377–1417.
- Welch, R. M., S. K. Sengupta, A. K. Goroch, P. Rabindra, N. Rangaraj, and M. S. Navar, 1992: Polar cloud and surface classification using AVHRR imagery: An intercomparison of methods. *J. Appl. Meteor.*, **31**, 405–420.
- Wentz, F. J., 1994: *User's Manual SSM/I - 2 Geophysical Tapes*. Tech. Rep. 070194, Remote Sensing Systems, Santa Rosa, California, 20 pp.

- Wetherald, R.T., and S. Manabe, 1986: An investigation of cloud cover change in response to thermal forcing. *Clim. Change*, **8**, 5–23.
- Whitlock, C. H., T. P. Charlock, W. F. Staylor, R. T. Pinker, I. Laszlo, A. Ohmura, H. Gilgen, T. Konzelman, R. C. DiPasquale, C. D. Moats, S. R. LeCroy, and N. A. Richey, 1995: First global WCRP shortwave surface radiation budget data set. *Bull. Amer. Meteor. Soc.*, **76**, 905–922.
- Wielicki, B. A., and J. A. Coakley, Jr., 1981: Cloud retrieval using infrared sounder data: An error analysis. *J. Appl. Meteor.*, **20**, 37–49.
- Wielicki, B. A., B. R. Barkstrom, E. F. Harrison, R. B. I. Lee, G. L. Smith, and J. E. Cooper, 1996: Clouds and the Earth's Radiant Energy System (CERES): An Earth Observing System Experiment. *Bull. Amer. Meteor. Soc.*, **77**, 853–868.
- Wielicki, B. A., and L. Parker, 1992: On the determination of cloud cover from satellite sensors: The effect of sensor spatial resolution. *J. Geophys. Res.*, **97**, 12,799–12,823.
- Wielicki, B. A., J. T. Suttles, A. J. Heymsfield, R. M. Welch, J. D. Spinhirne, M. L. C. Wu, S. K. Cox, D. O'C. Starr, L. Parker, and R. F. Arduini, 1990: The 27–28 October 1986 FIRE IFO Cirrus case study: Comparison of radiative transfer theory with observations by satellite and aircraft. *Mon. Wea. Rev.*, **118**, 2356–2376.
- Wielicki, B. A., R. D. Cess, M. D. King, D. A. Randall, and E. F. Harrison, 1995: Mission to Planet Earth: Role of cloud and radiation in climate. *Bull. Amer. Meteor. Soc.*, **76**, 2125–2153.
- Williams, M., and R. A. Houze, Jr., 1987: Satellite-observed characteristics of winter monsoon cloud clusters. *Mon. Wea. Rev.*, **115**, 505–519.
- Wilson, C. A., and J. F. B. Mitchell, 1987: A doubled CO₂ climate sensitivity experiment with a global climate model including a simple ocean. *J. Geophys. Res.*, **92**, 13,315–13,343.
- Willson, R. C., 1973: Active cavity radiometer type III. *Appl. Optics*, **12**, 810.
- Willson, R. C., 1979: Active cavity radiometer type IV. *Appl. Optics*, **18**, 179.
- Willson, R. C., S. Gulkis, M. Janssen, H. S. Hudson, and G. A. Chapman, 1981: Observations of solar irradiance variability. *Science*, **234**, 1114–1116.
- Willson, R. C., 1982: Solar irradiance variations and solar activity. *J. Geophys. Res.*, **86**, 4319–4326.
- Willson, R. C., 1984: Measurements of solar total irradiance and its variability. *Space Science Reviews*, **38**, 203–242.
- Willson, R. C., and H. S. Hudson, 1986: Long-term downward trend in total solar irradiance. *Science*, **234**, 1114–1117.
- Willson, R. C., and H. S. Hudson, 1988: Solar luminosity variations in solar cycle 21. *Nature*, **332**, 810–812.
- Willson, R. C., and H. S. Hudson, 1991: The sun's luminosity over a complete solar cycle. *Nature*, **351**, 42–44.
- Willson, R. C., 1994: Irradiance Observations of SMM, Spacelab-1, UARS and ATLAS Experiments. *The Sun as a Variable Star*, IAU Col. 143 proc., J. Pap, C. Frohlich, H. Hudson and K. Salienc, Eds., Cambridge University Press, 54–62.
- Willson, R. C., 1995: Science rationale of the EOS/ACRIMSAT mission. *The Earth Observer*, Feb., 1995.
- Woodard, M. F., and H. S. Hudson, 1983: Frequencies, amplitudes, and line widths of solar oscillations from solar total irradiance observations. *Nature*, **318**, 449–450.
- Woodard, M. F., 1984: Upper limit on solar interior rotation. *Nature*, **309**, 530–532.
- Woodard, M. F., and R. W. Noyes, 1985: Change of solar oscillation eigenfrequencies with the solar cycle. *Nature*, **318**, 449–450.
- Wu, X., J. J. Bates, and S. J. S. Khalsa, 1993: A climatology of the water vapor band brightness temperatures from NOAA operational satellites. *J. Climate*, **6**, 1282–1300.
- Wylie, D. P., and W. P. Menzel, 1989: Two years of cloud cover statistics using VAS. *J. Climate*, **2**, 380–392.
- Xu, K. M., and S. K. Krueger, 1991: Evaluation of cloudiness parameterizations using a cumulus ensemble model. *Mon. Wea. Rev.*, **119**, 342–367.
- Yamanouchi, T., K. Suzuki, and S. Kawaguci, 1987: Detection of clouds in Antarctica from infrared multispectral data of AVHRR. *J. Meteor. Soc. Japan*, **65**, 949–962.
- Yang, H., and R. T. Pierrehumbert, 1994: Production of dry air by isentropic mixing. *J. Atmos. Sci.*, **51**, 3437–3454.
- Zhang, M. H., J. J. Hack, J. T. Kiehl, and R. D. Cess, 1994: Diagnostic study of climate feedback processes in atmospheric general circulation models. *J. Geophys. Res.*, **99**, 5525–5537.
- Zhu, T., J. Lee, R. C. Weger, and R. M. Welch, 1992: Clustering, randomness, and regularity in cloud fields: 2. Cumulus cloud fields. *J. Geophys. Res.*, **97**, 20,537–20,558.

Chapter 2 Index

- AATSR 67, 69
 absorption, scattering, and emission,
 aerosol 50
 absorption, scattering, and emission,
 cloud 51-52
 absorption, scattering, and emission,
 Earth's surface 52-55
 absorption, scattering, and emission,
 gas 49-50
 ACRIM 43-47, 66-67, 69, 91, 103
 ADEOS 69, 87, 89
 Agung 48
 AIRS/AMSU/HSB 50, 52, 55, 59, 62,
 67-71, 78-82, 94-99, 102, 105
 AMIP 55, 80, 86
 AMSR 55, 62, 75-76, 79, 87-88, 95,
 97, 101, 104-105
 AMSR-E 52, 62, 67, 72, 75-76, 79, 87-
 88, 96-100
 ARM 50, 55, 72, 90, 91, 94, 102
 ASTER 52-55, 66, 69, 72, 94, 96
 ATLAS 44, 47
 atmospheric chemistry 48
 atmospheric temperature 49, 96-97,
 101
 ATSR 73
 AVHRR 52, 66-67, 75, 87, 90, 94
 biomass burning 50
 boundary layer fog 64
 boundary layer cloud 64
 BRDF 92
 BSRN 55, 70-71, 91, 102
 calibration 46-48, 66-69, 70-74, 82, 86,
 90-94, 99, 102, 104
 carbon cycle 101
 carbon dioxide (CO₂) 48-49, 56, 59,
 61, 65-66, 80, 84, 88, 91
 CART 102
 CEMs 63-64
 CERES 50-55, 62, 66-67, 69-71, 79,
 92-94, 102, 104
 CLIVAR 101-102
 cloud modeling 59-63
 cloud observations 57-58
 cloud property measurements 72, 94,
 104
 COARE 63-64, 83, 101
 convection 43-45, 56-58, 62-65, 77-83,
 87, 104-106
 convection and clouds in climate
 models 56, 80, 82
 CPR 52, 91
 DAAC 68-69
 data assimilation 55-57, 79, 81, 89, 97
 DFA 99
 DMSP 75, 88
 DoD 90
 DoE 102
 Earth's energy balance, cloud effects on
 56-57
 ECLIPS 102
 ECMWF 56, 81, 89
 EDC 54, 69, 72
 El Niño 52, 79, 83, 100
 ENSO 52, 79, 85-87, 103
 ENVISAT 66, 69, 73
 EOS AM 49, 52-54, 66-70, 92, 101-
 102
 EOS PM 55, 66, 75, 82, 88, 92, 101
 EOSDIS 48, 86
 EOSP 50, 52, 59, 62, 67, 72, 75-79, 94-
 97, 102, 104-105
 ERB 43-48, 54, 67-68
 ERBE 44, 49, 51-56, 59, 66-70, 89
 ERBS 44, 46-47
 ESA 46, 66, 72, 87
 ESCC 43
 ESMR 87
 EURECA 44
 FIRE 64, 70-76, 94, 100-101
 fluxes, radiative 48, 50, 52, 54, 65-66,
 71-72, 91, 93, 97, 102, 104-105
 fluxes, surface 48-49, 52, 54, 65, 67-
 70, 79, 83, 93, 104
 fluxes, TOA 51, 59, 66-72, 92-93, 104
 fluxes, within atmosphere 71-73
 FSSP 75
 GCIP 54-55, 91
 GCMs 48, 54, 58, 60-62, 65, 90, 102
 GEBA 70
 GENESIS 58
 GEOS 55-57, 79, 81
 GERB 92
 GEWEX 48, 54, 81, 90, 101
 GHCN 86
 GLAS 52, 66-69, 71-72, 74, 79, 94-96,
 101
 GLI 67, 69
 GMS 87
 GOALS 101
 GOES 80, 82, 87, 90
 GPCP 84-86
 GSFC 68-69
 GVAP 81
 HIRDLS 49, 78, 82, 94
 HIRS 67-68, 78, 82
 HSB 55, 59, 67-71, 78-79, 82, 87, 98-
 99, 105
 humidity 43, 52, 55, 59, 77-82, 88, 92-
 96, 98-99, 103, 105-106
 hydrology 54-55
 ICRCM 50
 IDS 48, 52, 55, 59, 62-64, 79-80
 interannual variability 43, 48, 52, 81,
 89, 96, 101
 IPCC 50, 84
 IR 66, 81, 86-87, 95, 99, 104
 ISCCP 49, 51-57, 59, 62, 64, 67-74,
 100
 ISLSCP 54
 ITCZ 83-87
 IWP 76
 land processes 103
 lidar 52, 67, 69, 71-74, 82, 89, 94, 96,
 99, 102
 lightning 97
 LIS 62, 97
 LW 48-59, 66-72, 92, 93
 LWP 62, 66, 69, 75-76, 97, 105
 MCS 64, 76-78
 measurement strategy 70
 MERIS 67, 69
 methane (CH₄) 49
 METOP 66, 69, 75, 87, 98, 100
 MIMR 88, 97-100, 104-105
 MISR 50-54, 66-67, 69-74, 79, 92-97,
 102, 104-105
 MLS 49, 77-78, 82, 97-99, 105
 MMS 63-65

modeling 48-49, 52-54, 59-64, 72, 77-80, 83-84, 89-90, 93, 99, 101-102, 105
 MODIS 50-55, 62, 66-76, 79, 92-105
 MOPITT 49
 MSG 92
 NASA 43, 54, 66, 89-90
 NASDA 69, 88
 NCAR 63
 NCDC 86
 NCEP 81
 NEXRAD 86
 NMC 81, 89, 91
 NOAA 67-68, 78, 81, 86-87, 90, 102
 NWP 54, 81
 OLR 49, 53-56, 93
 Pathfinder data 54
 POLDER 66, 69, 73-76
 PR 87
 precipitation 43-106
 PSU 63
 QuikSCAT 24, 89
 radiation in climate models 55
 RAMS 63-64
 RC 48
 SAGE III 78-79, 82, 94-99, 105
 salinity 83
 satellite measurements 87-89, 91, 99
 SCARAB 67-68
 SeaWinds 88, 99, 100
 SMM 43-47
 SMMR 75, 81, 87
 snow cover 83
 SOHO 44-47
 SPCZ 85
 SRB 54, 67-68
 SSM/I 67-68, 75-76, 81, 87-88
 SST 58, 60-61, 65, 80, 86-89, 100, 103
 sulfate 50
 sulfur 50
 surface flux 70, 72, 102
 surface forcing 102
 surface insolation 49
 surface observations 58, 74, 86, 99, 101
 SVAT 54
 SW 48-59, 66-71, 92-93
 temperature profiles 81, 97, 99
 TES 49-50, 96
 TMI 67-68, 75, 87-88
 TOGA 63-64, 83, 101
 topography 64
 TOVS 78-81
 trace gases 48-49
 TRMM 65-70, 75, 87, 92, 94, 97, 99, 101, 104-105
 TSI 43-47, 103
 USGCRP 55, 102
 USGS 54
 validation 54-55, 59-60, 64-75, 81-82, 86, 90-94, 99, 101-104
 variability, trend detection 105
 VIRGO 44, 46-47
 VIRS 52, 66-76, 87, 92, 94
 VIS 87, 104
 water vapor 43-106
 WCRP 51, 70-74, 90, 101-103
 wind 48, 55, 79, 88-89, 99-105
 WOCE 101
 WSR 86